Enhancing Piezo- and Electrical Properties of Bismuth Ferrite based Ceramics
Chemical and Physical Approaches

Tuluk, A.

DOI
10.4233/uuid:ccccf461-a401-4b52-8b95-fa58358b0e75

Publication date
2023

Document Version
Final published version

Citation (APA)
Tuluk, A. (2023). *Enhancing Piezo- and Electrical Properties of Bismuth Ferrite based Ceramics: Chemical and Physical Approaches*. [Dissertation (TU Delft), Delft University of Technology].
https://doi.org/10.4233/uuid:ccccf461-a401-4b52-8b95-fa58358b0e75

Important note
To cite this publication, please use the final published version (if applicable).
Please check the document version above.

ENHANCING PIEZO- AND ELECTRICAL PROPERTIES OF BISMUTH FERRITE BASED CERAMICS:
CHEMICAL AND PHYSICAL APPROACHES

ENHANCING PIEZO- AND ELECTRICAL PROPERTIES OF BISMUTH FERRITE BASED CERAMICS:
CHEMICAL AND PHYSICAL APPROACHES

Proefschrift

ter verkrijging van de graad van doctor
aan de Technische Universiteit Delft,
op gezag van de Rector Magnificus Prof. dr. ir. T. H. J. J. van der Hagen;
voorzitter van het College voor Promoties,
in het openbaar te verdedigen op dinsdag 19 september 2023 om 10:00 uur

door

Anton TULUK

Master of Science in Applied Physics,
Dnipro National University, Oekraïne and
Cracow Pedagogical University, Polen

geboren te Dnipro, Oekraïne

Dit proefschrift is goedgekeurd door de promotoren.
Prof. dr. dr.h.c. ir. S. van der Zwaag en Prof. dr. B. Dam

Samenstelling promotiecommissie bestaat uit :

Rector magnificus,	voorzitter
Prof. dr. ir. S. van der Zwaag	Technische Universiteit Delft, promotor
Prof. dr. B. Dam	Technische Universiteit Delft, promotor

Onafhankelijke leden:

Dr. J. Khaliq	Northumbria University, Verenigd Koninkrijk
Dr. H. Khanbareh	University of Bath, Verenigd Koninkrijk
Prof. C.A. Dransfeld	Technische Universiteit Delft
Prof.dr. A.J.A. Winnubst	Universiteit Twente
Prof.dr. M.J. Santofimia Navarro	Technische Universiteit Delft

Keywords: Ceramic, Piezoelectric, Ferroelectric, Bismuth ferrite

Printed by: IPSKAMP Printing B.V.

Cover by: Anton Tuluk

ISBN
An electronic version of this dissertation is available at https://repository.tudelft.nl/

Contents

1

INTRODUCTION

1.1 PIEZOELECTRIC EFFECT

The piezoelectric effect was discovered in 1880 by Pierre and Jacques Curie [1] who found that single crystals of certain materials such as quartz, tourmaline and zinc blende possess the ability to generate an electric potential in response to an applied mechanical stress. The German physicist Wilhelm G. Hankel gave this phenomenon the name “piezoelectricity” [2]. The crystallographic requirement for a material to exhibit piezoelectricity is the absence of centrosymmetry [3]. Although the prefix "piezo" implies the application of pressure for the effect to occur, the effect is also reversible giving rise to the converse piezoelectric effect. In the converse effect, the application of an electrical potential across a piezoelectric material result in an elastic strain in the material. In general, the piezoelectric effect occurs only in non- or barely electrically conductive materials, i.e. semi-conductors. Otherwise, with a high intrinsic conductivity, it will not be possible to achieve a sufficient and lasting charge separation. Piezoelectric materials can be divided into two main groups: single crystals and polycrystalline ceramics. The best-known piezoelectric material in the single crystal group is quartz (SiO_2), trigonal crystallized silica which is known as one of the most common crystals on the earth’s surface. In the polycrystalline ceramics group, a typical piezoelectric material is barium titanate ($BaTiO_3$), an oxide of barium and titanium [3], but the most frequently

used piezoceramics is the chemically more complex lead-zirconium-titanate ($Pb[Zr_xTi_{1-x}]O_3$) or PZT [3].

Polycrystalline ceramics consist of randomly oriented micron-sized crystallites. Each crystallite is further divided into tiny "domains," or regions having similar dipole arrangements [4]. The overall effect of randomly oriented polar domains is an initial lack of piezoelectric behavior. However, the material may be induced to exhibit macroscopic polarization in any given direction by subjecting it to a strong electric field, as shown in **Figure 1.1**. Such inducible materials are termed ferroelectric. Polarization is accomplished by applying a field higher than the internal coercive field (for common piezoelectric approximately 10-20 kV/cm) [5,6] across electrodes deposited on the outer surfaces of the sample. Once polarized, the ferroelectric material will remain polarized until it is depoled by an opposite field or by heating it to a temperature above its Curie temperature. At the Curie temperature the crystal structure changes from a non-symmetrical (piezoelectric) to a symmetrical (non-piezoelectric) form. When the temperature is above the Curie temperature, each perovskite crystal in the ceramic element has a simple cubic symmetry with no dipole moment. At temperatures below the Curie point, however, each crystal has a tetragonal or rhombohedral symmetry and a dipole moment. As the poling process puts the domains into a non-equilibrium configuration, the piezo properties will fade in time when the material is used at higher temperatures closer to the Curie temperature.

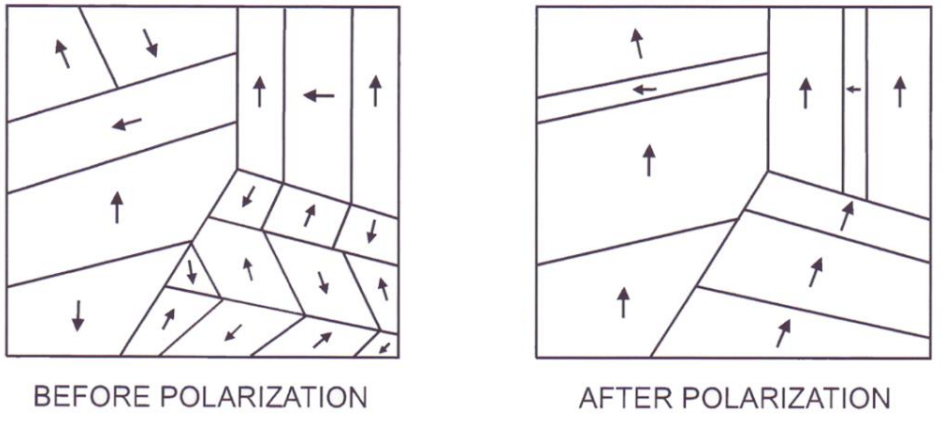

Figure 1.1 – Schematic diagram of the alignment of domains due to poling. [2]

We now can try and quantify the piezo-electric effect, linking the polarization of the material to the imposed mechanical load. As the piezoelectrical properties reflect the necessarily anisotropic atomic arrangements in the crystal structure they are anisotropic by default, so the relation requires a 3rd order tensorial relationship [3]

$$P_i = d_{ij} T_j \tag{1.1}$$

where the piezoelectric charge constant, d_{ij} (C/N), links the polarization (P_i (C/m²)) generated per unit of mechanical stress (T_j (Pa)) [1]. The piezoelectric charge coefficients for the direct and converse effect are thermodynamically identical, and the sign of the response is dependent upon the vector of either the mechanical or the electric field. The tensor notation can be quite complex but due to symmetry constraints in most piezoelectric systems a full tensor notation is not always necessary, but the dependence can be reflected in two scalar parameters for most common loading configurations e.g. d_{33} or d_{31}. The first subscript gives the direction of the charge motion associated with the applied stress. The second subscript gives the direction of mechanical stress. The piezoelectric coefficient d_{33} describes the generation of electric charge along the 3-axis in response to applied stress along the same 3-axis, without the presence of any other stresses. On the other hand, the piezoelectric coefficient d_{31} describes the generation of electric charge along the 3-axis in response to stress applied along the orthogonal 1-axis (or 2-axis), under similar conditions.

As already stated earlier, the temperature dependence of piezoelectric coefficients is extremely important when designing novel piezoelectric ceramics [7–9]. If a material has a Curie temperature significantly higher than room temperature, it suggests that a substantial amount of thermal energy is needed to disrupt its non-centrosymmetric state. As a result, the piezoelectric signal at room temperature is expected to be weak.

As discussed in a large number of publications [10–15] the magnitude of piezoelectric properties at room temperature may have to be sacrificed in order to achieve ceramics with a high T_C, i.e ceramics which can be used over a wide temperature domain. The thermal dependence of the piezoelectric

coefficients is linked to a number of factors, namely the intrinsic and extrinsic contributions. The intrinsic effect is dominated by distortions of the lattice. The temperature dependence of the intrinsic piezoelectric response can be approximated using Landau theory [16]:

$$d = \varepsilon_0 \varepsilon_r Q P_s \tag{1.2}$$

Where electrostriction coefficient (Q) is largely temperature independent [22], but the polarization (P_s) and permittivity ($\varepsilon_0 \varepsilon_r$) demonstrate strong temperature dependence.

Extrinsic contributions are often described as having the most profound effect on piezoelectric properties. The dominant extrinsic effect is related to the domain structure, in particular to the density and mobility of the domain walls. These are frequency, field and time dependent, nonlinear and lossy. Therefore, an understanding of and the ability to control the spatial mobility and clamping of the domain structure is important for any piezo-electrical system. As domain wall motion is a thermally activated process, the extrinsic effect increases with temperature [17–20].

As mentioned above the piezo-electrical response depends on temperature and (for polycrystalline materials) on poling conditions. However, the piezo electrical response can also be modified and improved by changing the chemical composition of the material. This can be done by replacing some of the atoms of the base material (substitutional atomic alloying with doping levels of up to 5 %), or by replacing some of the unit cells by unit cells of a different material ('unit cell' alloying in which at least two different metallic atoms and the corresponding oxygen atoms are added to the base structure). In the first case the changes at microstructural level are modest and the improvement in properties is primarily due to strengthening of the internal electrical field. In the second case, phase boundaries between the two parent ceramics may lead to new microstructural features which facilitate the accommodation of the elastic strains upon activation of the anisotropic piezoelectric effect, resulting in higher piezo-electric charge constants. The doping and alloying strategies will be discussed in section 1.3

1.2 $BiFeO_3$ AS A PIEZOELECTRIC MATERIAL

The perovskite $BiFeO_3$ (BFO) was discovered in the late 1950s [21]. BFO crystalizes in a perovskite type structure (**Figure 1.2a**), in particular in a rhombohedral structure belonging to the R3c space group (α – phase shown on **Figure 1.2b**) as determined by Michel in 1969 [22], which differs from earlier interpretations classifying it as to belonging to the R3m space group. The $BiFeO_3$ compound has a Neel temperature, T_N, of 370 °C and a ferroelectric T_C of 825 °C which has led to its wide use in binary compounds [23]. Around the T_C, a ferroelectric-paraelectric phase transition appears into the β phase which is followed by a sudden volume contraction [24]. Before this ferroelectric transition, BFO shows a very large spontaneous polarization ($P \approx 90 - 100 \mu C/cm^2$) [25,26] in the pseudocubic [111] direction. Despite extensive research, there is still not agreement about its crystal structure in the temperature range surrounding T_C, during the α – β phase transition [24,27,28].

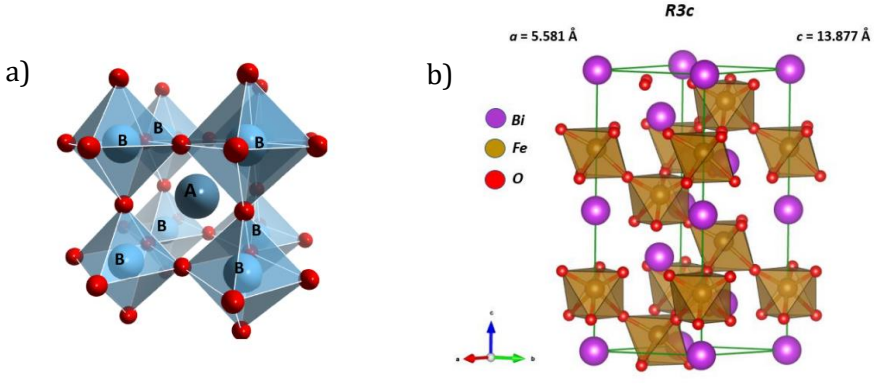

Figure 1.2 – a) perovskite type structures material is any material with a crystal structure having the formula ABO_3 (red spheres - oxygen), b) R3c crystal structure of $BiFeO_3$

Although other techniques have also been employed, solid state synthesis is the most commonly used method for synthesizing BFO. In the solid-state route Bi_2O_3 and Fe_2O_3 powders (in their stoichiometric ratio) are reacted at a temperature in the range of 750–830 °C to form BFO. The potential reactions can best be visualized in the Bi_2O_3-Fe_2O_3 phase diagram which was first investigated in detail by Maitre et al. [29] in 2004 and supplemented and

summarized by Palai et al. [30] in 2008 (**Figure 1.3**). As is visible in the phase diagram, except for the perovskite bismuth ferrite phase, two other stable phases exist: mullite $Bi_2Fe_4O_9$ and sillenite $Bi_{25}FeO_{39}$. The main reason for the formation of the secondary phases mullite and sillenite are local variations the reaction path [31] associated with the large difference in the diffusion coefficient of iron and bismuth ions [32] (as illustrated in **Figure 1.4**).

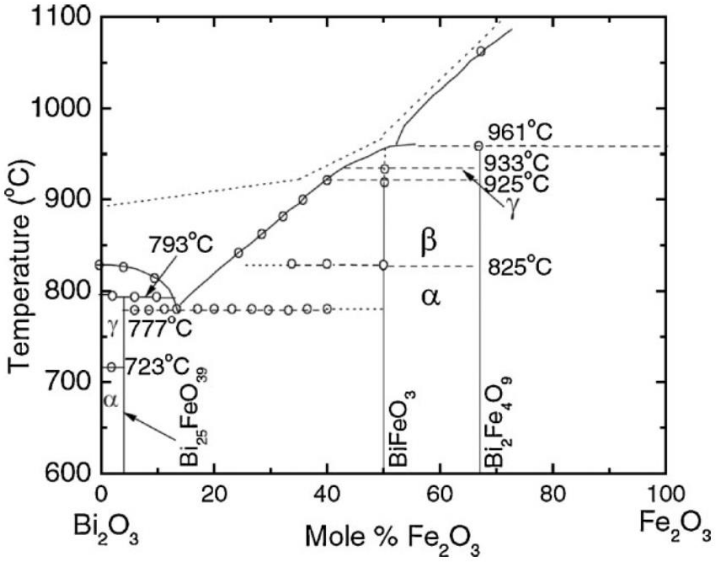

Figure 1.3 – Phase diagram Bi_2O_3-Fe_2O_3 system [30]

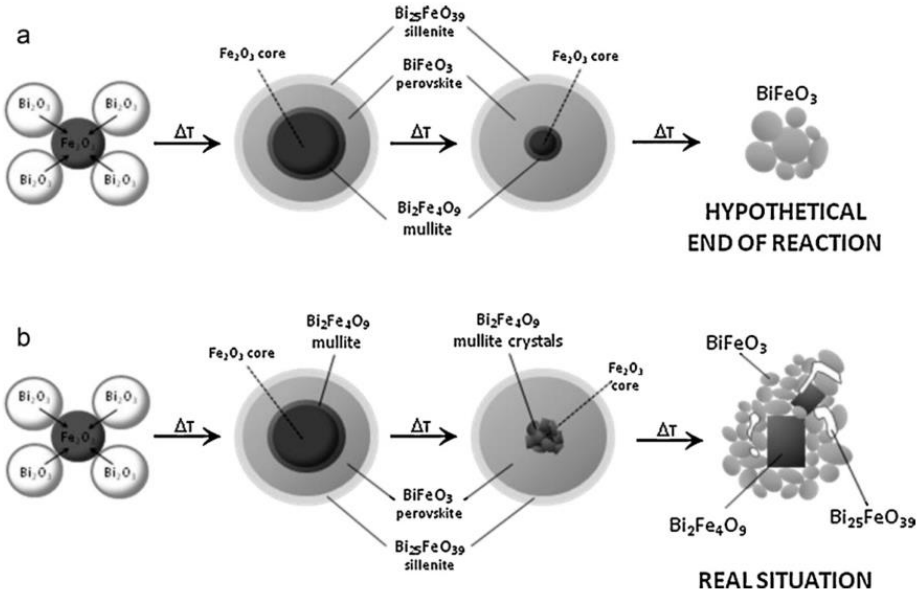

Figure 1.4 – Schematic diagram of the reaction paths in the solid-state synthesis of $BiFeO_3$. (a) Hypothetical end of the reaction and (b) experimental situation for practical conditions. [31]

1.3 ELEMENTAL DOPING

In the following we will discuss A-site, B-site and oxygen substitution of BFO and give specific examples for each case [33].

The process of A-site substitution involves the replacement of Bi^{3+} ions with other ions. As the electronic levels of A-site ions are distant from the Fermi level, A-site substitution can indirectly impact the band structure. This impact can be observed in terms of the control of band width and band filling. If A-site substitution is carried out using ions with a smaller ionic radius, it may lead to more buckling in the Fe-O-Fe bond angle [34] resulting in a higher electrical resistivity. Also, other physical properties can be manipulated through carrier doping. For instance, when divalent ions are inserted to replace trivalent A-site ions, a high-T_C piezoelectricity and a colossal magnetoresistance can be induced. Substituting Bi^{3+} with divalent ions such as Ca^{2+} [35] and Sr^{2+}[32] can result in novel conducting states of acceptor-doped BFO, provided other dopants like oxygen vacancies are not produced. The control of band filling

introduces hole carriers, while substitution with Ce^{4+} ions [36] results in the introduction of electron carriers.

B-site substitutions in BFO refer to the replacement of Fe^{3+} ions with other transition metal ions. The electronic structure of BFO is strongly related to the d orbital state of the Fe^{3+} ion, so substitutions can significantly influence the physical properties by altering the electronic structure near the Fermi level.

When considering B-site substitution, it is important to determine whether the dopant ions produce ordered or random structures. This factor is related to the ionic radius of the dopant ion.

Ordered structures are beneficial because they stabilize the crystal lattice and improve the materials' functional properties. In contrast, random distributions lead to the formation of defects, which can degrade the materials' properties. Therefore, it is important to carefully consider the choice of dopant ions and their ionic radius when making B-site substitutions in BFO.

B-site doping usually has been applied to BFO to reduce leakage currents. For example, doping BFO with Ti^{4+} has been shown to reduce leakage current by over three orders of magnitude [37]. This is because Ti^{4+} ions can introduce oxygen vacancies and compensate for naturally existing oxygen vacancies in BFO, leading to a reduction in the concentration of defects that contribute to the leakage current. Doping with Ni^{2+} [38] can increase the electrical conductivity of BFO by over two orders of magnitude. This is due to the fact that Ni^{2+} can donate electrons to the conduction band of BFO, increasing its carrier density and hence its conductivity. Similarly, doping with Cr or Mn has been shown to greatly reduce leakage currents in BFO films [39]. This is because Cr or Mn ions can act as acceptors, reducing the concentration of oxygen vacancies and thereby suppressing the formation of defects that contribute to leakage current. Overall, B-site doping of BFO with different transition metal ions can significantly modify its electronic and magnetic properties and reduce the leakage current, which is important for the development of high-performance electronic devices based on BFO.

Apart from elemental doping in which only small fraction of one of the elements of the initial material substituted, it is also possible to dope with significant amount of two or more other elements or even a different functional ceramic which can even lead to phase changes and microstructure and activate different effects.

1.4 MORPHOTROPIC PHASE BOUNDARIES AND UNIT CELL DOPING

A morphotropic phase boundary (MPB) is defined as a practically temperature independent phase boundary between two different crystal symmetries. While the original broader definition was "phase transitions due to compositional changes" [40], now the common parlance amongst researchers refers to MPB as a phase boundary that "separates tetragonal symmetry from rhombohedral symmetry by varying the composition in ferroelectrics" [41]. MPBs are frequently found in perovskite solid solution compositions and are the main component of the bulk of industrial electroceramics. Because of the higher polarizability caused by the interaction between two different crystallographic symmetries, there is a noticeable improvement in the dielectric and piezoelectric properties in this region. The property optimization using MPBs is used in the commercially dominating $PbZrO_3$-$PbTiO_3$ (PZT) system [42].

BFO has also been used to form solid solutions with satellite tetragonal end members in order to engineer an MPB to increase ferroelectric and piezoelectric properties [42].

The MPB composition in the $BiFeO_3$–$PbTiO_3$ system (adding both Pb and Ti atoms to the base BFO system) offers a high Curie temperature (635 °C) [43], but are extremely hard to pole due to the large spontaneous strain, and the conductivity due to p-type defects is too high for high temperature applications. On the other hand, other tetragonal end-members result in the breakdown of long-range order, a reduction in T_C, and the onset of relaxor behavior. As a general rule, increasing the number of cations in a solid solution tends to further undermine polar coherence and deepen the relaxor nature; however, incorporation of $PbTiO_3$ in nano-polar systems tends to overcome the loss of coherence and favors the formation of long-range polar order. As stated above the large tetragonal distortion (c/a ratio 1.18) for $BiFeO_3$-$PbTiO_3$ solid solutions results in a large coercive field of E_C >100kV/cm, making such materials difficult to be fully poled [44].

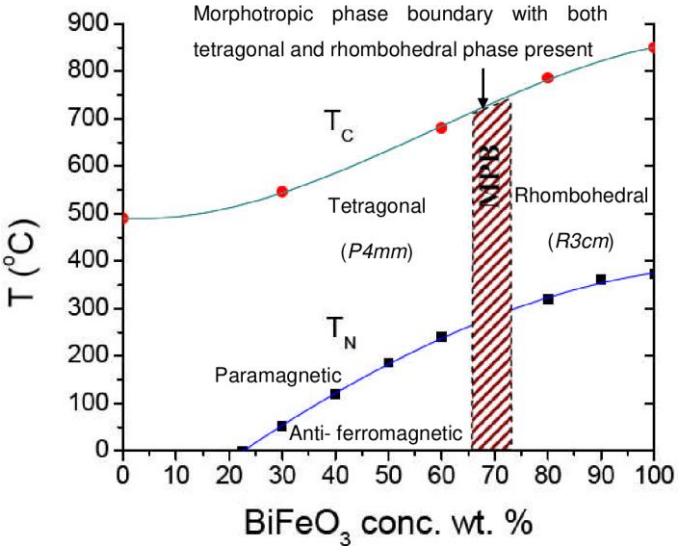

Figure 1.5 – Phase diagram of $BiFeO_3$–$PbTiO_3$ [45]

While binary system combinations offer many opportunities for property optimisation, the barely explored ternary systems may hold even more interesting opportunities.

The ternary approach is stimulated by the ternary alloys design for PZT-relaxors. The schematic phase diagram at RT for this system shown in **Figure 1.6**. Relaxor-PT piezoelectric materials, such as $Pb(Zn_{1/3}Nb_{2/3})O_3$-$PbTiO_3$ (PZN-PT) and $Pb(Mg_{1/3}Nb_{2/3})O_3$-$PbTiO_3$ (PMN-PT) [46], exhibit a morphotropic phase boundary (MPB) between the tetragonal and pseudocubic phases. In contrast, $PbZrO_3$ and $PbTiO_3$ have their MPB between the tetragonal and rhombohedral phases [42], while the PZN-PMN system shows no MPB The unique advantage of combining these materials in a ternary system is that it allows for the possibility of achieving a point where the two MPBs intersect, potentially resulting in a significant enhancement of material properties.

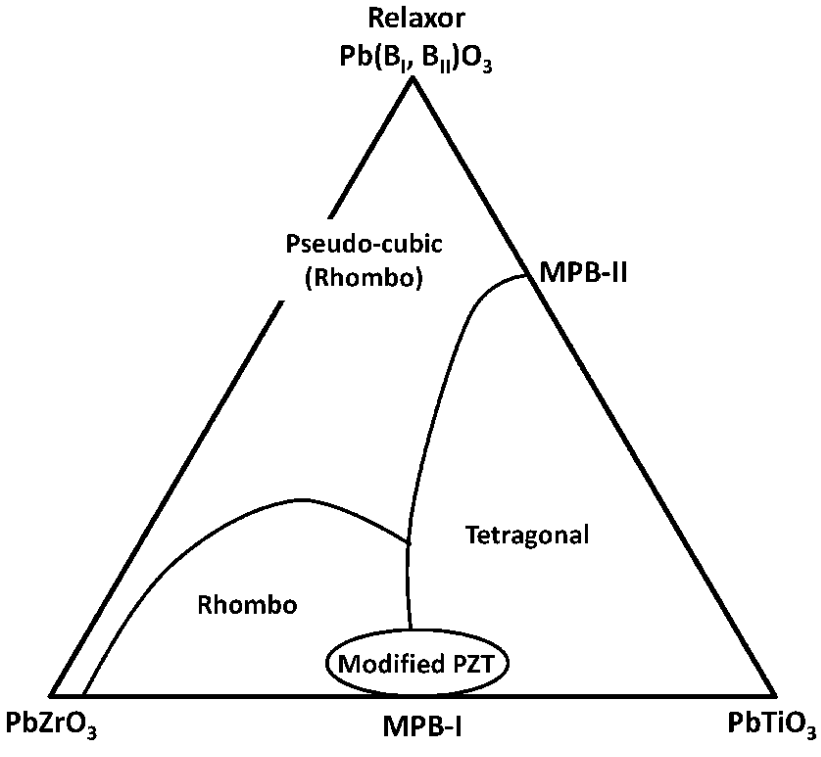

Figure 1.6 – Schematic ternary phase diagram (at room temperature) showing different phase behaviours for the binary subsystems [46].

For BFO based systems the example of $BiFeO_3$–$PbTiO_3$–$(K_{1/2}Bi_{1/2})TiO_3$ in which the largest weak-field d_{33} is located virtually mid-way between the $BiFeO_3$–$PbTiO_3$ MPB composition and the pseudo-cubic region of $BiFeO_3$–$(K_{1/2}Bi_{1/2})TiO_3$ [43] offers a high Curie temperature and a high d_{33} alternative to PZT.

1.5 QUENCHING

Tuning the properties of ferroelectric and piezoelectric materials through chemical modifications has been researched extensively. In comparison, the effect of (thermal) processing conditions on their properties has been studied less with attention going primarily to the determination of the sintering temperature leading to the highest density. However, tailoring the cooling rate

when lowering the temperature can be an attractive route to preserve desirable high temperature states and tune properties.

The quenching method, i.e a forced rapid cooling from a high temperature above or near the Curie temperature to room temperature, has shown potential in the literature as a tool to tailor the electromechanical properties and phase transitions in different ferroelectric and related materials. For example, quenching $Sr_xBa_{1-x}Nb_2O_6$ has been found to reduce disorder at the A-site, resulting in sharper phase transformations, reduced relaxor characteristics, and increased phase transition temperature.

In BFO, quenching has been a valuable method for minimizing the formation of the Bi- and Fe-rich secondary phases [23], which have been persistently observed in BFO ceramics processed by conventional mixed-oxide route. Additionally, quenching has been used to tailor the behaviour of charged point defects [47], particularly in terms of domain-wall pinning effects. These studies have provided invaluable information on the hardening behaviour of BFO, making it possible to truly unveil the effect of point defects on the switching and sub switching properties of BFO, and even atomistic details of domain walls. Furthermore, quenching may prevent the formation of spurious satellite phases. In a recent study [48], the piezoelectric properties of BFO were enhanced by modifying the heat-treatment process to avoid the intermediate temperature range where secondary phases tend to form. As a result of these modifications, the direct piezoelectric sensor coefficient d_{33} was significantly improved, increasing from 120 to 250 pC/N (**Figure 1.7a**).

Apart from quenching also annealing (i.e. isothermal holding at a fixed temperature) may be used to tune properties, such as in a recent study on the the effect of annealing on the piezoelectric properties of quenched $Na_{0.5}Bi_{0.5}TiO_3$-$BaTiO_3$ (NBT-BT) ceramics [49], which was shown to control the presence of the non-uniform domains in the ceramics formed by quenching. Another study investigated the effect of annealing on the piezoelectric properties of NBT-based ceramics quenched from different cooling temperatures. They found that the piezoelectric coefficients thermal stability of the ceramics could be significantly improved by annealing at temperatures above 800 °C after quenching [50]. However, after subsequent annealing a decrease in piezoelectric coefficient was observed (**Figure 1.7b**). The improvement in piezoelectric properties was attributed to the completion of

the formation of the perovskite structure and the relaxation of residual stresses.

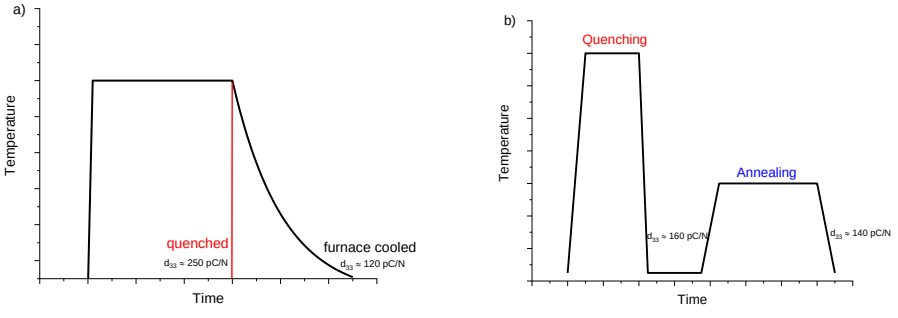

Figure 1.7 – a) piezoelectric properties of BFO-BT ceramic after quenching and furnace cooling [48] and b) piezoelectric properties of NBT-based ceramics after quenching and annealing [50]

Overall, while chemical modifications remain an attractive option to tailor material properties, the quenching and annealing method also offers promising avenues for optimizing the ferroelectric and piezoelectric properties.

1.7 THESIS OUTLINE

The goal of the research described in this thesis is to improve the piezo- and electrical properties of bismuth ferrite-based (BFO) piezoceramics at room and elevated temperatures. To that aim, each chapter addresses a different scientific question, and the answers together build up a more complete understanding of the problem in use of BFO-based piezoceramics and ways to improve their properties by using different approaches.

The main goal of **Chapter 2** was to identify problems in the synthesis, as well as the shortcomings and limitations of BFO piezoceramics. Determination of the optimal values for temperature and time in the synthesis and sintering of BFO ceramics formed the first focus of the study. The second aim of this study was to investigate the contribution of oxygen vacancies to the high electrical conductivity of BFO by conducting electrical conductivity measurements on samples cooled under different oxygen potentials.

Chapter 3 describes a method to determine the best estimate of piezoelectric properties of conductive piezo-materials by placing them in a non-conductive matrix and to reach a fully poled state of the BFO particles when poling the particulate composite. To this aim the permittivity of the matrix should be matched to that of the ceramic particles, in order to fully polarize the ceramic and accurately measure the true values of the piezoelectric properties of (ceramic) BFO by extrapolation of the data for the composites with different filling fractions.

In **chapter 4** the effect of titanium and cobalt doping on electrical conductivity and piezoelectric properties is studied. The main goal is to reduce oxygen vacancies, the presence of which was studied in Chapter 2, while maintaining good piezoelectric properties. The work focussed on determining the (opposing) effects of Cobalt and Titanium as well as a search for any synergetic effects due to dual doping.

In chapter 5, we investigated the potential of BFO-rich bulk piezoceramics, specifically the $BiFeO_3$–$PbTiO_3$–$SrTiO_3$ system, for high-temperature applications. The goal of the study was investigate and optimize the piezoelectric properties of BFO-rich bulk piezoceramics, specifically focusing on the effects of dual ('unit cell' doping) with $PbTiO_3$ and $SrTiO_3$ on the Curie temperature, crystal structure, and temperature stability of piezoelectric properties in relation to the distance to the triple point MPB composition. Also, the study aims to determine the effect of temperature (following different thermal treatments) on the piezoelectric properties of the most promising ternary systems.

In **chapter 6** the effect of various heat treatments on the piezoelectric properties of the $BiFeO_3$-$PbTiO_3$-$Bi_{0.5}Li_{0.5}TiO_3$ ternary system was investigated. The goals of this study are to investigate the effects of thermal processing conditions, including quenching and annealing, on the final properties of the material. This includes studying the temperature dependence of the electrical conductivity and piezoelectric charge constant. The aim is to identify optimal properties and evaluate the suitability of the new material for high temperature sensors.

The thesis ends with a Summary in which the main findings of the research are compiled.

REFERENCES

[1] J. Curie, P. Curie, *Développement par compression de l'électricité polaire dans les cristaux hémièdres à faces inclinées* [Development by compression of polar electricity in hemihedral crystals with inclined faces], Bull. La Société Minéralogique Fr. 3 (1880) 90–93. https://www.persee.fr/doc/bulmi_0150-9640_1880_num_3_4_1564.

[2] A. Ballato, Piezoelectricity: History and new thrusts, Proc. IEEE Ultrason. Symp. 1 (1996)575–583.https://doi.org/10.1109/ultsym.1996.584046.

[3] J. Holterman, P. Groen, An Introduction to Piezoelectric Materials and Applications, An Introd. to PiezoelectricMaterials Appl. (2013) 15–17. www.applied-piezo.com.

[4] T. Granzow, S. Glinsek, E. Defay, Piezoelectric Ceramics, Encycl. Smart Mater. 17 (2021) 22–34. https://doi.org/10.1016/B978-0-12-815732-9.00043-7.

[5] J. Fialka, P. Beneš, Comparison of methods of piezoelectric coefficient measurement, 2012 IEEE I2MTC - Int. Instrum. Meas. Technol. Conf. Proc. (2012) 37–42. https://doi.org/10.1109/I2MTC.2012.6229293.

[6] V.D. Kugel, L.E. Cross, Behavior of soft piezoelectric ceramics under high sinusoidal electric fields, J. Appl. Phys. 84 (1998) 2815–2830. https://doi.org/10.1063/1.368422.

[7] R.E. Eitel, C.A. Randall, T.R. Shrout, P.W. Rehrig, W. Hackenberger, S.E. Park, New high temperature morphotropic phase boundary piezoelectrics based on Bi(Me)O3-PbTiO3 ceramics, Japanese J. Appl. Physics, Part 1 Regul. Pap. Short Notes Rev. Pap. 40 (2001) 5999–6002. https://doi.org/10.1143/jjap.40.5999.

[8] T. Sebastian, I. Sterianou, D.C. Sinclair, A.J. Bell, D.A. Hall, I.M. Reaney, High temperature piezoelectric ceramics in the Bi(Mg1/2Ti 1/2)O3-BiFeO3-BiScO3-PbTiO 3 system, J. Electroceramics. 25 (2010) 130–134. https://doi.org/10.1007/s10832-010-9600-0.

[9] Z. Ning, Y. Jiang, J. Jian, J. Guo, J. Cheng, H. Cheng, J. Chen, Achieving both large piezoelectric constant and high Curie temperature in BiFeO3-PbTiO3-BaTiO3 solid solution, J. Eur. Ceram. Soc. 40 (2020) 2338–2344. https://doi.org/10.1016/j.jeurceramsoc.2020.01.059.

[10] I. Kim, K. Jang, I. Kim, L. Li, Higher-order Landau phenomenological models for perovskite crystals based on the theory of singularities: a new phenomenology of BaTiO 3, Phase Transitions. 91 (2018) 239–253. https://doi.org/10.1080/01411594.2017.1350960.

[11] T. Rojac, M. Makarovic, J. Walker, H. Ursic, D. Damjanovic, T. Kos,

Piezoelectric response of BiFeO3ceramics at elevated temperatures, Appl. Phys. Lett. 109 (2016). https://doi.org/10.1063/1.4960103.

[12] A. Hussain, X. Xu, G. Yuan, Y. Wang, Y. Yang, J. Yin, J. Liu, Z. Liu, The development of BiFeO 3 -based ceramics, Chinese Sci. Bull. 59 (2014) 5161–5169. https://doi.org/10.1007/s11434-014-0648-0.

[13] J. Bennett, T.R. Shrout, S.J. Zhang, P. Mandal, A.J. Bell, T.J. Stevenson, T.P. Comyn, Temperature dependence of the intrinsic and extrinsic contributions in BiFeO3-(K0.5Bi0.5)TiO3-PbTiO3piezoelectric ceramics, J. Appl. Phys. 116 (2014) https://doi.org/10.1063/1.4894443.

[14] M. Yashima, K. Omoto, J. Chen, H. Kato, X. Xing, Evidence for (Bi,Pb)-O covalency in the high T C ferroelectric PbTiO3-BiFeO3 with large tetragonality, Chem. Mater. 23 (2011) 3135–3137. https://doi.org/10.1021/cm201184y.

[15] P.M. Weaver, T. Stevenson, T. Quast, G. Bartl, T. Schmitz-Kempen, P. Woolliams, A. Blumfield, M. Stewart, M.G. Cain, High temperature measurement and characterisation of piezoelectric properties, J. Mater. Sci. Mater. Electron. 26 (2015) 9268–9278. https://doi.org/10.1007/s10854-015-3285-8.

[16] L.L. Ilhwan Kim, Kumok Jang , Ilhun Kim, Higher-order Landau-Devonshire theory for BaTiO3, 22 (2005) 552–555.

[17] S. Takahash, Effects Of Impurity Doping In Lead Zirconate-Titanate Ceramics,Ferroelectrics.41(1982)143-156. https://doi.org/10.1080/00150198208210617.

[18] A. Bencan, G. Drazic, H. Ursic, M. Makarovic, M. Komelj, T. Rojac, Domain-wall pinning and defect ordering in BiFeO3 probed on the atomic and nanoscale, Nat. Commun. 11 (2020) 1–9. https://doi.org/10.1038/s41467-020-15595-0.

[19] M. Makarovic, M.Ç. Bayir, H. Ursic, A. Bradesko, T. Rojac, Domain wall conductivity as the origin of enhanced domain wall dynamics in polycrystalline BiFeO3, J. Appl. Phys. 128 (2020). https://doi.org/10.1063/5.0017374.

[20] A.N. Morozovska, R.K. Vasudevan, P. Maksymovych, S. V. Kalinin, E.A. Eliseev, Anisotropic conductivity of uncharged domain walls in BiFeO 3, Phys. Rev. B - Condens. Matter Mater. Phys. 86 (2012) 1–9. https://doi.org/10.1103/PhysRevB.86.085315.

[21] J. Gebhardt, A.M. Rappe, Doping of BiFeO3: A comprehensive study on substitutional doping, Phys. Rev. B. 98 (2018) 1–16. https://doi.org/10.1103/PhysRevB.98.125202.

[22] C. Michel, J.M. Moreau, G.D. Achenbach, R. Gerson, W.J. James, The atomic

structure of BiFeO3, Solid State Commun. 7 (1969) 701–704. https://doi.org/10.1016/0038-1098(69)90597-3.

[23] M. Makarovic, A. Bencan, J. Walker, B. Malic, T. Rojac, Processing, piezoelectric and ferroelectric properties of (x)BiFeO3-(1-x)SrTiO3 ceramics, J. Eur. Ceram. Soc. 39 (2019) 3693–3702. https://doi.org/10.1016/j.jeurceramsoc.2019.04.044.

[24] G. Marschick, J. Schell, B. Stöger, J.N. Gonçalves, M.O. Karabasov, D. Zyabkin, A. Welker, M. Escobar C., D. Gärtner, I. Efe, R.A. Santos, J.E.M. Laulainen, D.C. Lupascu, Multiferroic bismuth ferrite: Perturbed angular correlation studies on its ferroic α-β Phase transition, Phys. Rev. B. 102 (2020) 224110. https://doi.org/10.1103/PhysRevB.102.224110.

[25] H. Zhu, Y. Yang, W. Ren, M. Niu, W. Hu, H. Ma, J. Ouyang, Rhombohedral BiFeO3 thick films integrated on Si with a giant electric polarization and prominent piezoelectricity, Acta Mater. 200 (2020) 305–314. https://doi.org/10.1016/j.actamat.2020.09.022.

[26] G.L. Yuan, S.W. Or, Y.P. Wang, Z.G. Liu, J.M. Liu, Preparation and multi-properties of insulated single-phase $BiFeO_3$ ceramics, Solid State Commun. 138 (2006) 76-81 https://doi.org/10.1016/j.ssc.2006.02.005.

[27] S.M. Selbach, T. Tybell, M.A. Einarsrud, T. Grande, Phase transitions, electrical conductivity and chemical stability of BiFeO3 at high temperatures, J. Solid State Chem. 183 (2010) 1205–1208. https://doi.org/10.1016/j.jssc.2010.03.014.

[28] J.F. Scott, R. Palai, A. Kumar, M.K. Singh, N.M. Murari, N.K. Karan, R.S. Katiyar, New phase transitions in perovskite oxides: BiFeO 3 , SrSnO 3 , and Pb(Fe 2/3 W 1/3) 1/2 Ti 1/2 O 3, J. Am. Ceram. Soc. 91 (2008) 1762–1768. https://doi.org/10.1111/j.1551-2916.2008.02404.x.

[29] A. Maître, M. François, J.C. Gachon, Experimental Study of the Bi2O3-Fe2O3 Pseudo-Binary System, J. Phase Equilibria Diffus. 25 (2004) 59–67. https://doi.org/10.1361/10549710417687.

[30] R. Palai, R.S. Katiyar, H. Schmid, P. Tissot, S.J. Clark, J. Robertson, S.A.T. Redfern, G. Catalan, J.F. Scott, β phase and γ-β metal-insulator transition in multiferroic BiFeO3, Phys. Rev. B - Condens. Matter Mater. Phys. 77 (2008) 1–11. https://doi.org/10.1103/PhysRevB.77.014110.

[31] M.S. Bernardo, T. Jardiel, M. Peiteado, A.C. Caballero, M. Villegas, Reaction pathways in the solid state synthesis of multiferroic BiFeO3, J. Eur. Ceram. Soc. 31 (2011) 3047-3053. https://doi.org/10.1016/j.jeurceramsoc.2011.03.018.

[32] R. Dahiya, A. Agarwal, S. Sanghi, A. Hooda, P. Godara, Structural,

magnetic and dielectric properties of Sr and v doped BiFeO3 multiferroics, J. Magn. Magn. Mater. 385 (2015) 175–181. https://doi.org/10.1016/j.jmmm.2015.03.013.

[33] V.A. Khomchenko, D.A. Kiselev, M. Kopcewicz, M. Maglione, V. V. Shvartsman, P. Borisov, W. Kleemann, A.M.L. Lopes, Y.G. Pogorelov, J.P. Araujo, R.M. Rubinger, N.A. Sobolev, J.M. Vieira, A.L. Kholkin, Doping strategies for increased performance in BiFeO3, J. Magn. Magn. Mater. 321 (2009) 1692–1698. https://doi.org/10.1016/j.jmmm.2009.02.008.

[34] A. Tamilselvan, S. Balakumar, M. Sakar, C. Nayek, P. Murugavel, K. Saravana Kumar, Role of oxygen vacancy and Fe-O-Fe bond angle in compositional, magnetic, and dielectric relaxation on Eu-substituted BiFeO3 nanoparticles, Dalt. Trans. 43 (2014) 5731–5738. https://doi.org/10.1039/c3dt52260a.

[35] V.A. Khomchenko, D.A. Kiselev, J.M. Vieira, L. Jian, A.L. Kholkin, A.M.L. Lopes, Y.G. Pogorelov, J.P. Araujo, M. Maglione, Effect of diamagnetic Ca, Sr, Pb, and Ba substitution on the crystal structure and multiferroic properties of the BiFeO3 perovskite, J. Appl. Phys. 103 (2008). https://doi.org/10.1063/1.2836802.

[36] S.K. Pradhan, B.K. Roul, Electrical behavior of high resistivity Ce-doped BiFeO 3 multiferroic, Phys. B Condens. Matter. 407 (2012) 2527–2532. https://doi.org/10.1016/j.physb.2012.03.061.

[37] S.J. Kim, S.H. Han, H.G. Kim, A.Y. Kim, J.S. Kim, C. Il Cheon, ? Multiferroic properties of Ti-doped BiFeO3 ceramics, J. Korean Phys. Soc. 56 (2010) 439–442. https://doi.org/10.3938/jkps.56.439.

[38] F. Azough, R. Freer, M. Thrall, R. Cernik, F. Tuna, D. Collison, Microstructure and properties of Co-, Ni-, Zn-, Nb- and W-modified multiferroic BiFeO3 ceramics, J. Eur. Ceram. Soc. (2010). https://doi.org/10.1016/j.jeurceramsoc.2009.09.016.

[39] D. Bensaid, N.-E. Benkhettou, A. Kourdassi, Structural and Electronic Properties of Bixo₃ (X = Mn, Fe, Cr), J. Mod. Phys. 02 (2011) 642–650. https://doi.org/10.4236/jmp.2011.27075.

[40] M. Ahart, M. Somayazulu, R.E. Cohen, P. Ganesh, P. Dera, H.K. Mao, R.J. Hemley, Y. Ren, P. Liermann, Z. Wu, Origin of morphotropic phase boundaries in ferroelectrics, Nature. 451 (2008) 545–548. https://doi.org/10.1038/nature06459.

[41] D. Kobor, M. Tine, A. Hajjaji, L. Lebrun, S. Pruvost, D. Guyomar, Comparative characterization of rhombohedral and tetragonal PZN-PT single crystals, AIP Adv. 1 (2011). https://doi.org/10.1063/1.3599587.

[42] D. Alikin, A. Turygin, A. Kholkin, V. Shur, Review ferroelectric domain structure and local piezoelectric properties of lead-free (K0.5Na0.5)NbO3 and BiFeO3-based piezoelectric ceramics, Materials (Basel). 10 (2017). https://doi.org/10.3390/ma10010047.

[43] A.J. Bell, T.P. Comyn, T.J. Stevenson, Expanding the application space for piezoelectric materials, APL Mater. 9 (2021). https://doi.org/10.1063/5.0035416.

[44] M.R. Suchomel, P.K. Davies, Enhanced tetragonality in (x)PbTiO 3-(1-x)Bi(Zn 1/2Ti 1/2)O 3 and related solid solution systems, Appl. Phys. Lett. 86 (2005) 1–3. https://doi.org/10.1063/1.1978980.

[45] T.E. Hooper, A.J. Bell, Landau-Devonshire derived phase diagram of the BiFeO3-PbTiO3 solid solution, J. Appl. Phys. 127 (2020). https://doi.org/10.1063/1.5144151.

[46] J. Luo, S. Zhang, Advances in the growth and characterization of relaxor-PT-based ferroelectric single crystals, Crystals. 4 (2014) 306–330. https://doi.org/10.3390/cryst4030306.

[47] J. Lv, X. Lou, J. Wu, Defect dipole-induced poling characteristics and ferroelectricity of quenched bismuth ferrite-based ceramics, J. Mater. Chem. C. 4 (2016) 6140–6151. https://doi.org/10.1039/c6tc01629d.

[48] M.H. Lee, D.J. Kim, H.I. Choi, M.H. Kim, T.K. Song, W.J. Kim, D. Do, Thermal Quenching Effects on the Ferroelectric and Piezoelectric Properties of BiFeO3-BaTiO3Ceramics, ACS Appl. Electron. Mater. 1 (2019) 1772–1780. https://doi.org/10.1021/acsaelm.9b00315.

[49] J. Zhang, R.X. Wang, L. Li, J.Y. Wu, Y.S. Cui, Z. Bin Gu, H. Zhang, M.W. Zhu, S.T. Zhang, B. Yang, Highly enhanced thermal stability in quenched Na0.5Bi0.5TiO3-based lead-free piezoceramics, J. Eur. Ceram. Soc. 39 (2019) 4705–4711. https://doi.org/10.1016/j.jeurceramsoc.2019.06.052.

[50] L.K. Venkataraman, Influence of quenching and subsequent annealing on the conductivity and electromechanical properties of Na1/2Bi1/2TiO3-BaTiO3, Materials (Basel). 14 (2021). https://doi.org/10.3390/ma14092149.

2

CONTROLLING THE OXYGEN DEFECTS CONCENTRATION IN A PURE $BiFeO_3$ BULK CERAMIC

ABSTRACT

$BiFeO_3$ is a multiferroic material with a perovskite structure which has a lot of potential for use in sensors and transducers. However, obtaining pure single-phase $BiFeO_3$ ceramic with a low electrical conductivity via solid state reactions remains a problem that limits its application. In this work, the suppression of secondary phases in $BiFeO_3$ was studied by varying the compositional parameters and the sintering temperature. The addition of 1% Bi_2O_3 to the stoichiometric precursors mixture prevented the formation of secondary phases observed when sintering stoichiometric precursors. The phase pure ceramic had a p-type conductivity and a 3 decades lower electrical conductivity as measured by impedance spectroscopy. Annealing of optimally synthesized material at different partial pressures of oxygen in an oxygen-nitrogen gas atmosphere showed that the reason for this type of conductivity lies in the high concentration of defects associated with oxygen. By annealing in various mixtures of nitrogen and oxygen, it is possible to control the concentration of these defects and hence the conductivity, which can go down another 2 decades. At a $pO_2 \leq 10$ % the conductivity is determined by intrinsic charge carriers in the material itself.

This chapter has been published in Materials 15, 19 (2022)

2.1 INTRODUCTION

Bismuth ferrite ($BiFeO_3$), and the solid solutions based on it, are promising multiferroic materials for use in sensors and transducers due to its high Curie temperature, T_C, of 825 °C[1]. In principle, this allows for the possibility of using it as a lead-free high-temperature piezoceramic [2]. Although bismuth ferrite was discovered already in the late 1950s, obtaining it in a single phase form remains a challenge due to the easy formation of the stable secondary phases of Sillenite ($Bi_{25}FeO_{39}$) and Mullite ($Bi_2Fe_4O_9$) [3]. The presence of these secondary phases leads to large electrical leakage currents, which imposes serious restrictions on its use in actual sensor applications. Due to the high coercive field required to pole this material, it is important to increase its insulating properties [4]. Therefore, before studying the electrical properties, it is necessary to obtain high-density ceramics as free from secondary phases as possible. In previous works, various methods of obtaining pure bismuth ferrite were used, such as solid-state synthesis [5,6], rapid liquid reaction [7], mechano-chemical activation [8], wet-chemical methods [9] as well as others. But the formation of secondary phases could not be avoided in any of them. To eliminate secondary phases present after synthesis, leaching in nitric acid [10] was proposed, which shows good results, but probably leads to uncontrolled changes in the composition of the material which will impact the defect chemistry. Given the versatility and cost-effectiveness in the synthesis of inorganic solid materials [11] and the recent developments of the method [12–15], in this work solid state sintering at different temperatures and using non-stoichiometric powder mixtures is employed to try and synthesize phase pure $BiFeO_3$.ceramic samples.

For pure and impure material alike the defect configuration of bismuth ferrite is very dependent on sample preparation [10], which of course affects the conductivity of the material. However, the nature of defects is mainly studied theoretically [16],[17],[18]. As shown in previous works the high temperature sintering of Bi-based systems can lead to the creation of oxygen vacancies by the release of electrons [19]. The increase in oxygen vacancies can also induce a change in the valence state of Fe^{3+}. If the released electrons bind with the Fe^{3+} ions in the system, a charge transformation from Fe^{3+} to Fe^{2+} will take place.

The oxygen defect nature and level are probably not only affected by the obvious sintering conditions but also by the annealing environment, in

particular the oxygen partial pressure, during high temperature processing. But no systematic studies of the oxygen partial pressure, pO_2, during high temperature processing on the electrical conductivity can be found in the literature; this may be due to the notorious difficulty of obtaining phase-pure bulk $BiFeO_3$ ceramics with low leakage currents and thermal instability of this phase at higher temperature which makes it difficult to reproduce the results due to changes in the sample during the annealing process. Furthermore, annealing samples at high temperatures under well-controlled oxygen levels is non-trivial and requires special equipment usually not available in most laboratories.

Electrical impedance spectroscopy is a useful approach to study the electrical properties of electroceramics including ferroelectrics [20]. The impedance data can be used to calculate the DC conductivity, to distinguish between long range polarization and charge carrier diffusion processes. Also, the impedance data can be presented in the form of an electrical modulus, which gives more information about the short-range polarization processes in the material. The electrical modulus can give an insight into the dielectric processes occurring inside the material [21]. The low frequency side of the peak in electrical modulus represents the range of frequencies in which the charge carriers can move over a long distance (charge carriers can perform successful hopping from one site to the neighbouring site). The high frequency side of the electric modulus represents the range of frequencies in which the charge carriers are spatially confined to their potential wells, and thus can only make localized motions inside the well. The frequency at which the peak occurs is an indication of the transition from long-range to short-range conduction. Asymmetrical behavior of the electrical modulus peak demonstrates non-Debye-type relaxation phenomena which are in good agreement with the observations from the conductivity spectrum. An increase in the frequency of the peak is consistent with an increasing activation energy of conductivity representing long-range movement. Although the impedance spectra or electrical modulus do not uniquely specify the nature of the observed polarization and conductivity phenomena, it is possible to obtain the correlation between of certain types of defects and conductivity or polarization by comparing differently processed or annealed samples and infer the mechanism.

The present work is devoted to optimization of making pure $BiFeO_3$ ceramics by classic solid-state reaction for subsequent investigations of the defect chemistry. The effect of the calcination temperature on phase formation is studied. Furthermore, the influence of excess Bi_2O_3 addition is investigated. Impedance spectroscopy on the as-made ceramics is performed to investigate the influence of phase purity on the electrical properties. Furthermore, to vary and control the concentration of oxygen related defects, optimally sintered samples were annealed in nitrogen-oxygen gas mixtures with different oxygen concentrations during heating, holding at 750 °C and subsequent cooling to room temperature. The oxygen concentration was maintained throughout the entire experiment.

2.2 EXPERIMENTAL PROCEDURE

$BiFeO_3$ samples with and without 1 mol% excess Bi_2O_3 were prepared by a solid-state reaction from pre-milled Bi_2O_3 and Fe_2O_3 powder in the appropriate ratios. Milling was performed using 2 mm Y_2O_3-stabilized ZrO_2 balls in hexane using a Retsch PM100 planetary ball mill. The powders were dried and calcined at a range of temperatures between 700 and 825 °C in air for 1 h with a heating rate of 600 °C/h. The reacted powder with an average particle size of 1 µm was ground again and cold pressed into pellets using an uniaxial press. After that, the samples were sintered at temperatures between 750 °C to 850 °C in air for 1 h at a heating rate of 600 °C/h. (see **Figure 2.S1** of the Supporting Information for an photograph of a typical sample). The block diagram of the sintering experiments is shown in **Figure 2.S2** of the Supporting Information section.

Optimally sintered samples (1% excess Bi_2O_3 and sintered at 750 °C) were then annealed in a quartz tube furnace at 750 °C for 1h in a mixture of pure nitrogen and oxygen gases with different oxygen fraction (100%, 20%, 10%, 1%). The flows were controlled by Bronkhorst Nederland mass flow controllers of type F-201CV-20-RAD-22-V. The N_2 and O_2 were supplied by Linde, the Netherlands, and were of quality 5N. Nitrogen was filtered for hydrocarbons, water and oxygen. Oxygen was filtered for hydrocarbons and water. The filters were supplied by Messer Griesheim, Germany. The flows for the different annealing were as follows:

O_2 (%)	N_2 flow (ml/min)	O_2 flow (ml/min)	Total flow (ml/min)
1	2970	30	3000
10	225	25	250
20	200	50	250
100	0	250	250

In order to achieve 1% oxygen concentration in the gaseous atmosphere in the quartz tube furnace, the nitrogen gas flow had to be increased to 2970 ml/min, because the lowest controlled setting for the oxygen mass flow controllers was 20 ml/min. The other experiments were carried out at a lower total gas flow in order to reduce gas consumption. The gas conditions were maintained during heating, holding and cooling. The block diagram for the annealing environment experiments is given in **Figure 2.S3** in the Supporting Information section.

Phase purity of the crushed $BiFeO_3$ samples was analysed by X-ray diffraction analysis using a Rigaku Miniflex 600 tabletop diffractometer and Cu Kα radiation at room temperature. The density was determined by the Archimedes' method in water. The microstructures of sintered ceramics were investigated using scanning electron microscopy (SEM), using a Jeol JSM-7500F field emission scanning electron microscope. For electrical measurements, gold electrodes were deposited on the ceramics by DC sputtering using a Quorum Q300T sputter coater. Electrical measurements were performed with a Novocontrol Alpha Dielectric Analyser in the frequency range from 1 Hz to 10 MHz at temperature from 25 to 200 °C. This temperature range was chosen such that a sufficiently wide temperature window is available to determine activation energies, but the upper temperature is low enough not to change the defect concentration during the electrical measurements. The complete reversibility was verified by measuring the conductivity during a complete heating up and cooling down cycle.

The DC conductance was calculated by fitting the low-frequency conduction region using Jonscher's power law[22]:

$$\sigma = \sigma_{DC} + A\omega^n \qquad (2.1)$$

where σ – total conductivity, σ_{DC} – the direct current conductivity of the sample, $A\omega^n$ – pure dispersive component of AC conductivity having a characteristic of

power law in terms of angular frequency ω and exponent n, and *A* is a constant which determines the strength of polarizability. All measurements were conducted in air.

2.3 RESULTS AND DISCUSSION

Figure 2.1 shows the X-ray diffraction patterns of $BiFeO_3$ ceramics using stoichiometric starting powder calcined at different temperatures. In all samples, the major phase is the perovskite bismuth ferrite, but all samples contain substantial concentrations of the two secondary phases: one rich in bismuth – $Bi_{25}FeO_{39}$ and one iron rich – $Bi_2Fe_4O_9$. By comparing the intensity of the most intense peaks of the secondary phases with the major peak of the bismuth ferrite (110) (**Figure 2.2**) the amount of each secondary phase present in each sample could be estimated. The peaks of $Bi_{25}FeO_{39}$ decrease with increasing synthesis temperature, while the peaks of $Bi_2Fe_4O_9$ increase. This may be due to the loss of bismuth during the synthesis. The lowest concentration for both secondary phases was obtained for the sample calcined at 750 °C.

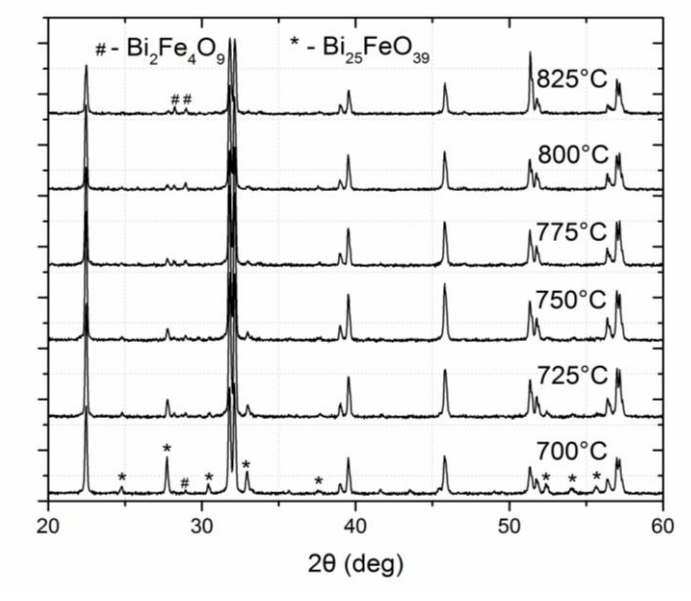

Figure 2.1 – X-ray diffraction patterns of bismuth ferrite synthesized at different temperatures using stoichiometric starting material.

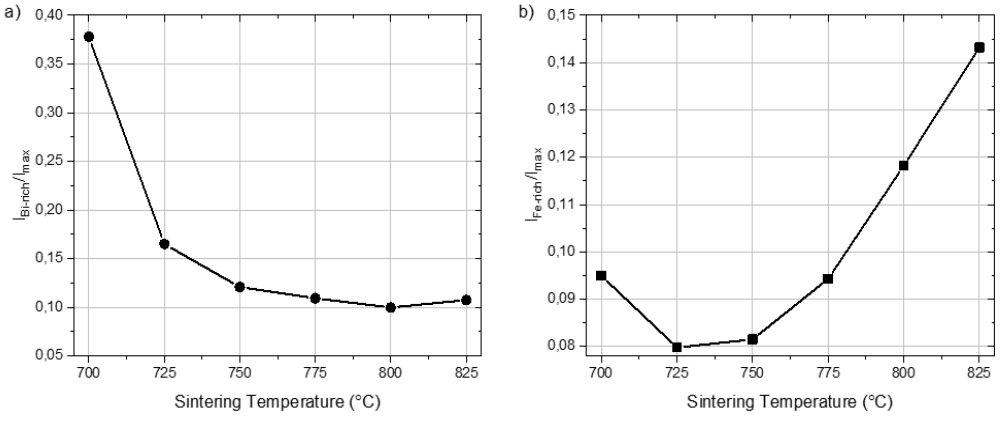

Figure 2.2 – Comparison of intensities of secondary phases with the major peaks of bismuth ferrite for sample produced with a stoichiometric precursor (a – $Bi_{25}FeO_{39}$, b – $Bi_2Fe_4O_9$).

Figure 2.3 shows the relative density and the SEM micrographs of the fracture surfaces of the samples prepared by for stoichiometric precursors. For each temperature 10 samples were prepared. SEM micrographs clearly show an increase in grain size with increasing sintering temperature. At temperatures above 825 °C, the morphology of the samples is radically different, which is due to the proximity to the melting point of $Bi_{25}FeO_{39}$ [1]. When sintering at temperatures of 825 and 850 °C, two separate microstructures can be observed to coexist: square cuboid particles and smooth shapeless crystallites. The shapeless crystallites can be attributed to bismuth ferrite and the bismuth-rich phase. The square cubic crystallites are likely to be an iron-rich phase that has a high melting point [23]. A maximum average density of 95% has been observed for the samples sintered at 775 °C.

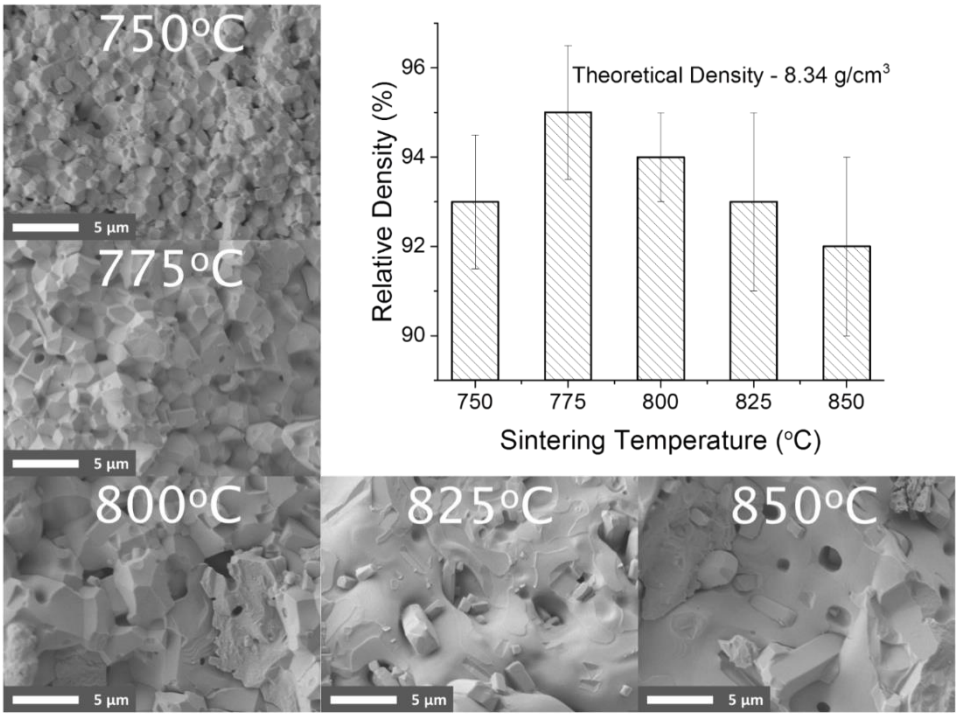

Figure 2.3 – SEM micrographs of structure and density values for ceramics sintered from stoichiometric precursors at different temperatures.

Clearly, bismuth ferrite obtained from stoichiometric precursors contains a high amount of secondary phases. Therefore, 1% excess of bismuth oxide was added to the precursors to compensate for the loss of Bi which might occur during the sintering process to increase the phase purity of bismuth ferrite. The XRD pattern of the sample calcined and sintered from the stoichiometric precursors (**Figure 2.4a**) shows both secondary phases $Bi_{25}FeO_{39}$ and $Bi_2Fe_4O_9$. But in the XRD pattern of the sample with excess bismuth (**Figure 2.4b**) these secondary phases and their diffraction peaks are not detectable at the level of background noise.

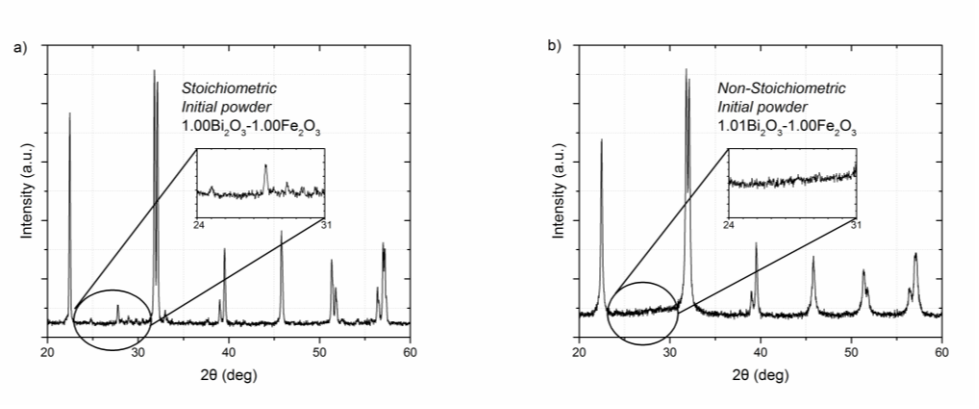

Figure 2.4 – X-ray diffraction analysis of samples prepared with and without the addition of extra bismuth. (*a - Equal amounts of iron and bismuth in the precursor; b – 1 mol% extra bismuth oxide added to precursor*).

Figure 2.5 shows the results of impedance data for different temperatures for the stoichiometric and Bi-enriched samples that correspond to the XRD patterns shown in Fig. 4. From these spectra, two processes which contribute to electrical conductivity are noticeable. While the nature of these processes is still under discussion, there is a noticeable decrease in the conductivity of the phase pure sample when compared to the sample that contains secondary phases. This may be associated with a decrease in the concentration of bismuth and oxygen vacancies with the addition of extra bismuth, or the absence of easy conductivity path via the secondary phases.

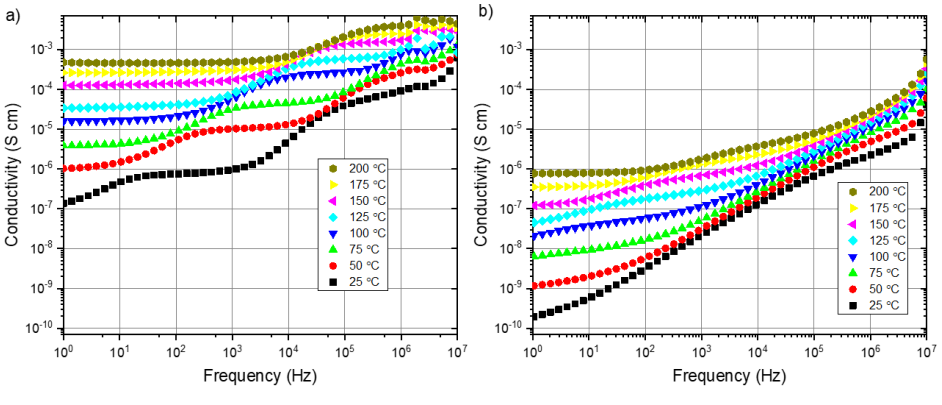

Figure 2.5 – AC Conductivity measurements (a – from stoichiometric precursor $BiFeO_3$, b – from 1% Bi_2O_3 enriched precursor $BiFeO_3$).

In **Figure 2.6** the Arrhenius plot is given for the DC conductivity using samples prepared from the stoichiometric and non-stoichiometric precursors. The DC conductivity in the phase pure sample synthesized from the non-stoichiometric precursor is significantly lower than the conductivity of the samples containing secondary phases. It is clearly visible from Fig. 6 that for both materials the conductivity is a thermally activated process with a similar activation energy of about 0.25 eV. This strongly suggests that the conductivity mechanism for both samples is of the same nature.

Investigation of the effect defect concentration on electrical conductivity was performed by annealing pure $BiFeO_3$ ceramic samples in gasses with different oxygen content. As shown in **Figure 2.6a**, a decrease in conductivity with decreasing oxygen concentration in the gas environment during annealing can be observed, which is not surprising for a material demonstrating p-type conductivity. It should be noted that the conductivity decreases very rapidly with a relatively small decrease in oxygen in the gas mixture. The activation energy of that conduction mechanism increases with a decrease of oxygen pressure leading to much higher values than for the as-sintered samples.

The oxygen vacancies involved in conduction mechanism may be associated with the volatility of Bi_2O_3:

$$2Bi_{Bi}^{X} + 3O_{O}^{X} \rightarrow 2V'''_{Bi} + 3V_{O}^{\cdot\cdot} + Bi_2O_3 \qquad (2.2)$$

where Bi_{Bi}^{X} – Bi position occupied by Bi, O_{O}^{X} – O position occupied by O, V'''_{Bi} – bismuth vacancy, $V_{O}^{\cdot\cdot}$ – oxygen vacancy. The hole concentration was controlled by annealing and can be described by the following reaction:

$$2V_{O}^{\cdot\cdot} + O_2 \rightarrow 2O_{O}^{X} + 4h^{\cdot} \qquad (2.3)$$

where $h^{\cdot}$ – electron hole and $e^{'}$ – free electron. As the oxygen concentration in the atmosphere decreases, the balance shifts to the left, reducing the concentration of free charge carriers, and as a result, the overall conductivity. This behaviour is confirmed in the experiments, confirming the p-type conductivity in the material. Hole conduction behaviour in $BiFeO_3$-based ceramics was previously attributed to oxidation of Fe^{3+} to Fe^{4+} [24]. However, excess Bi_2O_3 was introduced in the starting materials of BFO to suppress its volatility during processing. The Bi non-stoichiometry can further lead to significant change of conduction behaviour. As a result, the oxygen loss can be compensated by electrons:

$$2O_O^X \rightarrow 2V_O^{\cdot\cdot} + O_2 + 4e^{'} \quad (2.4)$$

leading to an n-type conductivity which is not observed here.

As shown in **Figure 2.6a** samples that were annealed at different partial oxygen pressures show two trends in conductivity (from RT till around 100 °C and from 100 °C to 200 °C). This can be explained by the fact that the concentration of carriers generated by impurities is much higher than that of thermally generated intrinsic carriers at temperatures below 100 °C, and the effect of mobility reduction caused by electron-phonon collisions is small. The concentration of charge carriers generated from impurities weakly depends on temperature, and the slope can be explained by the change in their mobility during heating, and therefore the electronic conductivity decreases slightly when cooled due to the low mobility of these charges. Samples not having received this post-synthesis annealing treatment do not show this dual conduction behaviour, most likely due to the very high concentration of charge carrier impurities. The activation energy of conduction increases for annealed samples due to a decrease in the concentration defects or compensation of free charge carriers.

Figure 2.6b shows the pO_2 dependence of DC conductivity for the phase pure BFO. As can be seen, for the region pO_2 greater than 0.1 atm, the total conductivity exhibits a positive slope when plotted against the oxygen concentration, which reflects the hole contribution. For low oxygen concentrations the conductivity becomes independent of the oxygen concentration, which indicates an increased contribution of the ion conduction [24].

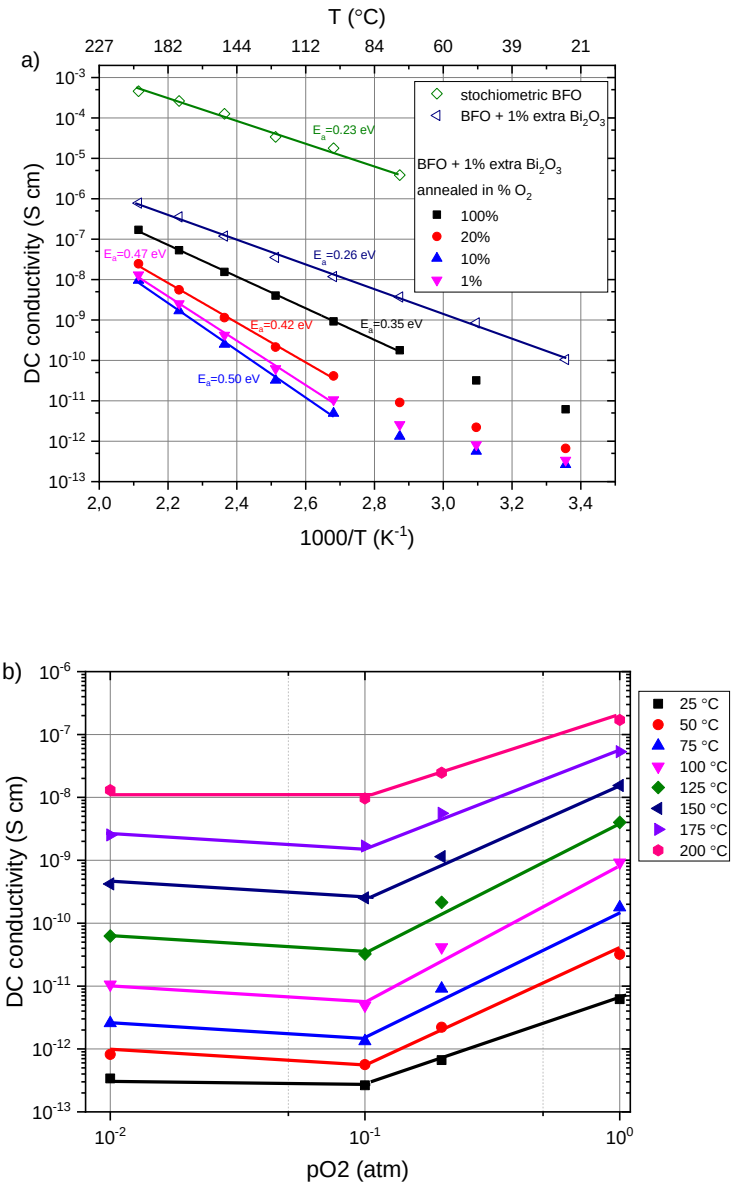

Figure 2.6 – Conductivity of BFO samples prepared and annealed in different atmospheres: a) Arrhenius plot of DC conductivity as a function of inverse temperature for reheated samples after annealing and linear cooling from 750°C and b) DC conductivity measured in air over the temperature range from 25 till 200 °C for samples synthesized from non-stoichiometric precursors for various oxygen partial pressures during high temperature processing.

A comparison of the impedance with the electric modulus data allows the determination of the bulk response in terms of localized or non-localized conduction [16]. In **Figure 2.7a**, the imaginary part of electrical modulus and imaginary part of impedance as a function of frequency at 200 °C are shown. The overlap of the peak positions of the M" and Z" curves is evidence of delocalized or long-range relaxation [16]. However, for the present the peaks do not overlap perfectly but are very close, suggesting that conduction contains components from both long-range and localized relaxations. **Figure 2.7b** shows the electrical modulus and impedance peak frequency as a function of pO_2 at a fixed measurement temperature 200 °C. As can be seen, the frequency shift for the electrical modulus and impedance does not change with a change in the oxygen concentration, which can serve as an indirect confirmation of the assumption that oxygen related defects dominate the conductivity of the obtained samples and the contribution of other conductivity mechanisms is small. In other studies, this is presented as evidence of a long-range conductivity range for free oxygen vacancies [25,26]. The dependence of the maximum frequency of the peaks of the electric modulus and impedance on pO_2 is in complete agreement with the inferred dependence of the conductivity on defects and the actual lattice.

As stated earlier, measurements were made at temperatures below 200 °C to ensure that the defect population remains the same and only reflects the state resulting from the annealing condition (annealing at a temperature of 750 °C followed by linear cooling under controlled oxygen partial pressure). Given that thermal cycling in air up to a temperature of 200 °C does not change the conductivity, we indirectly established that the defect state in the samples was established at a temperature between 750 °C and 200 °C. Our experiments were not set up to properly establish the exact conditions at which the defect state reached its 'frozen' state, nor could it be establish whether the 'frozen' state was determined by thermodynamics or kinetics. The frozen state obtained at a partial oxygen pressure below 0.1 atm shows a purely ionic nature, which shows us that the generation of oxygen vacancies defects has reached saturation point with the concentration of charge carriers remaining the same. This fully confirms our assumption that the nature of the high conductivity is associated with oxygen vacancies.

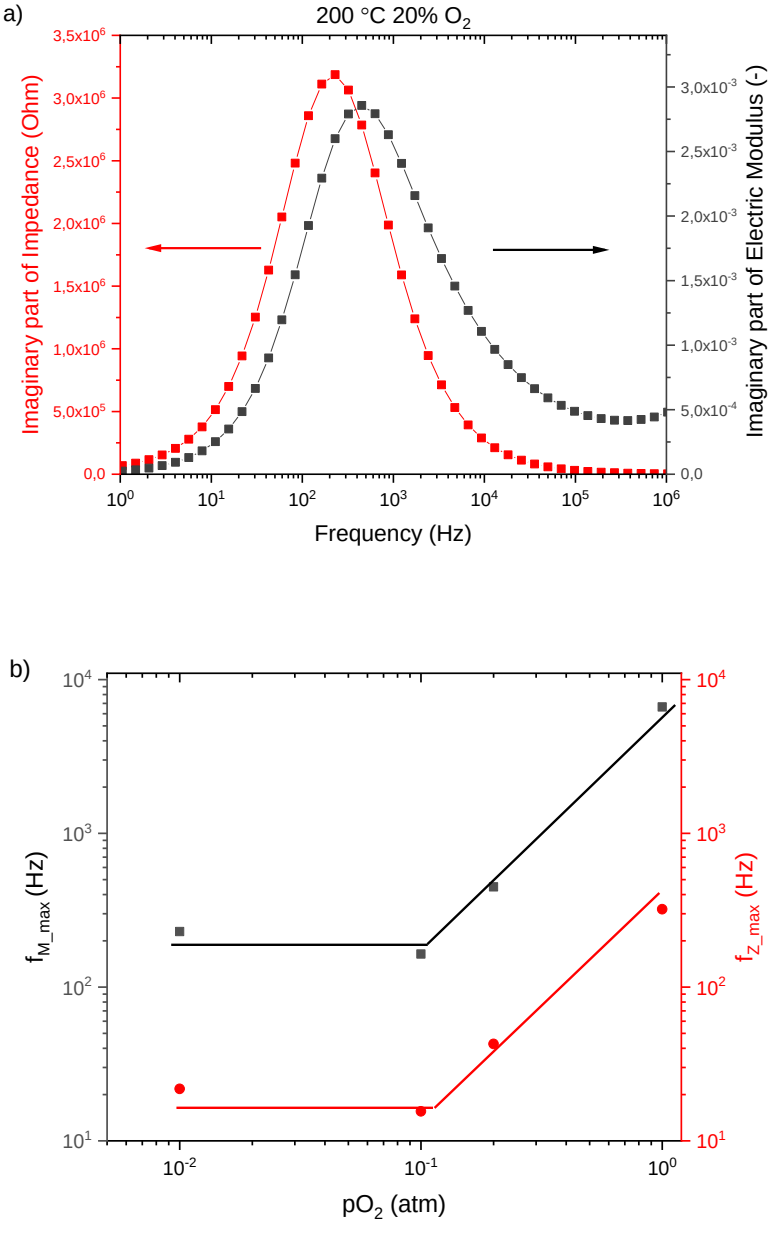

Figure 2.7 – Results of impedance spectroscopy analysis for data measured at 200 °C: a) impedance and electric modulus spectroscopic plots for samples annealed in 20% O_2; b) electrical modulus peak and impedance peak frequency as a function of pO_2

2.4 CONCLUSIONS

Pure $BiFeO_3$ with a relatively low electrical conductivity can be obtained by conventional solid-state sintering at 750 ^{0}C starting from a non-stoichiometric composition of precursors. Adding 1% excess of Bi_2O_3 compensates for the loss of bismuth during synthesis and sintering. The absence of secondary phases resulted in a reduction of the electrical conductivity by more a factor 1000. Annealing pure $BiFeO_3$ in mixtures of nitrogen and oxygen gases at various oxygen partial pressures reduced the conductivity further. Hence control of the oxygen partial pressure in the atmosphere during high temperature processing is a novel tool to manipulate the oxygen-related defects, which play a major role in the conductivity of $BiFeO_3$. In case the oxygen concentration in the gaseous environment is below 10% the conductivity seems to be determined by other intrinsic charge carriers.

2.5 SUPPORTING INFORMATION

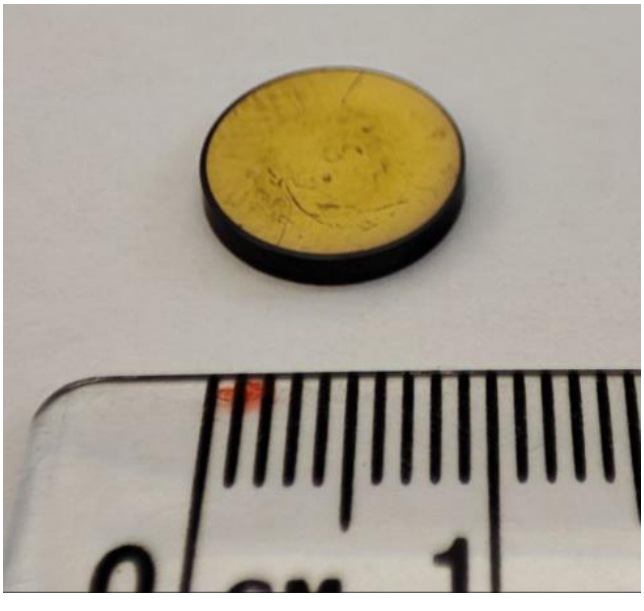

Figure 2.S1 – Photo of the sample after electrical measurement with gold electrodes

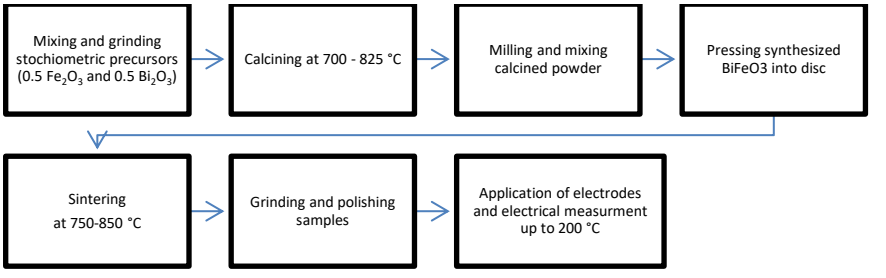

Figure 2.S2 – Block diagram of the synthesis and sintering of $BiFeO_3$ and its subsequent analysis to optimize the preparation process

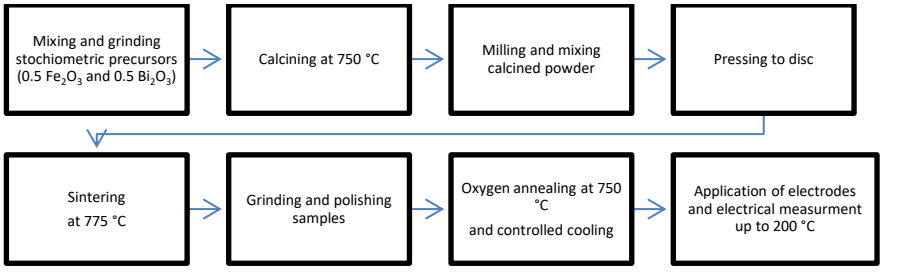

Figure 2.S3 – Block diagram of the synthesis and sintering of bismuth ferrite and subsequent annealing, to study the effect of oxygen defects on conductivity

REFERENCES:

[1] R. Palai, R.S. Katiyar, H. Schmid, P. Tissot, S.J. Clark, J. Robertson, S.A.T. Redfern, G. Catalan, J.F. Scott, β phase and γ-β metal-insulator transition in multiferroic BiFeO3, Phys. Rev. B - Condens. Matter Mater. Phys. 77 (2008) 1–11. https://doi.org/10.1103/PhysRevB.77.014110.

[2] T. Stevenson, D.G. Martin, P.I. Cowin, A. Blumfield, A.J. Bell, T.P. Comyn, P.M. Weaver, Piezoelectric materials for high temperature transducers and actuators, J. Mater. Sci. Mater. Electron. 26 (2015) 9256–9267. https://doi.org/10.1007/s10854-015-3629-4.

[3] T. Rojac, A. Bencan, B. Malic, G. Tutuncu, J.L. Jones, J.E. Daniels, D. Damjanovic, BiFeO3 ceramics: Processing, electrical, and electromechanical properties, J. Am. Ceram. Soc. 97 (2014) 1993–2011. https://doi.org/10.1111/jace.12982.

[4] J. Wu, Z. Fan, D. Xiao, J. Zhu, J. Wang, Multiferroic bismuth ferrite-based materials for multifunctional applications: Ceramic bulks, thin films and nanostructures, Prog. Mater. Sci. 84 (2016) 335–402. https://doi.org/10.1016/j.pmatsci.2016.09.001.

[5] H. Han, J.H. Lee, H.M. Jang, Low-Temperature Solid-State Synthesis of High-Purity BiFeO3 Ceramic for Ferroic Thin-Film Deposition, Inorg. Chem. 56 (2017). https://doi.org/10.1021/acs.inorgchem.7b01893.

[6] Y. Yao, B. Ploss, C.L. Mak, K.H. Wong, Pyroelectric properties of BiFeO3ceramics prepared by a modified solid-state-reaction method, Appl. Phys. A Mater. Sci. Process. 99 (2010) 211–216. https://doi.org/10.1007/s00339-009-5499-1.

[7] Y.P. Wang, L. Zhou, M.F. Zhang, X.Y. Chen, J.-M. Liu, Z.G. Liu, Room-temperature saturated ferroelectric polarization in BiFeO3 ceramics synthesized by rapid liquid phase sintering, Appl. Phys. Lett. 84 (2004) 1731–1733. https://doi.org/10.1063/1.1667612.

[8] D. Maurya, H. Thota, K.S. Nalwa, A. Garg, BiFeO3 ceramics synthesized by mechanical activation assisted versus conventional solid-state-reaction process: A comparative study, J. Alloys Compd. 477 (2009) 780–784. https://doi.org/10.1016/j.jallcom.2008.10.155.

[9] J. Silva, A. Reyes, H. Esparza, H. Camacho, L. Fuentes, BiFeO3: A review on synthesis, doping and crystal structure, Integr. Ferroelectr. 126 (2011) 47–59. https://doi.org/10.1080/10584587.2011.574986.

[10] H.M. Hashem, M.H. Hamed, Preparation parameters optimization and structure investigation of multiferroic bismuth ferrite, Mater. Chem. Phys. 211 (2018) 445–451. https://doi.org/10.1016/j.matchemphys.2018.03.012.

[11] A. Kumar, S. Dutta, S. Kwon, T. Kwon, S.S. Patil, N. Kumari, S. Jeevanandham, I.S. Lee, Solid-State Reaction Synthesis of Nanoscale Materials: Strategies and Applications, Chem. Rev. (2022). https://doi.org/10.1021/acs.chemrev.1c00637.

[12] A. Qasem, P. Xiong, Z. Ma, M. Peng, Z. Yang, Recent Advances in Mechanoluminescence of Doped Zinc Sulfides, Laser Photonics Rev. 15 (2021) 1–20. https://doi.org/10.1002/lpor.202100276.

[13] S. Zhao, Q. Mo, B. Wang, W. Cai, R. Li, Z. Zang, Inorganic halide perovskites for lighting and visible light communication, Photonics Res. 10 (2022) 1039. https://doi.org/10.1364/prj.450483.

[14] L. Yuan, Y. Jin, Y. Su, H. Wu, Y. Hu, S. Yang, Optically Stimulated Luminescence Phosphors: Principles, Applications, and Prospects, Laser Photonics Rev. 14 (2020) 1–34. https://doi.org/10.1002/lpor.202000123.

[15] H.C. Thong, Z. Li, J.T. Lu, C.B.W. Li, Y.X. Liu, Q. Sun, Z. Fu, Y. Wei, K. Wang, Domain Engineering in Bulk Ferroelectric Ceramics via Mesoscopic Chemical Inhomogeneity, Adv. Sci. 2200998 (2022) 1–9. https://doi.org/10.1002/advs.202200998.

[16] P. Baettig, C. Ederer, N.A. Spaldin, First principles study of the multiferroics BiFeO3, Bi2FeCrO6, and BiCrO3: Structure, polarization, and magnetic ordering temperature, Phys. Rev. B. 72 (2005) 214105. https://doi.org/10.1103/PhysRevB.72.214105.

[17] S.J. Clark, J. Robertson, Energy levels of oxygen vacancies in BiFeO3by screened exchange, Appl. Phys. Lett. 94 (2009). https://doi.org/10.1063/1.3070532.

[18] T.R. Paudel, S.S. Jaswal, E.Y. Tsymbal, Intrinsic defects in multiferroic BiFeO 3 and their effect on magnetism, Phys. Rev. B - Condens. Matter Mater. Phys. 85 (2012). https://doi.org/10.1103/PhysRevB.85.104409.

[19] C. Ang, Z. Yu, L. Cross, Oxygen-vacancy-related low-frequency dielectric relaxation and electrical conduction, Phys. Rev. B - Condens. Matter Mater. Phys. 62 (2000) 228–236. https://doi.org/10.1103/PhysRevB.62.228.

[20] J. Kolte, P.H. Salame, A.S. Daryapurkar, P. Gopalan, Impedance and AC conductivity study of nano crystalline, fine grained multiferroic bismuth ferrite (BiFeO3), synthesized by microwave sintering, AIP Adv. 5 (2015). https://doi.org/10.1063/1.4931818.

[21] X. Zhao, R. Liao, N. Liang, L. Yang, J. Li, J. Li, Role of defects in determining the electrical properties of ZnO ceramics, J. Appl. Phys. 116 (2014). https://doi.org/10.1063/1.4886416.

[22] A.K. Jonscher, The 'universal' dielectric response - review article, Nature. 267 (1997) 673–679. https://doi.org/10.1007/978-0-387-29185-7_10.

[23] T. Rojac, M. Kosec, B. Budic, N. Setter, D. Damjanovic, Strong ferroelectric domain-wall pinning in BiFeO3 ceramics, J. Appl. Phys. 108 (2010). https://doi.org/10.1063/1.3490249.

[24] N. Masó, A.R. West, Electrical properties of Ca-doped BiFeO 3 ceramics: From p-type semiconduction to oxide-ion conduction, Chem. Mater. 24 (2012) 2127–2132. https://doi.org/10.1021/cm300683e.

[25] V. Sharma, R. Kaur, M. Singh, R. Selvamani, S.M. Gupta, V.S. Tiwari, A.K. Karnal, A. Singh, Conductivity relaxation and oxygen vacancies-related electron hopping mechanism in $Pb_{1-x}La_{x/2}Sm_{x/2}Ti_{1-x}Fe_xO_3$ solid solutions, J. Asian Ceram. Soc. 6 (2018) 222–231. https://doi.org/10.1080/21870764.2018.1489941.

[26] P. Gupta, P.K. Mahapatra, R.N.P. Choudhary, T. Acharya, Structural, dielectric, impedance, and modulus spectroscopy of La3TiVO9 ceramic, Phys. Lett. Sect. A Gen. At. Solid State Phys. 384 (2020) 126827. https://doi.org/10.1016/j.physleta.2020.126827.

3

ESTIMATING THE TRUE PIEZOELECTRIC PROPERTIES OF $BiFeO_3$ FROM MEASUREMENTS ON $BiFeO_3$-PVDF TERPOLYMER COMPOSITES

ABSTRACT

$BiFeO_3$ is an interesting multiferroic material with potential use in sensors and transducers. However, the high coercive field and low dielectric strength of this material make the poling process extremely difficult. Poling becomes a lot easier if the ceramic particles are incorporated in a non-conductive polymer with comparable dielectric properties. In this work, unstructured composites consisting of $BiFeO_3$ particles in a non-piezoactive PVDF terpolymer matrix are made with a ceramic volume fraction ranging from 20 to 60 %. The highest piezoelectric charge and voltage constant values (d_{33} = 31 pC/N and g_{33} =47 mV·m/N) are obtained for a $BiFeO_3$-PVDF terpolymer composite with a volume fraction of 60 %. The Poon model is chosen to analyse the volume fraction dependence of the dielectric constant while the modified Yamada model is used to analyse the piezoelectric charge constant data. It is concluded that the maximum possible piezoelectric constant for bulk $BiFeO_3$ can be as high as 56 pC/N.

This chapter has been published in Journal of Journal of Alloys and Compounds 868: 159186 (2021)

3.1 INTRODUCTION

$BiFeO_3$, also called Bismuth Ferrite or BFO, like many piezoelectrics, crystallises with a distorted rhombohedral perovskite-type structure and was first discovered in the late 1950s by Royen and Swars [1]. However, interest in this material only rose in the early 2000s due to the high Curie temperature (~825 °C [2]) and the high spontaneous polarization: 50–60 μC/cm² in thin films [3], ~100 μC/cm² in single crystals along the $[111]_{pc}$ direction [4] and 45 μC/cm² in bulk ceramics [5]. But studies on the piezoelectric properties of bulk ceramics of $BiFeO_3$ never yielded the high values reported for the thin films (120 pm/V [6])and its true potential was never demonstrated. This is largely due to the problems of electrical leakage and phase purity, which created difficulties in realising the potential maximal properties of bulk $BiFeO_3$. The presence of secondary phases in $BiFeO_3$ leads to large electrical leakage currents, which impose serious restrictions on its industrial use. Furthermore, large leakage currents become increasingly prohibitive at high fields. Thus, due to the high coercive field required to pole $BiFeO_3$, it is important to increase its insulating properties to reduce the leakage currents [7].

One way to prevent leakage and short circuiting is to incorporate $BiFeO_3$ particles into a non-conductive matrix, such as another ceramic [8,9] or a polymer [10–13]. The dielectric properties of different composite films of $BiFeO_3$-PVDF (with $BiFeO_3$ concentrations ranging from 13 to 34 vol%) were found to increase with increasing filler content [14]. Composites of one-dimensional (1D) multiferroic $BiFeO_3$ and poly(vinylidene fluoride-trifluoroethylene) (P(VDF-TrFE)) composites showed coexistence of electric and magnetic hysteresis for the composite materials at room temperature [15].

While the intrinsic piezoelectric properties of granular $BiFeO_3$ can in principle be derived from the volume fraction dependence of the piezoelectric properties of $BiFeO_3$-polymer composites, the analysis is only valid if the dielectric constants of the polymer and the piezoceramic are almost equal. Since $BiFeO_3$ ceramics have a relatively low value for the dielectric constant in comparison to other piezoelectric ceramics, this opens up possibilities for selecting a polymer matrix with a comparable dielectric permittivity. Hence in this work a relaxor polymer, polyvinylidene difluoride with tri-fluoroethylene and chlorofluoroethylene copolymers (P(VDF-TrFE-CFE), or in-short a PVDF terpolymer), with a high dielectric constant and without any piezoelectric

properties itself (even cast film 150 μm thick polarized at 350 kV/cm field for 20 minutes showed no piezoelectric response), is chosen as the matrix material. To minimize the contribution of particle-to-particle connectivity to the properties the work focusses on so-called 0-3 composites where the particles are homogeneously dispersed in the polymer matrix with minimal particle-particle contact. The volumetric dependence of the dielectric and the piezoelectric properties of the composites is then analysed in detail to determine an accurate estimate of the intrinsic piezoelectric properties of $BiFeO_3$ in granular form.

3.2 EXPERIMENTAL PROCEDURE

3.2.1 Composite manufacturing

Based on extensive synthesis trials single phase $BiFeO_3$ powder was obtained by solid state synthesis from pre-milled Bi_2O_3 and Fe_2O_3 in equal proportions with 1 at% excess Bi, as described previously [16]. This mixture of oxides was calcined at 750 °C for 1 h. The agglomerated powder was then dry milled using 2 mm yttria stabilized zirconia balls for 5 h by using a planetary ball mill. The particle size distributions of the milled powder in an aqueous solution as measured by a laser diffraction analyser were found to be d(10) = 0.67 μm, d(50) = 1.44 μm, and d(90) = 2.83 μm (d(X) signifies the point in the size distribution, up to and including which X% of the total volume of material in the sample is 'contained'. Therefore, d(50) is the size below which 50 % of the particles lie in the distribution). The powder was dried in a circulating air oven at 220 °C for 24 h prior to the experiment to avoid moisture adsorption. Phase purity of the powders was checked by X-ray diffraction analysis using a Rigaku miniflex600 tabletop diffractometer and Cu Kα radiation.

To produce the $BiFeO_3$ – polymer composites, solutions of polyvinylidene difluoride with tri-fluoroethylene and chlorofluoroethylene copolymers (P(VDF-TrFE-CFE)) (obtained from Piezotech Arkema) in dimethylformamide (DMF) were prepared. For low volume fractions of filler particles (< 30 vol%) a solution of 20 wt% P(VDF-TrFE-CFE) in DMF was used while for higher volume fractions a 13 wt% solution was used. The $BiFeO_3$ particles were mixed into this solution using a Hauschild DAC 150 FVZ planetary speed mixer at 750 rpm for 5 minutes. The mixture formed a viscous liquid that was degassed before casting on a glass substrate for the preparation of the thin films. Cast

composites were dried in a vacuum oven at 60 °C for 1 hour before annealing at 100°C for 1 hour. The final thickness of the dried samples varied between 120 and 160 µm. Once annealing was completed, a number of discs (12 mm diameter) were cut from the composite for electrical testing. Finally, gold electrodes of 10.9 mm diameter were deposited on both sides of the composite samples with a magnetron sputtering apparatus (Balzers Union, SCD 040).

3.2.2 Measurement procedures

Scanning Electron Microscope (SEM) images were taken using a Jeol JSM-7500F field emission scanning electron microscope. Prior to SEM measurements a thin (15 nm) layer of gold was deposited on the sample. In order to examine the cross sections of the composites they were first frozen in liquid N_2 to obtain a brittle fracture mode.

Electrical measurements were performed using a Novocontrol Alpha Dielectric Analyzer in the frequency range from 1 Hz to 10 MHz at temperatures from -50 to 120 °C at a fixed potential difference of 1 V. The piezoelectric constant, d_{33}, measurements were performed with a high precision PM300 Piezometer from Piezotest Piezosystems, at 110 Hz and a static and dynamic force of 10 and 0.25 N respectively. At least 4 samples of each composite were tested. Inter-sample variability was found to be modest (±0.5 pC/N).

3.3 RESULT AND DISCUSSION

3.3.1 Phase purity of $BiFeO_3$

Figure 3.1 shows the Rietveld refined XRD patterns of the $BiFeO_3$ ceramic powder. The material crystallises in a rhombohedral perovskite structure type with space group R3c. The refined unit cell parameters of a = 5.57564(7) Å and c = 13.8626(2), are in good agreement with the values reported in the literature [17]. The sample also contains minor amounts of the bismuth-rich phase, $Bi_{25}FeO_{39}$ (0.9 wt%), and the iron-rich phase ,$Bi_2Fe_4O_9$ (1.4 wt%) (for more details see **Figure 3.1S**), which are formed due to the addition of extra bismuth and evaporation of bismuth oxide during the calcination process as indicated in the previous work [16].

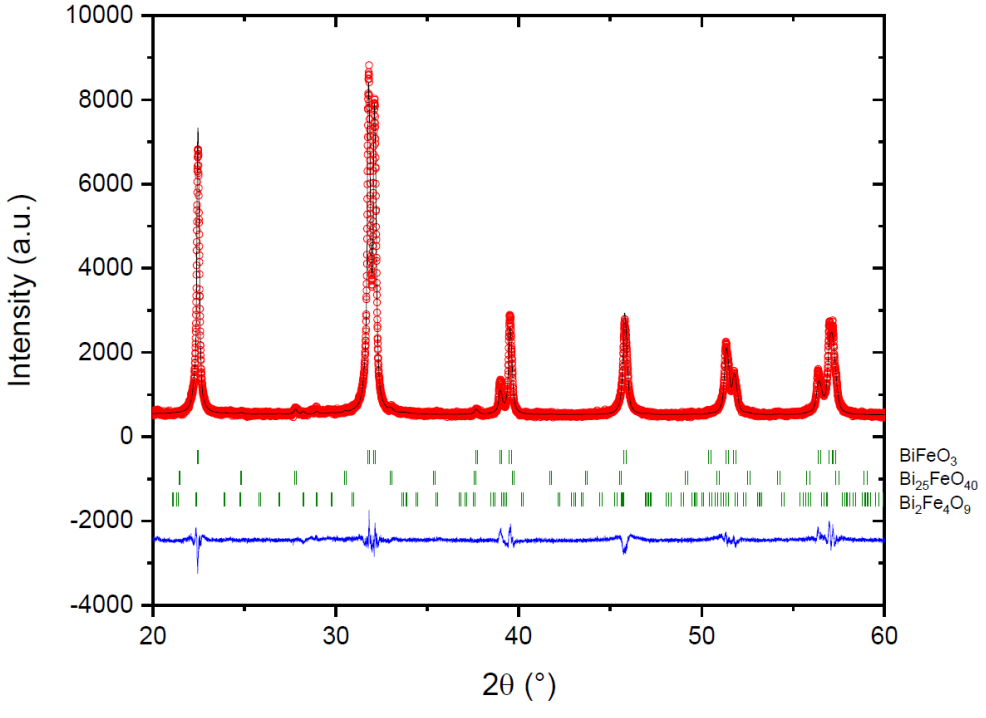

Figure 3.1 – Rietveld refined XRD patterns of the calcined $BiFeO_3$ ceramic powder. R-Bragg for the main phase is 3.21 %.

3.3.2 Microstructure of composites

Figure 3.2 shows scanning electron microscope images of the cross-section of $BiFeO_3$-PVDF terpolymer composites. Piezoceramic particles appear to be homogeneously distributed in the polymer matrix and only show minor degrees of agglomeration for composite with 20 and 30 vol%, as shown by the porous agglomerates on **Figure 3.2b** and **3.2c**. No signs of sedimentation problems were encountered. Although dark fissure-like zones in the micrographs appear due to the uneven height of the cross-section created by inducing brittle fracture, no microcracks were present in the as-produced samples. The average particle size as determined by SEM corresponded well with the results obtained from particle size analysis.

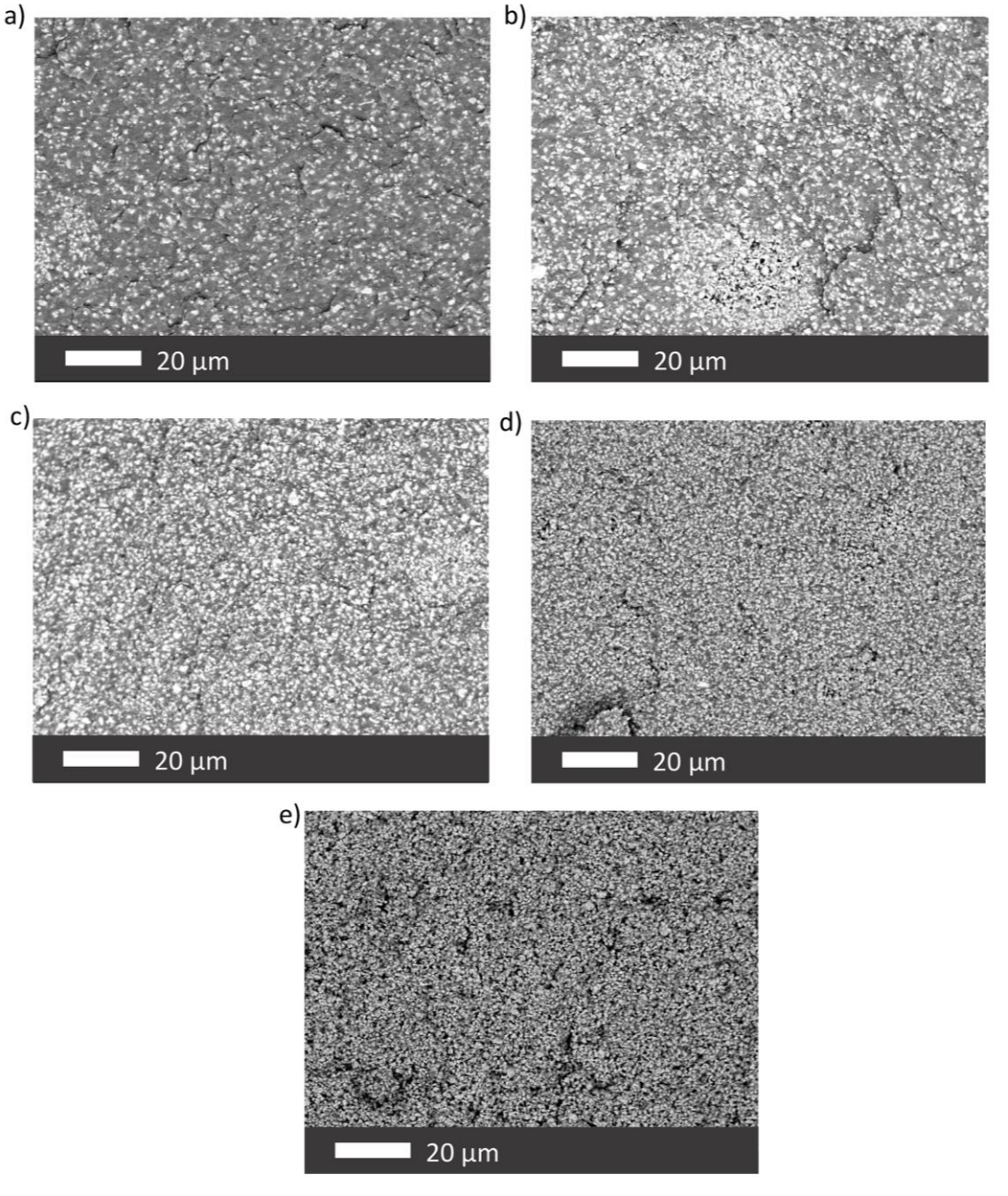

Figure 3.2 – SEM picture cross-section of $BiFeO_3$-PVDF composites: a) 20 vol%; b) 30 vol%; c) 40 vol%; d) 50 vol%; e) 60 vol%

3.3.3 Dielectric and electrical properties of the constituent materials

Samples of pure polymer and $BiFeO_3$ ceramics were prepared to determine the dielectric constants of the polymer and $BiFeO_3$. PVDF terpolymer films with a thickness of around 200 µm were prepared by the same method as for the composites. $BiFeO_3$ bulk ceramics were sintered at a temperature of 775 °C for 1 hour (details in [16]). **Figure 3.3** shows the temperature dependence of the dielectric constant of the polymer (a) and $BiFeO_3$ (b) at different frequencies. It can be seen in **Figure 3.3a** that, due to its relaxor nature[18], the PVDF terpolymer film demonstrates a strong and clearly non-linear dependence of the dielectric constant on temperature and frequency with a maximum value at around 25 °C. In contrast, the dielectric constant of $BiFeO_3$ (**Figure 3.3b**) increases linearly with temperature due to an increase in the conductivity of the sample. Since measurements of the piezoelectric charge constant of the composites were carried out at 25 °C and a frequency of 100 Hz, we are particularly interested in the difference in dielectric strength of the two materials at this frequency and at this temperature. As can be seen in the **Figure 3.3** at this temperature and this frequency, the values of the dielectric constant of $BiFeO_3$ and the polymer are 85 and 61 respectively leading to an unusually small mismatch between the polymer matrix and the ceramic filler particles when compared to other piezoelectric ceramic-polymer composites.

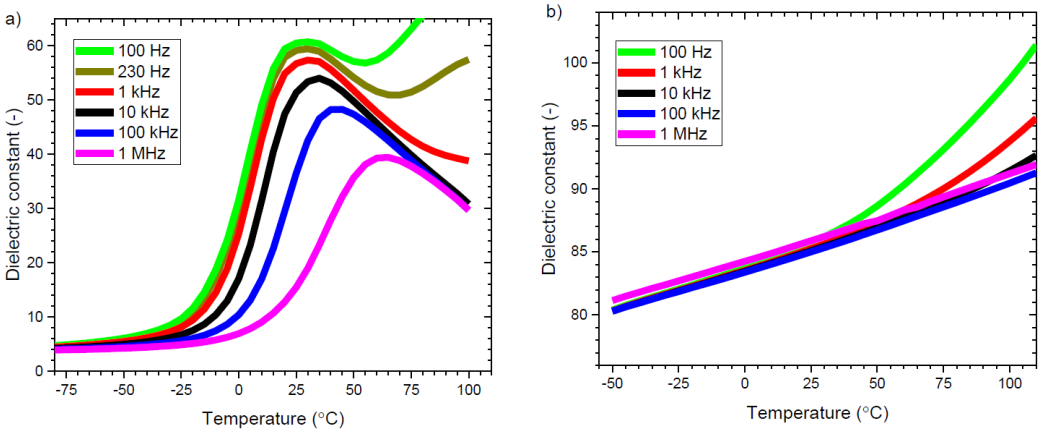

Figure 3.3 – Dielectric constant as a function of the temperature: a) PVDF terpolymer film and b) sintered $BiFeO_3$ bulk ceramic

Figure 3.4 shows the temperature dependence of the DC conductivity for both the polymer and the bulk ceramic. The electrical conductivity of $BiFeO_3$ increases almost linearly with temperature, while the conductivity of the polymer rises sharply over the temperature region of 10-50 °C and then increases more linearly. Such a sharp increase in conductivity over a limited temperature range can be explained by the relaxor phase transition [19]. The origin of the high dielectric response of this class of terpolymers is its ferroelectric phase and the polar nanodomains. The former is responsible for almost frequency independent dielectric maxima (sharp phase transition), while the latter leads to a strong frequency dependence of dielectric spectra (relaxor phase transition). Such a ferroelectric relaxation is associated with short segmentation mobility in the nanodomains [20]. Considering that there are no free protons in our polymer, the conductivity is most likely associated with the transfer of ions by induced segmental dynamics in the nanodomains, [21].

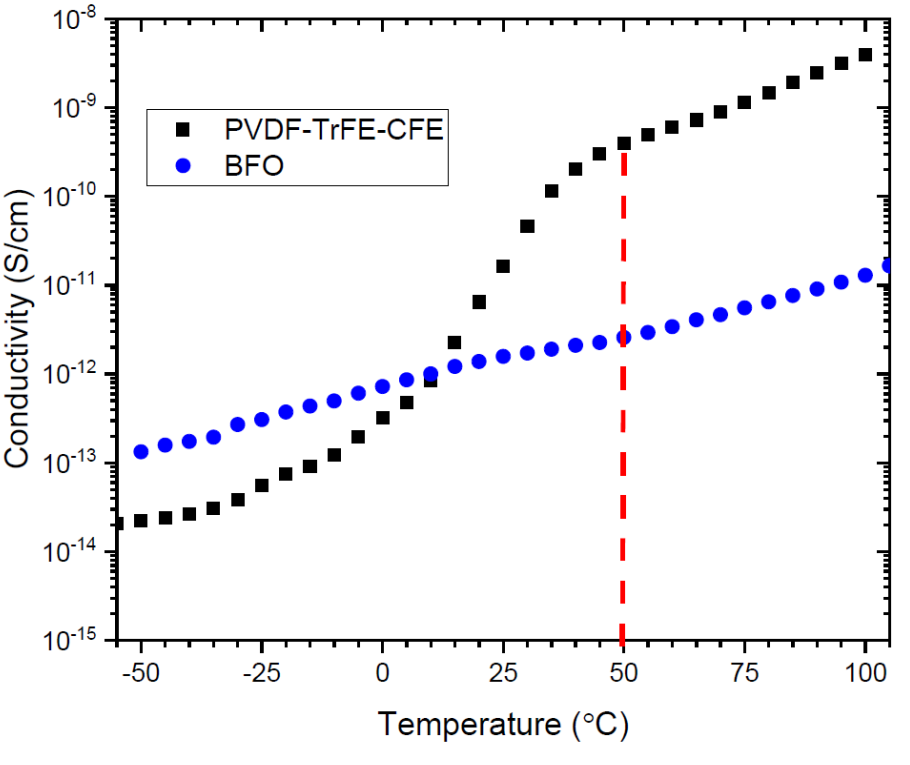

Figure 3.4 – DC conductivity PVDF-terpolymer film and bulk $BiFeO_3$ ceramic as a function of the temperature

3.3.4 Dielectric and electrical properties of the composite materials

Figure 3.5 shows the dielectric measurements of the composite with a 50 vol% $BiFeO_3$ (Other samples show similar behavior; this concentration is chosen as to analyse the material behaviour because of its optimal properties and uniform microstructure). It can be seen that the temperature response is similar to that observed for a pure polymer. At low temperatures, the dielectric constant is most notably changed by the ceramic filler which increases the dielectric constant from a value of 5 for the pure polymer to a value of 20 for this composite. The relaxation peak at higher temperatures is less pronounced than for the pure polymer due to the linear temperature behaviour of the dielectric constant of the $BiFeO_3$.

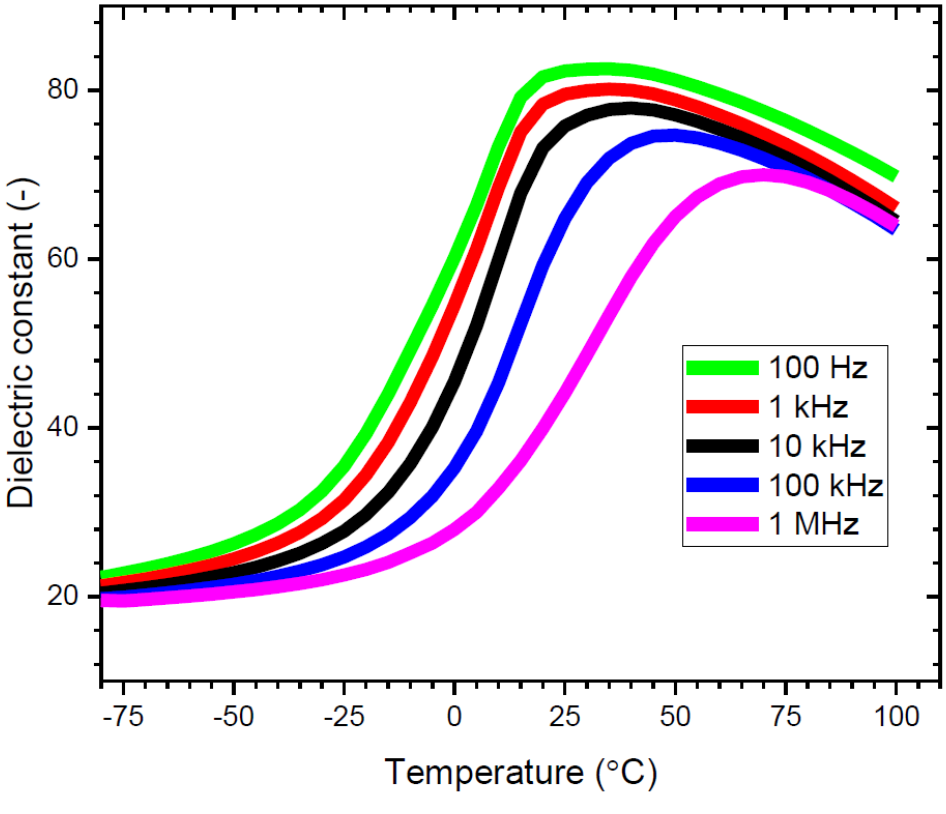

Figure 3.5 – Dielectric constant of 50 vol% $BiFeO_3$-PVDF terpolymer composite as a function of temperature

To fit the temperature dependent dielectric constant of the composites multiple models (as presented in **Table 3.1**) are available. **Figure 3.6a** shows a comparison of these models with the experimental results. All models lead to a linear behavior up to 35 °C, which corresponds to the dielectric peak temperature for the polymer. Above this temperature, all models show a deviation in the prediction of the dielectric constant. The Poon and Shin model was identified as the most optimal for the current dataset. This model shows good results over the entire temperature and frequency range (**Figure 3.6b**), as well as for different concentrations of ceramic filler (**Figure 3.6c**).

Table 3.1 – Dielectric constant approximation models for 0-3 composites. The subscript c refers to the ceramic filler particle, the subscript p refers to the polymer matrix and the parameter ν refers to the volume fraction.

Model	Equation
Maxwell-Garnett [22]	$\varepsilon_{eff} = \varepsilon_p \frac{2\varepsilon_p + \varepsilon_c + 2\nu(\varepsilon_c - \varepsilon_p)}{2\varepsilon_p + \varepsilon_c - \nu(\varepsilon_c - \varepsilon_p)}$
Yamada [23]	$\varepsilon_{eff} = \varepsilon_p(1 + \frac{n\nu(\varepsilon_c - \varepsilon_p)}{n\varepsilon_p + (1-\nu)(\varepsilon_c - \varepsilon_p)})$
Lichtenecker [24]	$\ln(\varepsilon_{eff}) = (1-\nu)\ln(\varepsilon_p) + \nu \ln(\varepsilon_p)$
Jayasundere [25]	$\varepsilon_{eff} = \frac{\varepsilon_p(1-\nu) + \varepsilon_c\gamma}{(1-\nu) + \gamma}$ $\gamma = \frac{3\varepsilon_p\nu}{2\varepsilon_p + \varepsilon_c}(1 + 3\nu\frac{(\varepsilon_c - \varepsilon_p)}{2\varepsilon_p + \varepsilon_c})$
Poon [26]	$\varepsilon_{eff} = \varepsilon_p + \frac{\nu(\varepsilon_c - \varepsilon_p)}{\nu + (1-\nu)\frac{\varepsilon_c + 2\varepsilon_p - \nu(\varepsilon_c - \varepsilon_p)}{3\varepsilon_p}}$

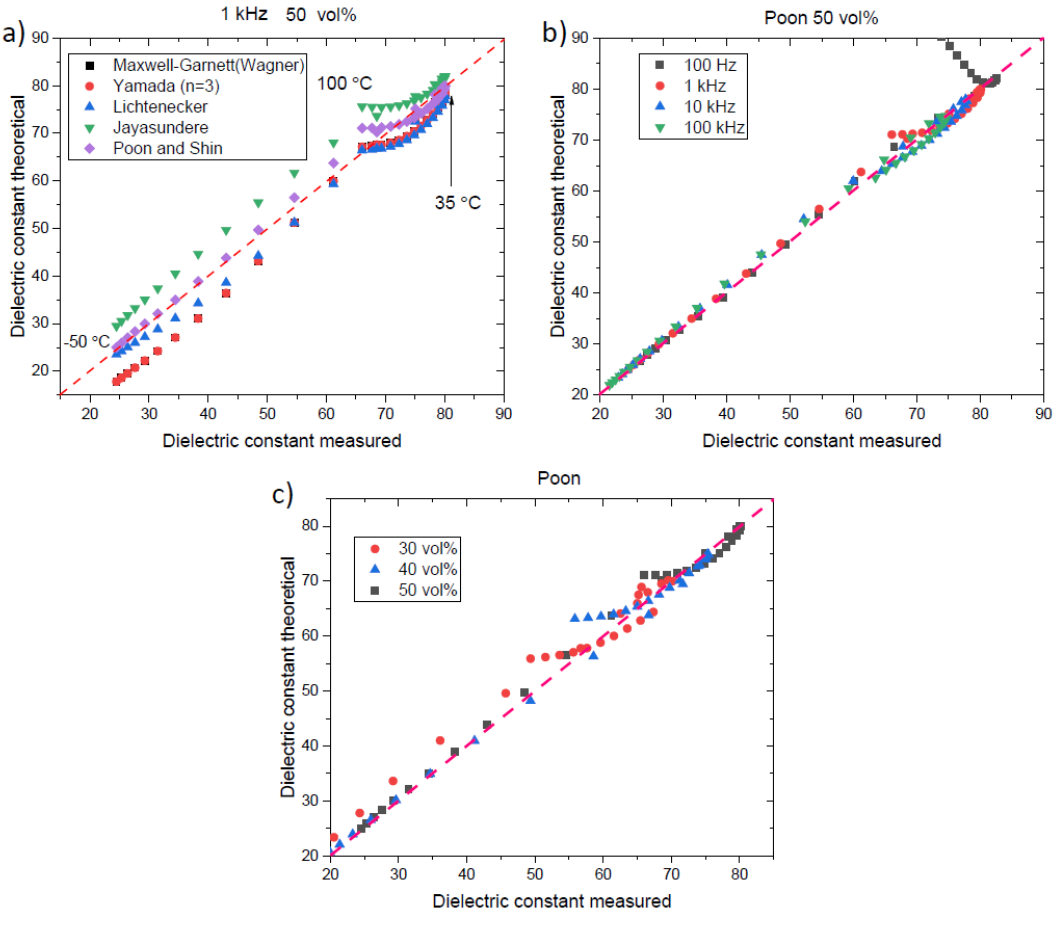

Figure 3.6 – Comparing different theoretical models for ceramic-polymer composites: a) comparison of the predicted dielectric constant versus the measured value; b) comparison of the predicted dielectric constant against the measure value as a function of the frequency for the Poon model; c) comparison of the predicted dielectric constant against the measure value as a function of the volume fraction for the Poon model

Figure 3.7 shows in more detail the approximation of the experimental data for the 50 vol% composite using the Poon model. It can be seen that the predicted behaviour matches the recorded values rather well with only minor deviations above 35 °C which may be attributed either to the polymer matrix behaving marginally different due to the constraining effect of the ceramic filler particles or some inter-particle connectivity not accounted for.

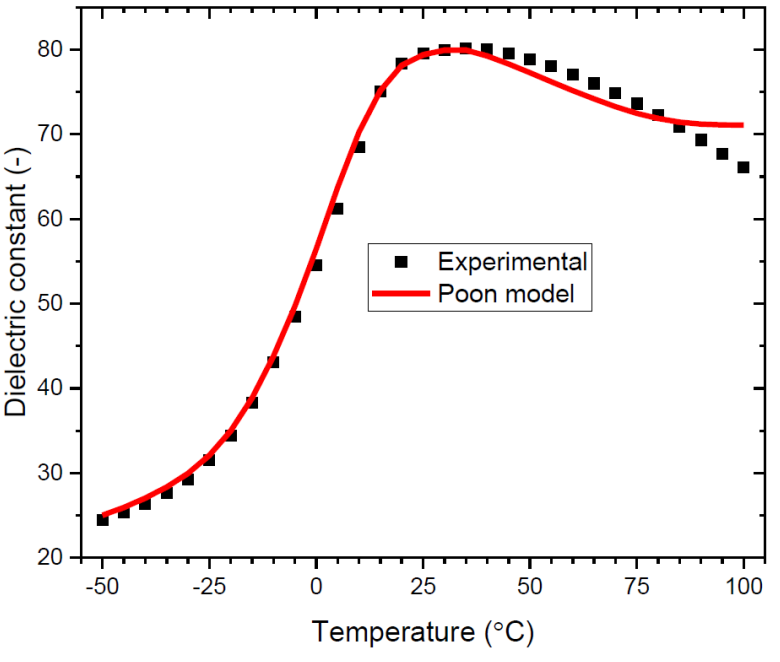

Figure 3.7 – Fitting of the temperature dependence of the dielectric constant at 1 kHz for the 50 vol% $BiFeO_3$-PVDF composite to the Poon model using the data from **Figure 3.3**

3.3.5 Poling study

The effect of poling field and temperature on the piezoelectric charge constants of the $BiFeO_3$ –PVDF terpolymer composites is shown in **Figure 3.8**. The electric field was kept constant at 250 kV/cm while investigating the effect of temperature, and temperature was held constant at 60 °C during the electric field magnitude study. All samples were polarized for 20 minutes. As can be seen in **Figure 3.8a**, as the field increases to 225 kV/cm, the piezoelectric charge constant also increases and then stabilizes abruptly. This is a clear indication that the sample is optimally polarized at a field of 225 kV/cm. The decrease in the piezoelectric constant at a field of 275 kV/cm is attributed to damage to the electrodes during polarization. As shown in **Figure 3.8b**, a modest increase in d_{33} with poling temperature is observed.

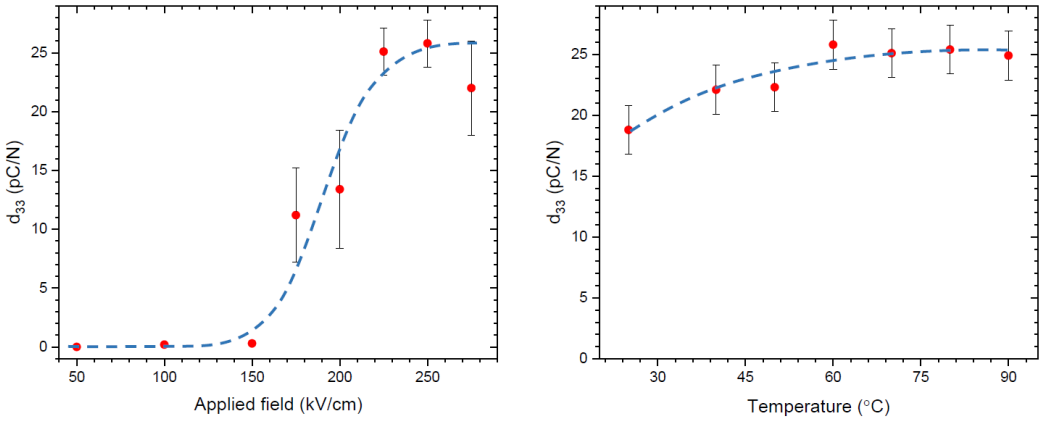

Figure 3.8 – Poling study of the $BiFeO_3$-PVDF 50 vol% composite. a) as function of applied field at 60 °C and b) as a function of the poling temperature at 250 kV/cm. The fit lines are to guide the eye and are not based on model predictions

The observed optimal poling temperature can be explained on the basis of the competing temperature dependences of the DC conductivity [27] and that of the dielectric constant of the polymer matrix.

3.3.6 Piezoelectrical properties

The piezoelectric charge constant (d_{33}) of the composites as a function of the $BiFeO_3$ volume fraction is shown in **Figure 3.9a**. As expected, with an increase in the volume fraction of $BiFeO_3$, the piezoelectric constant also increases. The maximum value of d_{33} at 60 vol% is 31 pC/N. Since the dielectric constant of the matrix material (about 61 at room temperature) is very similar to that of $BiFeO_3$ (about 85), the field distribution in the composite should be rather uniform and the piezoelectric constant should grow almost linearly with increasing ceramic loading. The piezoelectric voltage constant (g_{33}) is proportional to the piezoelectric charge constant and inversely proportional to the dielectric constant, and because the dielectric constants of the matrix and the filler differ insignificantly, g_{33} should also grow almost linearly with increasing ceramic content. The maximum value of the piezoelectric voltage constant experimentally measured at 60 vol% is 47 mV·m/N. **Table 3.2** presents the ceramic volume fraction, permittivity, piezoelectric charge and piezoelectric voltage constants of our composite compared with composites

and ceramics reported by others. As the value of the dielectric constant is low compared to that of PZT or different composites, the measured piezoelectric voltage constants of the present composites are quite high and compare favorably with those of other composites. Due to the fact that the dielectric constant is higher than that of other composites, devices based on this family of composites will have a higher capacitance, which expands the frequency range (Reducing the cutoff frequency at low frequencies) of applications and makes the $BiFeO_3$-PVDF terpolymer composite a promising material for sensor applications.

Table 3.2 – Comparing piezoelectric properties of 0-3 ceramic-polymer composites. A volume percent of 100 indicates the pure material.

Material	Volume (%)	ε_r (-)	d_{33} (pC/N)	g_{33} (mV·m/N)
$BiFeO_3$ ceramic [5]	100	-	45	-
PZT507 [28]	100	3950	875	25
PVDF [29]	100	12	23	220
PT-PEO [27]	30	21	7.5	40
KNLN-Epoxy [30]	60	48	32	75
PZT-Epoxy [30]	60	48	18	42
BT-Epoxy [30]	60	47	10	24
KNLN-PU [30]	60	65	29	50
PZT-PU [30]	60	50	12	27
BT-PU [30]	60	40	4	11
PT-PEI [31]	30	10	4	45
$BiFeO_3$-PVDF [this work]	60	80	31	47

3.3.7 Piezoelectrical properties

Since incorporation of $BiFeO_3$ particles in the polymer matrix selected allowed us to increase the electric field for poling, it opened up the possibility to indirectly measure the maximum or intrinsic piezoelectric properties of the

granular $BiFeO_3$ particles. In order to extract the piezoelectric constant of ceramics from the effective piezoelectric constant of the 0-3 $BiFeO_3$-PVDF terpolymer composites measured, we used Yamada's model:

$$d_{33} = \frac{n\nu\alpha\varepsilon_{eff}d_{33c}}{n\varepsilon_{eff}+\varepsilon_c-\varepsilon_{eff}} \quad (3.1)$$

Where ν is again the filler volume fraction, α is the poling efficiency and ε_{eff} is the effective dielectric constant. The Yamada model also incorporates shape anisotropy effects of the particles by the parameter n. If n = 3, the particles are spherical while n > 3 reflects elongated particles. The Yamada model has been modified in part to account for changes in the effective dielectric constant as described by the Poon model.

Based on the poling results obtained the poling efficiency, α, was chosen as 1. Since, in our model, the actual value of n does not matter much, and almost equal final results of the piezoelectric constant (with a deviation of 3 pC/N) are obtained for 3 <n <10the value for the shape factor, n, was chosen as 3, since this corresponds to a spherical shape of the particles, which is the closest to the morphology of our particles.

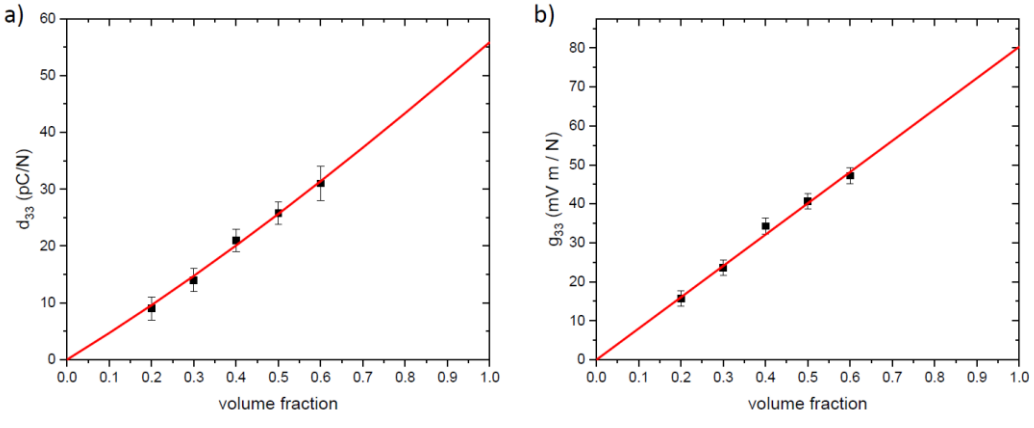

Figure 3.9 – d_{33}(a) and g_{33}(b) values for $BiFeO_3$–PVDF terpolymer composites with fitted theoretical model predictions according to the Yamada model

If we assume that this model is valid up to 100 vol% loading, we predict that the piezoelectric charge constant of ideally poled granular $BiFeO_3$ could be as high as 56 pC/N, which is 25 % higher than highest observed bulk value shown (~45 pC/N) in recent studies [32]. Assuming that routes for non-leaking $BiFeO_3$ bulk ceramics will be found in future, the combination of the predicted

high value for the piezoelectric voltage constant g_{33} of about 80 mV·m/N, and a high Curie temperature (~825 °C [2]) , would make $BiFeO_3$ a truly attractive material for high-temperature sensors.

3.4 CONCLUSIONS

Embedding $BiFeO_3$ granular material in a non-conducting PVDF terpolymer having a comparable dielectric constant allowed for proper poling of the $BiFeO_3$ particles and a correct interpretation of the volume fraction dependence of the dielectric and piezoelectric properties of the composites made. By combining the Poon model for the dielectric properties and the Yamada model for the piezoelectric properties, the piezoelectric charge and voltage constants of granular $BiFeO_3$ could be determined and were found to be as high as 56 pC/N for d_{33} and 80 mV·m/N for g_{33}. These values, in combination with the high Curie temperature, reconfirm the great potential of $BiFeO_3$ as a high temperature sensor material.

3.5 SUPPORTING INFORMATION

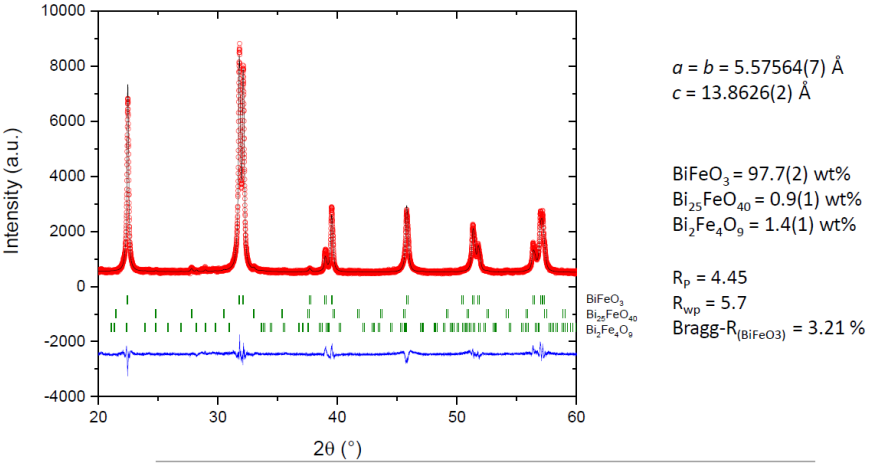

Atom	x	y	z	B_{iso}	Occ.
Bi	0.0	0.0	0.0	1.51(1)	0.987(5)
Fe	0.0	0.0	0.723(2)	2.12(6)	1.0
O	0.44(1)	0.009(8)	0.948(4)	2.05(17)	0.997(7)

Figure 3.1S – Details and results of the Rietveld refined XRD pattern of the calcined $BiFeO_3$ ceramic powder. Numbers in brackets indicate the standard deviation on the digit immediately preceding them

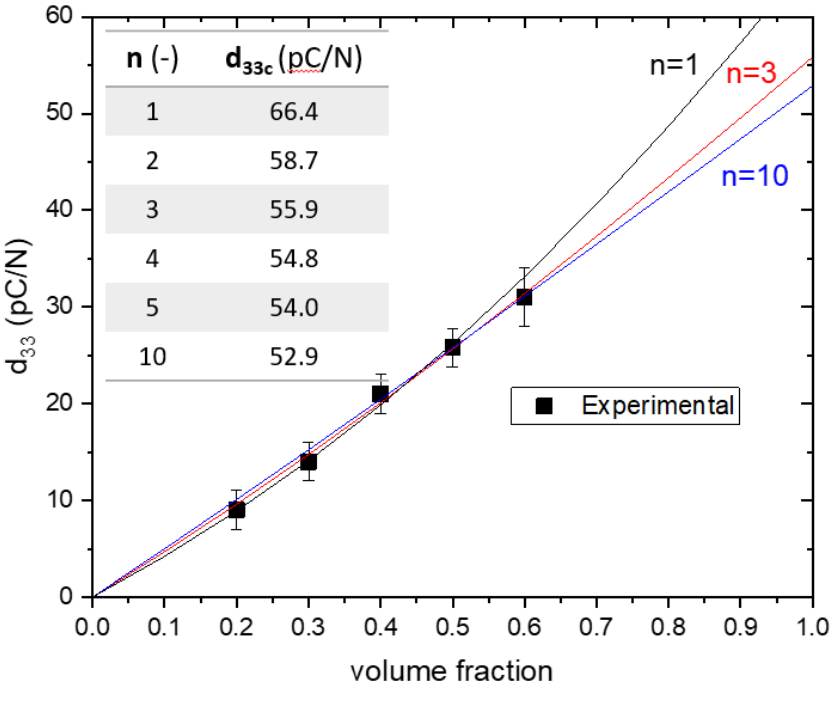

Figure 3.2S – d_{33} values for $BiFeO_3$–PVDF terpolymer composites with fitted theoretical model predictions according to the Yamada model with different shape factor

REFERENCES:

[1] P. Royen, K. Swars, Das System Wismutoxyd-Eisenoxyd im Bereich von 0 bis 55 Mol% Eisenoxyd, Angew. Chemie. 69 (2007) 779–779. https://doi.org/10.1002/ange.19570692407.

[2] R. Palai, R.S. Katiyar, H. Schmid, P. Tissot, S.J. Clark, J. Robertson, S.A.T. Redfern, G. Catalan, J.F. Scott, β phase and γ-β metal-insulator transition in multiferroic BiFe O3, Phys. Rev. B - Condens. Matter Mater. Phys. 77 (2008) 1–11. https://doi.org/10.1103/PhysRevB.77.014110.

[3] J. Wang, J.B. Neaton, H. Zheng, V. Nagarajan, S.B. Ogale, B. Liu, D. Viehland, V. Vaithyanathan, D.G. Schlom, U. V. Waghmare, N.A. Spaldin, K.M. Rabe, M. Wuttig, R. Ramesh, Epitaxial BiFeO3 multiferroic thin film heterostructures, Science (80-.). 299 (2003) 1719–1722. https://doi.org/10.1126/science.1080615.

[4] J. Yu, J. Chu, Progress and prospect for high temperature single-phased magnetic ferroelectrics, Chinese Sci. Bull. 53 (2008) 2097–2112. https://doi.org/10.1007/s11434-008-0308-3.

[5] L. Liu, T. Rojac, J. Kimpton, J. Walker, M. Makarovic, J.F. Li, J. Daniels, Poling-induced inverse time-dependent microstrain mechanisms and post-poling relaxation in bismuth ferrite, Appl. Phys. Lett. 116 (2020). https://doi.org/10.1063/5.0002235.

[6] H. Zhu, Y. Yang, W. Ren, M. Niu, W. Hu, H. Ma, J. Ouyang, Rhombohedral BiFeO3 thick films integrated on Si with a giant electric polarization and prominent piezoelectricity, Acta Mater. 200 (2020) 305–314. https://doi.org/10.1016/j.actamat.2020.09.022.

[7] J. Wu, Z. Fan, D. Xiao, J. Zhu, J. Wang, Multiferroic bismuth ferrite-based materials for multifunctional applications: Ceramic bulks, thin films and nanostructures, Prog. Mater. Sci. 84 (2016) 335–402. https://doi.org/10.1016/j.pmatsci.2016.09.001.

[8] A. Hussain, M.A. Qaiser, J. Zhang, S.T. Zhang, Y. Wang, Y. Yang, Z. Liu, G. Yuan, High-temperature piezoelectric properties of 0-3 type CaBi4Ti4O15:x wt%BiFeO3 composites, J. Am. Ceram. Soc. 100 (2017) 3522–3529. https://doi.org/10.1111/jace.14879.

[9] M.A. Qaiser, A. Hussain, J. Zhang, Y. Wang, S. Zhang, L. Chen, G. Yuan, 0–3 type Bi3TaTiO9:40wt%BiFeO3 composite with improved high-temperature piezoelectric properties, J. Alloys Compd. 740 (2018) 1–6. https://doi.org/10.1016/j.jallcom.2017.12.365.

[10] K. Yoshiyama, M. Mori, M. Hagiwara, S. Fujihara, Effect of particle size and morphology on the performance of BiFeO3-PDMS piezoelectric generators, CrystEngComm. 22 (2020) 2919–2925. https://doi.org/10.1039/d0ce00067a.

[11] S. Moharana, R.N. Mahaling, High performance of hydroxylated BiFeO3/polystyrene composite films with enhanced dielectric constant and low dielectric loss, J. Aust. Ceram. Soc. 56 (2020) 751–760. https://doi.org/10.1007/s41779-019-00393-9.

[12] S. Dash, R.N.P. Choudhary, M.N. Goswami, Enhanced dielectric and ferroelectric properties of PVDF-BiFeO3 composites in 0–3 connectivity, J. Alloys Compd. 715 (2017) 29–36. https://doi.org/10.1016/j.jallcom.2017.04.310.

[13] M.K. Mishra, S. Moharana, R.N. Mahaling, Enhanced dielectric properties of poly(vinylidene fluoride)–surface functionalized BiFeO3 composites using sodium dodecyl sulfate as a modulating agent for device applications, J. Appl. Polym. Sci. 134 (2017) 1–9. https://doi.org/10.1002/app.45040.

[14] A. Kumar, K.L. Yadav, Enhanced magnetocapacitance sensitivity in BiFeO 3- poly(vinylidene-fluoride) hot pressed composite films, J. Alloys Compd. 528 (2012) 16–19. https://doi.org/10.1016/j.jallcom.2012.02.125.

[15] S. You, C. Liu, H. Liu, X. Yu, S. Li, W. Liu, S. Guo, X. Zhao, The preparation and characterization of 1D multiferroic BFO/P(VDF-TrFE) composite nanofibers using electrospinning, Mater. Lett. 130 (2014) 157–159. https://doi.org/10.1016/j.matlet.2014.05.118.

[16] A.Y. Tuluk, T.R. Mahon, S. van der Zwaag, P. Groen, BiFeO3 synthesis by conventional solid-state reaction, 2019 IEEE Int. Symp. Appl. Ferroelectr. ISAF 2019-Proc. (2019) 3-6. https://doi.org/10.1109/ISAF43169.2019.9034976.

[17] G. Catalan, J.F. Scott, Physics and applications of bismuth ferrite, Adv. Mater. 21 (2009) 2463–2485. https://doi.org/10.1002/adma.200802849.

[18] Y. Wang, S.G. Lu, M. Lanagan, Q. Zhang, Dielectric relaxation of relaxor ferroelectric P(VDF-TrFE-CFE) terpolymer over broad frequency range, IEEE Trans. Ultrason. Ferroelectr. Freq. Control. 56 (2009) 444–449. https://doi.org/10.1109/TUFFC.2009.1063.

[19] A. Pramanick, N.C. Osti, N. Jalarvo, S.T. Misture, S.O. Diallo, E. Mamontov, Y. Luo, J.K. Keum, K. Littrell, Origin of dielectric relaxor behavior in PVDF-based copolymer and terpolymer films, AIP Adv. 8 (2018). https://doi.org/10.1063/1.5014992.

[20] H.M. Bao, J.F. Song, J. Zhang, Q.D. Shen, C.Z. Yang, Q.M. Zhang, Phase transitions and ferroelectric relaxor behavior in P(VDF-TrFE-CFE) terpolymers, Macromolecules. 40 (2007) 2371–2379. https://doi.org/10.1021/ma062800l.

[21] Q. Liu, X. Yin, C. Richard, J.F. Capsal, Influence of the crystallization on the molecular mobility and ionic DC conductivity behaviors of relaxor ferroelectric P(VDF-TrFE-CTFE) terpolymers, J. Polym. Sci. Part B Polym. Phys. 54 (2016) 1645–1657. https://doi.org/10.1002/polb.24068.

[22] C.W. Nan, Comment on "Effective dielectric function of a random medium," Phys. Rev. B - Condens. Matter Mater. Phys. 63 (2001) 5–7. https://doi.org/10.1103/PhysRevB.63.176201.

[23] T. Yamada, T. Ueda, T. Kitayama, Piezoelectricity of a high-content lead zirconate titanate/polymer composite, J. Appl. Phys. 53 (1982) 4328–4332. https://doi.org/10.1063/1.331211.

[24] F. Carpi, D. De Rossi, Improvement of electromechanical actuating performances of a silicone dielectric elastomer by dispersion of titanium dioxide powder, IEEE Trans. Dielectr. Electr. Insul. 12 (2005) 835–843. https://doi.org/10.1109/TDEI.2005.1511110.

[25] N. Jayasundere, B. V. Smith, Dielectric constant for binary piezoelectric 0-3 composites, J. Appl. Phys. 73 (1993) 2462–2466. https://doi.org/10.1063/1.354057.

[26] Y.M. Poon, F.G. Shin, A simple explicit formula for the effective dielectric constant of binary 0-3 composites, J. Mater. Sci. 39 (2004) 1277–1281. https://doi.org/10.1023/B:JMSC.0000013886.21054.e4.

[27] H. Khanbareh, S. van der Zwaag, W.A. Groen, Piezoelectric and pyroelectric properties of conductive polyethylene oxide-lead titanate composites, Smart Mater. Struct. 24 (2015) 45020. https://doi.org/10.1088/0964-1726/24/4/045020.

[28] V.L. Stuber, D.B. Deutz, J. Bennett, D. Cannel, D.M. de Leeuw, S. van der Zwaag, P. Groen, Flexible Lead-Free Piezoelectric Composite Materials for Energy Harvesting Applications, Energy Technol. 7 (2019) 177–185. https://doi.org/10.1002/ente.201800419.

[29] Piezoelectric Film | PVDF Film | Piezotech, (n.d.). https://www.piezotech.eu/en/Applications/piezoelectric-film/ (accessed November 25, 2020).

[30] V.L. Stuber, T.R. Mahon, S. van der Zwaag, P. Groen, The effect of the intrinsic electrical matrix conductivity on the piezoelectric charge constant of piezoelectric composites, Mater. Res. Express. 7 (2019). https://doi.org/10.1088/2053-1591/ab5bb3.

[31] H. Khanbareh, M. Hegde, J.C. Bijleveld, S. van der Zwaag, P. Groen, Functionally graded ferroelectric polyetherimide composites for high temperature sensing, J. Mater. Chem. C. 5 (2017) 9389–9397. https://doi.org/10.1039/c7tc02649h.

[32] T. Rojac, M. Makarovic, J. Walker, H. Ursic, D. Damjanovic, T. Kos, Piezoelectric response of BiFeO3ceramics at elevated temperatures, Appl. Phys. Lett. 109 (2016). https://doi.org/10.1063/1.4960103.

4

TUNING PIEZOPROPERTIES OF $BiFeO_3$ CERAMIC BY COBALT AND TITANIUM DUAL DOPING

ABSTRACT

Bismuth ferrite is a potentially interesting lead-free piezoelectric material for use in high temperature applications due to its high Curie temperature. However, the high coercive field and high leakage currents of pure BiFeO3 (BFO) prevent reaching its theoretical performance level. The classic approach in tailoring piezo ceramics properties to their desired use conditions is the use of doping. In this work, we produce bulk BFO piezoceramic by the conventional sintering method with single element doping with cobalt (0.125-3 at%) or titanium (1-5 at%) and dual doping (Co and Ti added simultaneously). Cobalt doping reduces the required field for poling, but also increases the leakage currents. Titanium doping reduces the leakage currents but destroys the piezoelectric properties as the coercive field strength cannot be reached. However, when both elements are used simultaneously at their appropriate levels (0.25 at% each) a piezoelectric ceramic material is obtained requiring a low field for full poling (9 kV/mm) and showing excellent room temperature performance such as a d33 = 40 pC/N, a dielectric constant in the region of 100 and dielectric losses less than 1%.

This chapter has been published in Journal of Applied Physics 131, 21 (2022)

4.1 INTRODUCTION

For a long time, piezoelectric sensors have been regarded as the most efficient devices for measuring pressure, acceleration and stress at room temperature. For example, piezoelectric ceramic sensors offer significant advantages over other non-destructive testing methods such as: low cost, ease of operation and the ability to conduct *in-operando* measurements[1], but this advantage disappears when the sensor is exposed to high temperatures. The widespread use of piezoelectric ceramics in various applications has become possible due to property tuning via the use of donor or acceptor dopants[2]. Currently most piezoelectric sensors are based on a modified PZT with the chemical formula: $PbZr_xTi_{1-x}O_3$, which is one of the most widely studied systems from a fundamental and functional point of view but is also a system with no high temperature application potential. PZT is a perovskite ferroelectric with a cubic symmetry above its Curie temperature and with tetragonal, monoclinic, or rhombohedral distortion in the polar state at lower temperatures, depending on its composition [3]. The ferroelectric or piezoelectric characteristics of the PZT can be tuned towards "hard" or "soft" characteristics by proper doping. The terms "soft" and "hard" PZT ceramics refer to minimal field required to achieve a permanently poled state which in itself depends on the mobility of dipoles or domains, as well as the behaviour of polarization and depolarization. "Soft" PZTs are obtained by doping with donor ions such as La^{+3} and W^{+6} (for site A) and Nb^{+5}, Sb^{+5} (for site B), which leads to the creation of vacancies at site A in the lattice [4]. The characteristic features of attractive poling elements are those leading to a relatively high mobility of the domain walls and, as a consequence, a "soft" ferroelectric behaviour (easily polarizable). The advantages of "soft" PZT materials are thus their large piezoelectric charge constant, moderate dielectric constant and high coupling factors, which makes them interesting for actuators, sensors such as conventional vibration sensors, ultrasonic transmitters and receivers for flow or level measurements, electroacoustic applications such as sound transducers and microphones[5] . "Hard" PZT is doped with acceptor ions such as K^{+1}, Na^{+1} (for site A) and Fe^{+3}, Al^{+3}, Mn^{+3} (for site B), creating oxygen vacancies in the lattice[6]. Such PZT materials can be subjected to high electrical and mechanical stresses, without a change in performance, hence showing good stability. This makes "hard" PZT materials suitable for high power and high

frequency applications. Other advantages of "hard" PZT ceramics are a moderate dielectric constant value, large piezoelectric coupling factors and low dielectric losses, which facilitate their further use in the resonant mode only with low internal heating of the component. "Hard" PZT based piezoelectric elements are used for ultrasonic cleaning, ultrasonic processors, in biomedical fields, in transducers, hydroacoustic technologies, etc. The large difference in physical properties between "soft" and "hard" groups is mainly due to the contribution of the motion of the domain wall [2,7], and not so much to a change in the crystal lattice values. However, the mechanisms of hardening and softening are not fully understood.

Irrespective of the doping element used to tune the properties of PZT-based piezoelectric sensors, their maximal operating temperatures are around 260 °C or lower due to the intrinsic PZT transformation temperature and the modest effect of doping at that temperature range[8]. Therefore, considerable efforts are now aimed at developing new (i.e. non PZT based) materials that can satisfy the growing demand for piezoelectric elements with an operating temperature in the range of 350-600 °C. One such material is $BiFeO_3$ (BFO), with an exceptionally high Curie temperature, T_C, of 825 °C [9] and the added benefit of having a lead-free composition. This high T_C makes BFO an ideal candidate for use as a high temperature lead-free piezoceramic[1]. Unfortunately, research on bulk ceramics of BFO has not been very successful and did not demonstrate a high piezoelectric coefficient. This was largely due to the problems of electrical leakage and phase purity, which created difficulties in realising the potential of bulk bismuth ferrite.

As with PZT, one of the ways to solve these problems is to tune the properties of bismuth ferrite by doping. Macroscopic hardening of the ferroelectric behaviour of the BFO doped up to 3 at% by Co was recently shown by Makarovic et al[10]. In this work, it was shown that the assumptions about the p-type conductivity are correct and the main reason for the hardening is an increase in the concentration of Co_{Fe}-V_O pinning centers. This mechanism has clear parallels with those in acceptor doped ("hard") PZT. Continuing the analogy with PZT, it can be assumed that doping with donors such as Ti^{4+} should lead to softening of the BFO piezoelectric ceramics due to a decrease in the concentration of pinning centers. No increases in piezoelectric properties and softening were shown for Ti doped BFO, but only a decrease in tan δ with

an increase in the amount of Ti substitution, and this is explained by the assumption that Fe^{2+} ions (the predominant cause of high tan δ in BFO) were not formed due to Ti doping[11,12].

To study the mechanisms of hardening and softening of BFO ceramic, two types of dopants, cobalt and titanium, were chosen. Cobalt concentrations of 0.125, 0.25 and 0.5 at% were chosen since the concentration of cobalt close to 0.2 at% leads to an improvement in the ferroelectric and insulating properties of ceramics[10,13,14]. Higher dopant concentrations up to 3 at% Co have also been tested to ensure that there is an upward trend in conductivity. During the study, it was noticed that doping with cobalt reduces the required poling field to obtain piezoelectric properties in BFO.

To investigate the effect of donor doping on the piezoelectric properties of BFOs, titanium concentrations from 1 to 5 at% were chosen. When studying the insulating properties of BFO doped with titanium, at higher titanium concentrations, the leakage currents are steadily increasing[11,15].

Also, the effect of dual doping of cobalt and titanium is investigated and the concentration of doping in this case was selected based on the best results of previous experiments. The study has shown that dual doping, with the right concentration selection, allows us to combine the positive effects separate dopants.

4.2 EXPERIMENTAL PROCEDURE

$BiFeO_3$ samples were prepared by a conventional solid-state reaction using analytical grade commercially supplied raw materials: Bi_2O_3 (99.99% purity), Fe_2O_3 (99.95% purity), TiO_2 (99.99% purity) and Co_2O_3 (99.9% purity). All powders were weighed and grounded separately before mixing. Cobalt doping levels were varied between 0.125-3 at%. Titanium doping levels were varied between 1-5 at%. Based on results of the Co and Ti doped systems dual doping levels were chosen as 0.25-0.25, 0.5-0.5 and 0.25-1 at% Co-Ti. Grinding and mixing processes were performed in isopropanol using yttria-stabilized ZrO_2 balls. The particle size distributions composition of the milled powder is in the range of 0.5-1 microns according to the SEM images. The powders were dried and calcined at 775°C for 1 h and a heating rate of 600°C/h. Then the calcined powders were reground, granulated by mixing with 2 wt% QPAC 40 binder, and uniaxial pressed into disks (13 mm in diameter and 1 mm in thickness)

under 200-250 MPa. The pellets were sintered at 800–850 °C for 1 h, depending on their composition. Sintering temperatures were optimized to achieve the best density for a fixed sintering time of 1 h.

Scanning Electron Microscope (SEM) images of fracture surfaces were taken using a Jeol JSM-7500F field emission scanning electron microscope. Prior to SEM measurements a thin (15 nm) layer of gold was deposited on the sample. Grain size measurement based on SEM images and manual evaluation of typically 25 grains. To determine the phase purity of the various $BiFeO_3$ systems X-ray diffraction studies with Cu Kα radiation at room temperature were done using a Rigaku Miniflex 600 diffractometer. Given the absence of open porosity, the density was determined by the Archimedes' method in an aqueous medium.

Polarization–electric field hysteresis loops were measured at room temperature by a Radiant precision ferroelectric analyzer at 5 Hz and up to 110 kV/cm (4-5 kV depends on sample thickness and dielectric strength of samples). For this, gold electrodes were deposited on the ceramics by magnetron sputtering method. The samples were poled under a DC electric field of 60-110 kV/cm for 20 min in silicone oil at room temperature (Due to the risk of electrical breakdown at higher temperatures). The electrical properties of the piezoceramic were measured at room temperature using an Agilent 4263B LCR meter at 1 kHz and 1 V, while the piezoelectric properties were measured using a PM300 Berlincourt-type piezometer from Piezotest with a static force of 10 N and a dynamic force of 0.25 N peak-to-peak with sinusoidal excitation at 110 Hz.

4.3 RESULT AND DISCUSSION

4.3.1 MICROSTRUCTURE

Figure 4.1 shows SEM images of BFO ceramics, pure and doped with cobalt, titanium, or both, with relative densities reported as well. Macro pores are absent in all obtained ceramics. As can be seen from **Figure 4.1a**, low concentrations of cobalt (up to 1 at%) negatively affect the density of ceramics and increase the average grain size. At higher concentrations, the density of the ceramic increases with respect to the undoped BFO.

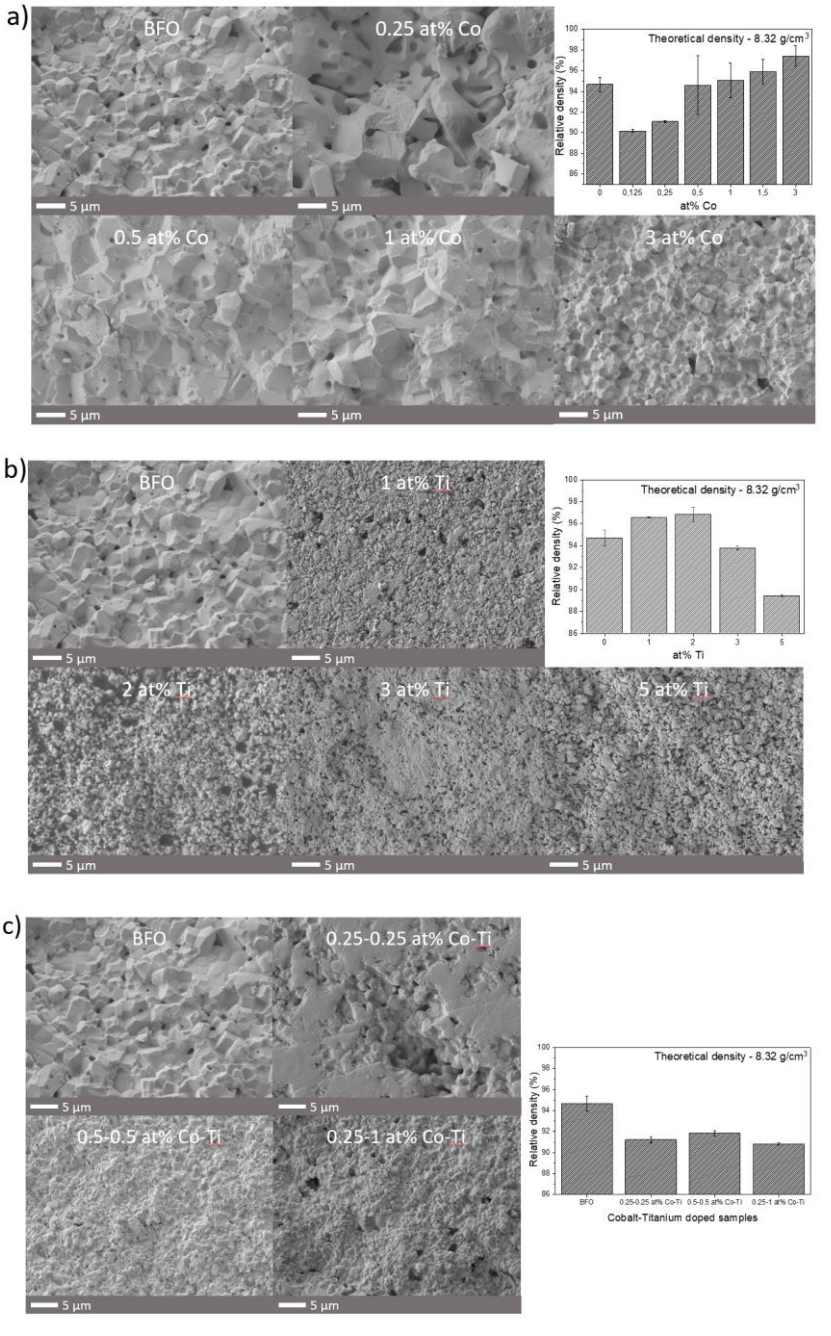

Figure 4.1 – SEM images of fracture surface and relative density in comparison to pure BFO ceramic of representative a) Co doped; b) Ti doped; c) dual doped BFO samples.

In contrast, low concentrations of titanium reduce the grain size, while high concentrations of Ti negatively affect the density of the ceramic (**Figure 4.1b**). This effect might be associated with an increase in the concentration of oxygen vacancies, which is reported to favorably affect the sintering and growth of ceramic grains[16].

Figure 4.1c shows the microstructure in dual doped samples. The effect of titanium on the microstructure of the samples dominates over the effect of cobalt since the grain size decreases in the same way as in the case of doping with titanium only.

4.3.2 CRYSTAL STRUCTURE

Figure 4.2a shows selected X-ray diffraction patterns of $BiFeO_3$ ceramic powder doped by Co, Ti or both. All materials crystallize in the form of a rhombohedral perovskite structure with space group *R3c*. According to the result of Rietveld's refinement (**Figure 4.1S**), all systems are practically free of secondary phases. The concentration of the secondary phases of undoped BFO is below 2 wt%, and even lower for the doped systems. Addition of these dopants does not affect the crystal structure, which is reflected in the absence of obvious changes in lattice parameters shown in **Figure 4.2b**. The differences in peak intensity between the various samples can be attributed to texturing and differences in grain size for differently doped samples.

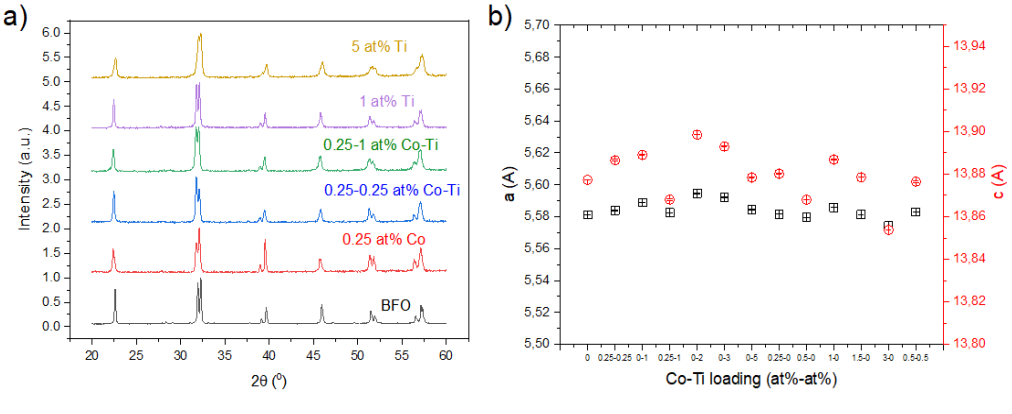

Figure 4.2 – a) X-ray diffraction pattern of the sintered $BiFeO_3$ ceramic with different dopants and concentrations and b) unit cell parameters of their *R3c* structure in hexagonal representation obtained by Rietveld refinement

4.3.3 FERROELECTRIC

As shown in many other works on bismuth ferrite[10,13,17], undoped bismuth ferrite has a high coercive field and demonstrates a pinched ferroelectric loop. In our case, as shown in **Figure 4.3**, the ferroelectric loop is clamped and only opens when a high field of 120 kV/cm in combination with a high temperature is reached. This may be due to an increase in the mobility of defects at elevated temperatures. A pinched hysteresis loop is often observed when the state of a ferroelectric domain wall is characterized by random internal electric fields. In our case, this may be due to the high oxygen vacancy content which forms defective dipoles.

Ferroelectric hysteresis loops for pure and cobalt-doped ceramics are shown in **Figure 4.4a**. All loops, except for pure BFO, have a pinched shape characteristic of BFO ceramics [13,14]. The addition of cobalt in our case does not lead to the hardening of BFO, as happens in the case of PZT, but rather leads to the opposite effect.

Figure 4.4b shows that the leakage currents increase with an increase in the cobalt concentration, which can also be associated with an increase in the concentration of oxygen vacancies. Several published experimental and theoretical studies demonstrate that unmodified BFO-based ceramics exhibit p-type (Fe^{4+}) conductivity when sintered in air[13,18–21]. According to a recent defect chemical model[22], an increase in electrical conductivity in the range of 0.125–3 at% Co (see **Figure 4.4b**) can be explained by an increase in the concentration of electron holes (Fe^{4+}). Samples with a doping concentration of 1.5 and 3 at% Co show electrical breakdown at fields above 10 kV/cm. The results show that Co acts as an acceptor dopant according to the defect response in equation (3.1), where the Co^{2+} acceptor replacing the Fe^{3+} position in BFO is supposed to compensate for the charge with oxygen vacancies ($V_O^{\bullet\bullet}$).

$$2CoO \rightarrow 2Co'_{Fe} + 2O_O^x + V_O^{\bullet\bullet} \qquad (4.1)$$

Considering that the concentration of $V_O^{\bullet\bullet}$ is closely related to the valence state of Fe, an increase in the concentration of $V_O^{\bullet\bullet}$ due to doping with Co will increase the p-type conductivity.

Leakage currents and ferroelectric loops of titanium-doped samples are shown in **Figure 4.5**. For all concentrations, the loops do not open, not even for the

highest field values of 150–160 kV/cm. If we consider the softening and hardening mechanisms inherent in PZT we would expect to see the opposite result when doping with a donor such as titanium. But as we can see, all ferroelectric and piezoelectric properties disappear. Leakage currents for Ti doped samples decreases until reaching a minimum at 2 at% Ti concentration, and then increase back with a subsequent increase in Ti concentration (till 5 at%), but still lower than undoped samples. This may be the result of a significant reduction in oxygen vacancies and the prevention of Fe^{4+} formation. Consequently, the dominant charge compensation mechanism in Ti^{4+} doped BFO is the filling of oxygen vacancies [12], although the creation of some Fe^{2+} ions or Fe^{3+} vacancies cannot be ruled out. Oxygen and iron ions are usually immobile at room temperature. Ionic conduction supported by the field can be due to the transfer of electrons between neighboring Fe^{2+} and Fe^{3+} ions in a strong field, so that the Fe^{2+} ions actually jump forward against the applied field.

The above results may be further evidence that oxygen vacancies are the main cause of the high leakage current in undoped BFO, and doping with higher valence ions reduces DC conductivity. However, this result can also be associated with a change in the microstructure, since the grain size decreases with titanium doping, which can also lead to a decrease in conductivity.

Ferroelectric loops and leakage currents of samples doped with cobalt and titanium are shown in **Figure 4.6**. At low concentrations of titanium and cobalt, it is possible to combine the positive aspects of both dopants: a decrease in the coercive field, due to cobalt, and a decrease in leakage current due to titanium. With an increase in the titanium concentration, the leakage currents decrease even more, but this also leads to a strong increase in the coercive field. For a sample with 0.5-0.5 at% Co-Ti, it can be seen that the effect of cobalt to increase conductivity dominates over the effect of adding titanium.

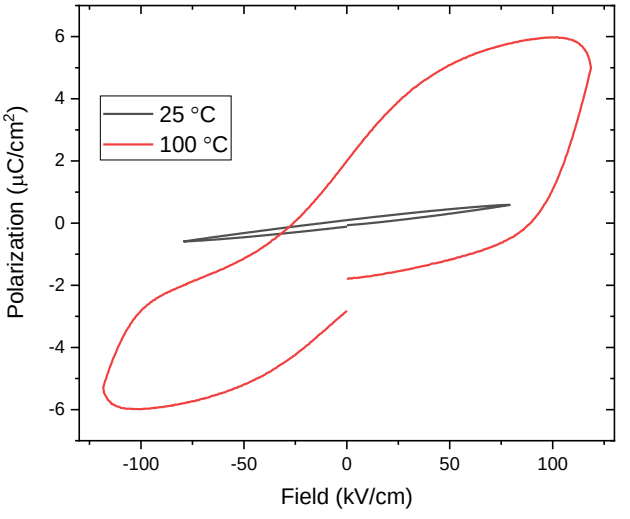

Figure 4.3 – Ferroelectric hysteresis loops of pure BFO ceramic samples at two temperatures

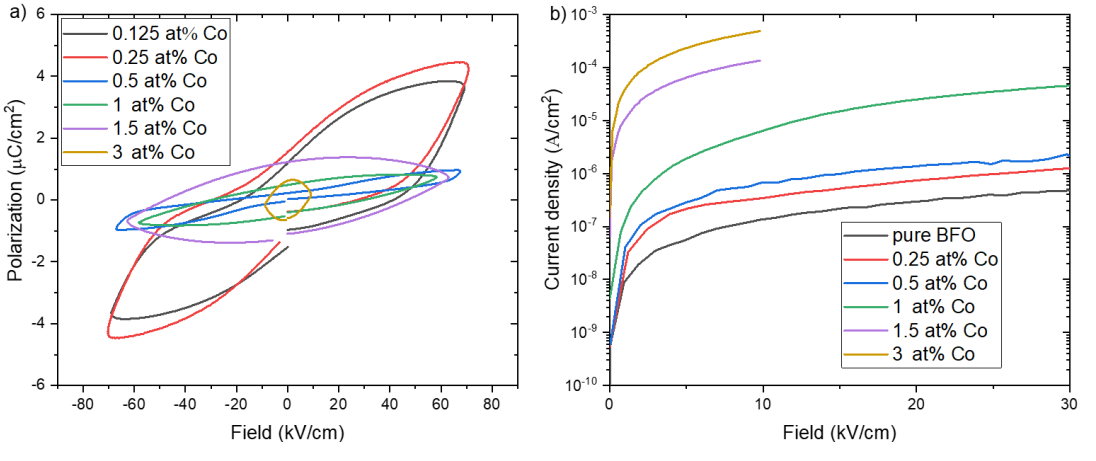

Figure 4.4 – a) Ferroelectric hysteresis loops and b) leakage current density of Co-doped BFO ceramic samples

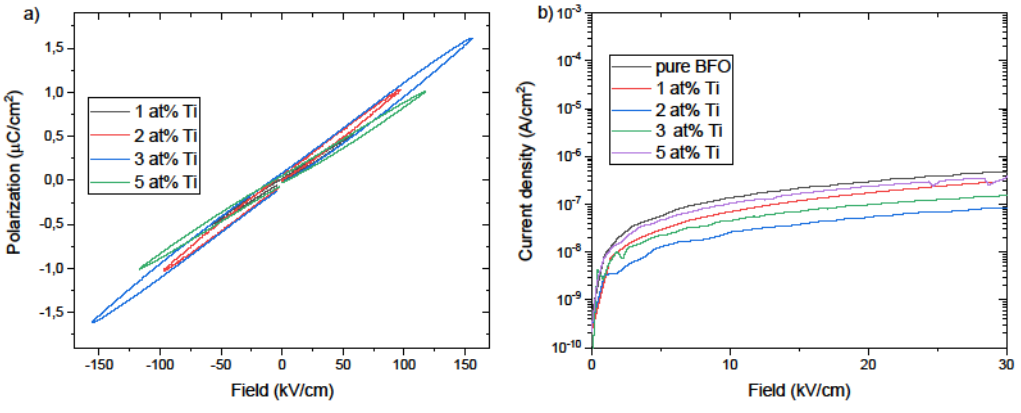

Figure 4.5 – a) Ferroelectric hysteresis loops and b) leakage current density of Ti-doped BFO ceramic samples

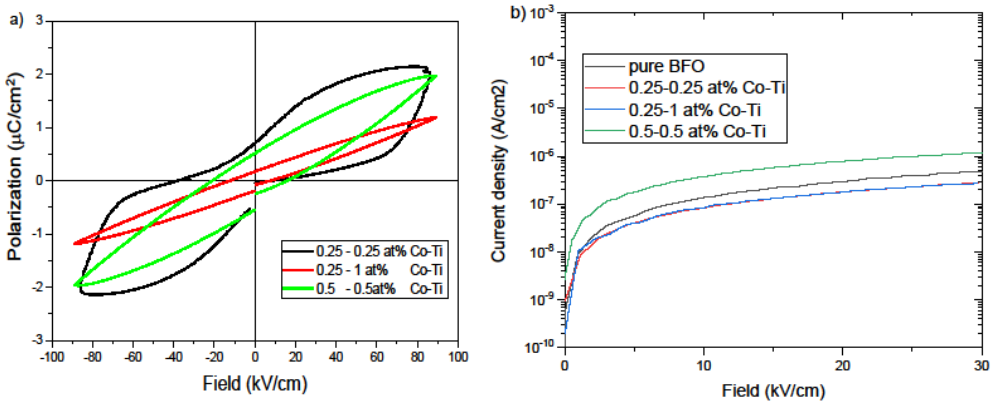

Figure 4.6 – a) Ferroelectric hysteresis loops and b) leakage current density of Co-Ti dual-doped BFO ceramic samples

4.3.4 PIEZOELECTRIC

Table 4.1 shows the piezoelectric and electrical properties of undoped and doped BFO samples. All samples were polarized at the maximum field ($\mathbf{E_p}$) at which no electrical breakdown occurs yet. As always, the piezoelectric properties of materials are dependent on their insulating properties which limit the maximum poling field that can be applied.

Thus, the low piezoelectric properties of undoped BFO can be explained by the high coercive field and the inability to reach it due to high leakage currents. Increasing the temperature during poling greatly increases the risk of electrical breakdown and cannot be used due to damage of samples. As we can see, with an increase in the concentration of cobalt, due to an increase in leakage current, the dielectric strength of the material also decreases, which leads to a decrease in the maximum field $\mathbf{E_p}$ that can be applied. However, at low concentrations of cobalt, this did not interfere with the successful polarization of the ceramics and led to a piezoelectric coefficient of 43 pC/N being achieved for samples with 0.25 at% Co.

On the other hand, doping with titanium at low concentrations increases the dielectric strength of the samples in comparison with that of undoped BFO. But even with a polarization at 130 kV/cm, piezoelectric properties were not obtained. With a subsequent increase in the concentration of titanium, the dielectric strength still decreases, but at higher concentrations compared to cobalt.

The results obtained are inconsistent with the typical behavior of piezoelectric ceramics upon doping with donors and acceptors and demonstrate opposite results, such as softening upon doping with a donor and hardening upon doping with an acceptor. In this regard, the results with samples doped with cobalt are of particular interest, since, despite the fact that leakage currents inevitably increase, the piezoelectric properties increase significantly. However, with a further increase in the concentration of cobalt, piezoelectric constant again decreases to zero, because we cannot impose a polarization field higher than the coercive field. An increase in piezoelectric properties by doping BFO with Co can be described as a softening of piezoelectric ceramics and a decrease in the coercive field, which some authors associate with an increase in the mobility of domain walls with an increase in their conductivity [23]. Whereas Ti doping, which reduces all types of conductivity and reduces the grain size of the ceramics, leads to a result where the coercive field increases even more, which completely destroys the effective piezoelectric properties.

Dual doping with cobalt and titanium, while maintaining the effect of reducing the required field to obtain piezoelectric properties, also reduces the dielectric loss of the resulting ceramic. The proposed explanation is that cobalt

presumably binds oxygen vacancies near the domain walls, increasing their conductivity and hence mobility. Whereas titanium evenly distributed throughout the sample reduces the overall conductivity of the BFO. By optimizing the concentration of both dopants, we managed to achieve a piezoelectric constant of 40 pC/N with dielectric losses below 1%

Table 4.1 – Summary of piezoelectric and electrical properties at room temperature

Composition	**E_p (kV/cm)**	**d_{33} (pC/N)**	**ε_r (-)**	**tan δ(-)**
BFO	100	9	80	0.005
BFO 0.125 at% Co	60	40	70	0.008
BFO 0.25 at% Co	60	43	80	0.017
BFO 0.5 at% Co	60	36	80	0.033
BFO 1.0 at% Co	30	-	80	0.166
BFO 1.5 at% Co	10	-	100	0.458
BFO 3.0 at% Co	10	-	130	0.939
BFO 1 at% Ti	130	1	100	0.006
BFO 2 at% Ti	110	1	110	0.006
BFO 3 at% Ti	60	-	110	0.007
BFO 5 at% Ti	60	-	115	0.007
BFO 0.25-0.25 at% Co-Ti	90	40	95	0.009
BFO 0.25-1 at% Co-Ti	90	2	100	0.014
BFO 0.5-0.5 at% Co-Ti	90	5	100	0.018

These results show that the correct manipulation of defects in the BFO ceramics allows tuning the piezoelectric and electrical properties, which in the future may allow the use of these ceramics at elevated temperatures conditions given its high Curie temperature in case the high electrical conductivity at high temperatures can be mitigated.

4.5 CONCLUSIONS

In this work, we studied the effect of doping BFO with cobalt and titanium on the electrical conductivity and piezoelectric properties. We found that doping with cobalt leads to a decrease in the coercive field of the piezoelectric ceramic and an increase in electrical conductivity. This effect is presumably associated with an increase in the concentration of oxygen vacancies due to the acceptor nature of doping. The decrease in the coercive field of the piezoceramics makes it possible to achieve the maximum possible piezoelectric constant in the region of 43 pC/N with a relatively small polarizing field in the region of 60 kV/cm.

Doping with titanium leads to a decrease in conductivity, which can be explained by a decrease in the concentration of oxygen vacancies. Also, doping with titanium significantly reduces the piezoelectric properties of BFO.

Dual doping with cobalt and titanium combines the positive effects of both dopants, such as a decrease in the coercive field for polarization, and an increase in the insulating properties of the material. When both elements are used simultaneously at their appropriate levels (0.25 at% each) a piezoelectric ceramic material is obtained that requiring a low field for full poling (90 kV/cm) and showing excellent room temperature performance such as a d_{33} = 40 pC/N, a dielectric constant in the region of 100 and dielectric losses less than 1%.

4.6 SUPPORTING INFORMATION

Table 4.1S – Results of Rietveld's refinement of pure and doped BFO samples

System	a(Å)	b(Å)	c(Å)	Volume (Å^3)	Bragg R factor
BFO	5.58123(2)	5.58123(2)	13.87698(1)	374.356(4)	5.83
0.125 at% Co	5.57531(24)	5.57531(24)	13.87268(72)	373.447(30)	2.29
0.25 at% Co	5.58169(13)	5.58169(13)	13.88015(64)	374.504(21)	2.68
0.5 at% Co	5.57957(8)	5.57957(8)	13.86793(36)	373.891(12)	1.06
1 at% Co	5.58578(8)	5.58578(8)	13.88686(36)	375.234(12)	8.69
1.5 at% Co	5.58123(7)	5.58123(7)	13.87851(27)	374.398(10)	6.98
3 at% Co	5.57419(4)	5.57419(4)	13.85378(18)	372.789(6)	0.65
1 at% Ti	5.58883(4)	5.58883(4)	13.88907(16)	375.704(6)	2.18
2 at% Ti	5.59455(7)	5.59455(7)	13.89853(30)	376.730(11)	0.62
3 at% Ti	5.59217(10)	5.59217(10)	13.89302(45)	376.260(16)	9.62
5 at% Ti	5.58452(15)	5.58452(15)	13.84841(66)	374.026(23)	1.28
0.25-0.25 at% Co-Ti	5.58389(10)	5.58389(10)	13.88652(39)	374.972(14)	2.61
0.5-0.5 at% Co-Ti	5.58314(12)	5.58314(12)	13.87736(42)	374.539(11)	1.73
0.25-1 at% Co-Ti	5.58244(18)	5.58244(18)	13.86805(57)	374.278(23)	0.84

Table 4.2S – Average grain size and density of pure and doped BFO samples

Composition	Grain size (microns)	Density (g/cm^3)	Relative Density (%)
BFO	2	7.9	95
BFO 0.125 at% Co	3.8	7.6	91
BFO 0.25 at% Co	3.8	7.8	94
BFO 0.5 at% Co	3.7	7.8	94
BFO 1.0 at% Co	5.7	7.8	94
BFO 1.5 at% Co	3.8	7.9	95
BFO 3.0 at% Co	3.1	8.0	96
BFO 1 at% Ti	1.0	8.0	96
BFO 2 at% Ti	1.1	8.1	97
BFO 3 at% Ti	0.6	7.8	94
BFO 5 at% Ti	1.1	7.5	90
BFO 0.25-0.25 at% Co-Ti	1.76	7.6	91
BFO 0.5-0.5 at% Co-Ti	1.63	7.6	91
BFO 0.25-1 at% Co-Ti	0.82	7.6	91

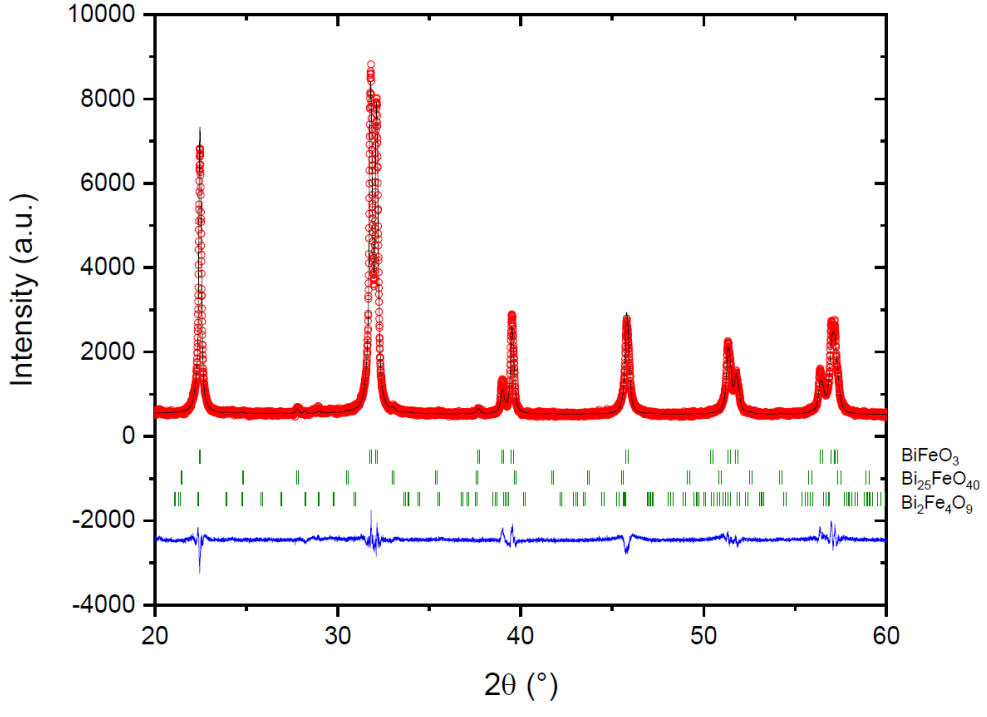

Figure 4.1S – Rietveld refinement of the XRD pattern of undoped BFO.

REFERENCES:

[1] T. Stevenson, D.G. Martin, P.I. Cowin, A. Blumfield, A.J. Bell, T.P. Comyn, P.M. Weaver, Piezoelectric materials for high temperature transducers and actuators, J. Mater. Sci. Mater. Electron. 26 (2015) 9256–9267. https://doi.org/10.1007/s10854-015-3629-4.

[2] S. Takahash, Effects Of Impurity Doping In Lead Zirconate-Titanate Ceramics, Ferroelectrics. 41 (1982) 143–156. https://doi.org/10.1080/00150198208210617.

[3] A.S. Bhalla, R. Guo, R. Roy, The perovskite structure – a review of its role in ceramic science and technology, Mat Res Innovat 4 (2000) 3–26. https://doi.org/10.1007/s100190000062.

[4] V.D. Kugel, L.E. Cross, Behavior of soft piezoelectric ceramics under high sinusoidal electric fields, J. Appl. Phys. 84 (1998) 2815–2830. https://doi.org/10.1063/1.368422.

[5] N. Horchidan, C.E. Ciomaga, R.C. Frunza, C. Capiani, C. Galassi, L. Mitoseriu, A comparative study of hard/soft PZT-based ceramic composites, Ceram. Int. 42 (2016) 9125–9132. https://doi.org/10.1016/j.ceramint.2016.02.179.

[6] M.I. Morozov, D. Damjanovic, Charge migration in Pb(Zr,Ti)O3 ceramics and its relation to ageing, hardening, and softening, J. Appl. Phys. 107 (2010). https://doi.org/10.1063/1.3284954.

[7] E.M. Bourim, H. Tanaka, M. Gabbay, G. Fantozzi, B.L. Cheng, Domain wall motion effect on the anelastic behavior in lead zirconate titanate piezoelectric ceramics, J. Appl. Phys. 91 (2002) 6662–6669. https://doi.org/10.1063/1.1469201.

[8] M.J. Schulz, M.J. Sundaresan, J. McMichael, D. Clayton, R. Sadler, B. Nagel, Piezoelectric Materials at Elevated Temperature, J. Intell. Mater. Syst. Struct. 14 (2003) 693–705. https://doi.org/10.1177/1045389X03038577.

[9] R. Palai, R.S. Katiyar, H. Schmid, P. Tissot, S.J. Clark, J. Robertson, S.A.T. Redfern, G. Catalan, J.F. Scott, β phase and γ-β metal-insulator transition in multiferroic BiFe O3, Phys. Rev. B - Condens. Matter Mater. Phys. 77 (2008) 1–11. https://doi.org/10.1103/PhysRevB.77.014110.

[10] M. Makarovic, N. Kanas, A. Zorko, K. Ziberna, H. Ursic, D.R. Smabraten, S.M. Selbach, T. Rojac, Tailoring the electrical conductivity and hardening in BiFeO3 ceramics, J. Eur. Ceram. Soc. 40 (2020) 5483–5493. https://doi.org/10.1016/j.jeurceramsoc.2020.06.037.

[11] G.D. Hu, S.H. Fan, C.H. Yang, W.B. Wu, Low leakage current and enhanced ferroelectric properties of Ti and Zn codoped BiFe O3 thin film, Appl. Phys. Lett. 92 (2008) 90–93. https://doi.org/10.1063/1.2918130.

[12] X. Qi, J. Dho, R. Tomov, M.G. Blamire, J.L. MacManus-Driscoll, Greatly reduced leakage current and conduction mechanism in aliovalent-ion-doped BiFeO3, Appl. Phys. Lett. 86 (2005) 1–3. https://doi.org/10.1063/1.1862336.

[13] T. Rojac, A. Bencan, B. Malic, G. Tutuncu, J.L. Jones, J.E. Daniels, D. Damjanovic, BiFeO3 ceramics: Processing, electrical, and electromechanical properties, J. Am. Ceram. Soc. 97 (2014) 1993–2011. https://doi.org/10.1111/jace.12982.

[14] J. Walker, H. Ursic, A. Bencan, B. Malic, H. Simons, I. Reaney, G. Viola, V. Nagarajan, T. Rojac, Temperature dependent piezoelectric response and strain-electric-field hysteresis of rare-earth modified bismuth ferrite ceramics, J. Mater. Chem. C. 4 (2016) 7859–7868. https://doi.org/10.1039/c6tc02000c.

[15] S.J. Kim, S.H. Han, H.G. Kim, A.Y. Kim, J.S. Kim, C. Il Cheon, ? Multiferroic properties of Ti-doped BiFeO3 ceramics, J. Korean Phys. Soc. 56 (2010) 439–442. https://doi.org/10.3938/jkps.56.439.

[16] R.D. Levi, Y. Tsur, The effect of oxygen vacancies in the early stages of BaTiO3 nanopowder sintering, Adv. Mater. 17 (2005) 1606–1608. https://doi.org/10.1002/adma.200401859.

[17] T. Rojac, M. Kosec, B. Budic, N. Setter, D. Damjanovic, Strong ferroelectric domain-wall pinning in BiFeO3 ceramics, J. Appl. Phys. 108 (2010). https://doi.org/10.1063/1.3490249.

[18] E. Markiewicz, B. Hilczer, M. Błaszyk, A. Pietraszko, E. Talik, Dielectric properties of BiFeO3 ceramics obtained from mechanochemically synthesized nanopowders, J. Electroceramics. 27 (2011) 154–161. https://doi.org/10.1007/s10832-011-9660-9.

[19] D. Maurya, H. Thota, K.S. Nalwa, A. Garg, BiFeO3 ceramics synthesized by mechanical activation assisted versus conventional solid-state-reaction process: A comparative study, J. Alloys Compd. 477 (2009) 780–784. https://doi.org/10.1016/j.jallcom.2008.10.155.

[20] M.I. Morozov, M.A. Einarsrud, T. Grande, Atmosphere controlled conductivity and Maxwell-Wagner relaxation in Bi0.5K0.5TiO3 - BiFeO3 ceramics, J. Appl. Phys. 115 (2014) 0–6. https://doi.org/10.1063/1.4863798.

[21] T. Rojac, A. Bencan, G. Drazic, N. Sakamoto, H. Ursic, B. Jancar, G. Tavcar, M. Makarovic, J. Walker, B. Malic, D. Damjanovic, Domain-wall conduction in ferroelectric BiFeO 3 controlled by accumulation of charged defects, Nat. Mater. 16 (2017) 322–327. https://doi.org/10.1038/nmat4799.

[22] E.T. Wefring, M.A. Einarsrud, T. Grande, Electrical conductivity and thermopower of (1 - X) BiFeO3-xBi0.5K0.5TiO3(x = 0.1, 0.2) ceramics near the ferroelectric to paraelectric phase transition, Phys. Chem. Chem. Phys. 17 (2015) 9420–9428. https://doi.org/10.1039/c5cp00266d.

[23] M. Makarovic, M.Ç. Bayir, H. Ursic, A. Bradesko, T. Rojac, Domain wall conductivity as the origin of enhanced domain wall dynamics in polycrystalline BiFeO3, J. Appl. Phys. 128 (2020). https://doi.org/10.1063/5.0017374.

5

EXPLORING THE $BiFeO_3$-$PbTiO_3$-$SrTiO_3$ TERNARY SYSTEM TO OBTAIN GOOD PIEZOELECTRIC PROPERTIES AT LOW AND HIGH TEMPERATURES

ABSTRACT

In this work we investigated the piezoelectric properties of $BiFeO_3$-rich (1-(y+x))·$BiFeO_3$– y·$PbTiO_3$–x·$SrTiO_3$ (0.1 ≤ x ≤ 0.35; 0.1 ≤ y ≤ 0.3) bulk piezoceramics as this system could potentially lead to bulk piezo electric ceramics suitable for high-temperature applications. Samples with various levels of $PbTiO_3$ and $SrTiO_3$ were prepared via a conventional solid-state route. X-ray diffraction confirmed a pure perovskite phase for the compositions explored without secondary phases. It was found that the addition of comparable levels of $PbTiO_3$ and $SrTiO_3$ to the $BiFeO_3$ ceramic resulted in higher piezoelectric properties compared to those of the pure $BiFeO_3$ and binary systems. The Curie temperature was significantly reduced by dual doping, with $SrTiO_3$ and $PbTiO_3$ additions resulting in comparable Curie temperature depressions. The locations of the phase boundary between the cubic, pseudocubic and rhombohedral crystal structure was determined. The highest piezoelectric properties d_{33} of 250 pC/N at room temperature were obtained for samples with the composition x=0.3, y=0.25, i.e. close to the cubic-pseudocubic phase boundary in the phase diagram. The temperature dependence of the piezoelectric properties varied depending on the previous thermal history, yet an appropriate heat treatment resulted in almost temperature stable d_{33} value. The ceramic with the lowest temperature sensititvity and a high Curie temperature of 350 °C was found for x=0.1, y=0.2 with d_{33} of 60 pC/N at RT and 71 pC/N at 300 °C (after poling at 60 kV/cm and a stabilizing heat treatment). However, the materials developed were still unsuitable for applications at high temperatures due to a common?? rapidly increasing electrical conductivity with temperature.

5.1 INTRODUCTION

Piezoelectric sensors have long been the most efficient devices for generating and measuring dynamic forces, below or not too far above room temperature. For example, conventional ultrasonic echography measurements of the wall thickness of pipes and tanks offer an advantage over other non-destructive testing methods such as: low cost, ease of operation and the ability to conduct in-operando measurements [1]. Piezoelectric sensors are already well established for this type of application but are limited to operating temperatures of up to 260 °C [2] due to most devices relying on the ubiquitous piezoelectric ceramic lead zirconate titanate or PZT. Therefore, considerable efforts are now aimed at developing materials that can satisfy the growing demand for piezoelectric elements with an operating temperature in the range of 350-600 °C.

One such material is $BiFeO_3$ (BFO), which has an exceptionally high Curie temperature, T_C, of 825 °C [3] and the additional benefit of being lead-free in composition. This high T_C makes BFO an ideal candidate for use as a high temperature lead-free piezoceramic [1]. Unfortunately, research on bulk BFO ceramics was not as successful as it did not demonstrate high piezoelectric coefficients and had serious temperature issues. This was largely due to the high electrical conductivity at temperatures >200 °C, which limits the use of this material in real devices.

For high temperature applications in actuators, transducers, sensors, and so on, solid state solutions of $BiMeO_3$–$PbTiO_3$ with a perovskite structure have been proposed as more sensitive prospective compositions due to their high Curie temperatures (T_C), especially those systems near morphotropic phase boundaries (MPB). For example, $BiScO_3$–$PbTiO_3$ (BS–PT) system was once expected to be the substitute for PZT for high temperature applications due to the excellent performance near its MPB. However, the high cost of the raw material Sc_2O_3 made it unsuitable for commercial applications [4]. Also widely studied is the $BiFeO_3$ - $PbTiO_3$ (BFO-PT) system, which had the highest T_C (T_C at MPB, around 630 °C) in the family of binary piezoceramics based on PT. However, it was difficult to obtain mechanically strong BFO-PT ceramics due to the negative temperature coefficient of expansion and the high tetragonality, as in the case of pure PT ceramics [5]. In addition, the large tetragonal

distortion (c/a ratio 1.18) for BFO-PT solid solutions results in a large coercive field of E_c >100kV/cm, making it difficult to have them fully poled [6].

It has been reported that the reduction of E_c and c/a of BFO-PT ceramics could be achieved by the substitution of large cations [7] to weaken the hybridization [8] between Pb^{2+}/Bi^{3+} and O^{2-} ions as well as strengthening the ferroelectric activity of B-site cations.

Popular strategies for improving piezoelectric response reported in the literature include chemical modification (doping of elements, substitution or formation of new solid solutions) to reduce tetragonality, which can be achieved by replacing large cations to expand the a-axis and weakly ferroactive cations to shorten the c-axis. For example, the introduction of La, Ca, Ba, Sr into the A site, Ga, Al, Ta, Nb into the B site or the combination of $PbZrO_3$, $BaZrO_3$, $BaTiO_3$ with BFO-PT will lead to a significant decrease in the c/a ratio and a significant improvement in piezoelectric properties and in particular their mechanical stability. Most recently, BFO-PT-based ternary solid solutions, such as BFO-PT-BT, BFO-PT-BZ, and BFO-PT-BZT have attracted great attention. Preliminary experiments showed high piezoelectric properties up to 300-400 pC/N (at room temperature), with a Curie temperature of about 300-400 °C. However, these piezoceramics generally have a high coercive field up to 60-100 kV/cm, which creates difficulties in fully activating the piezoelectric properties upon poling.

The current study adopted the method of site engineering, this time introducing $SrTiO_3$ (ST) into the BFO–PT system, forming a ternary system. Despite the fact that ST itself does not possess piezoelectric properties at room temperature, it can still stabilize BFO-PT structures and decrease conductivity at RT and elevated temperature. Furthermore, solutions of BFO–ST were reported to have different structures at varying $BiFeO_3$ contents, e.g., rhombohedral between 100 and 65 mol%, pseudocubic between 67 and 20 mol% and cubic below 20 mol% of BFO [9]. The introduction of Sr^{2+} in the A site, greatly influences the Pb/Bi–O bonding interaction and thus provides the additional flexibility to tailor the dielectric, piezoelectric and mechanical properties of BFO-PT- based solid solutions.

It is well known that BFO-PT and BFO-ST both can form solid solutions near the morphotropic phase boundary (MPB) region [9]–[12]. It is widely known that all functional properties of piezo materials with compositions near the

MPB region increase due to the coexistence of two phases. For BFO-PT the two phases in equilibrium are tetragonal and rhombohedral, for BFO-ST they are rhombohedral and cubic. For BFO-PT a continuous solid solution across its entire composition range, with a rhombohedral-tetragonal MPB at 0.7-0.8 BFO has been reported.

The formation of ternary solid solutions provides additional degrees of freedom in the material design to improve the comprehensive properties and to meet various materials requirements.

In the present study, bulk ceramics with pseudo-ternary compositions of (1-(y+x))BFO – y • PT – x • ST ($0.1 \leqslant x \leqslant 0.35$; $0.1 \leqslant y \leqslant 0.3$) were explored to obtain a combination of a high Tc and good piezo properties up to elevated temperatures. The ceramics were prepared by a conventional powder sintering method. The objectives of this study were: (1) to obtain high-strength piezo ceramics with a low electrical consductivity at room temperature and a suitable coercive field for complete polarization, (2) to study the softening effect of ST on BFO-PT ceramics and determine the position of the phase boundary, and (3) to study the temperature dependence of the piezoelectric and electrical properties for the most promising systems.

5.2 EXPERIMENTAL PROCEDURE

$BiFeO_3$-$PbTiO_3$-$SrTiO_3$ (BFO-PT-ST) samples were prepared by a conventional solid-state reaction process using analytical-grade powders as raw materials: Bi_2O_3, Fe_2O_3, PbO, TiO_2 and $SrCO_3$. All powders were ground separately before weighing and mixing. Grinding and mixing were performed using yttria stabilized ZrO_2 balls in isopropanol medium in polypropylene containers. The powders were dried and calcined at 775 °C for 1 h using a heating rate of 600 °C/h. After slow cooling the calcined powders were reground, granulated by mixing with 2 wt% QPAC 40 binder, and RT pressed uniaxial into disks (13 mm in diameter and about 1 mm in thickness) using a compaction pressure of 200-250 MPa. The final synthesis and sintering were performed at 1025, 1050 or 1075 °C for 1 h, depending on the system composition. Sintering parameters were optimized to achieve the highest density. In total 15 different compositions were explored.

Scanning Electron Microscope (SEM) images were taken using a Jeol JSM 7500F field emission scanning electron microscope. Prior to SEM measurements a

thin (15 nm) layer of gold was deposited on the sample. To determine the phase purity X-ray diffraction studies with Cu Kα radiation were done using a Rigaku MiniFlex tabletop XRD analyser. X-ray diffraction studies with Cu Kα radiation were done using a Bruker D8 Discover diffractometer at elevated temperatures. Scans were recorded at set temperatures: RT, 200 to 700 °C in steps of 25 °C for chosen systems. The density was determined by the Archimedes' method in an aqueous medium.

For electrical characterization, the samples were polished, coated with silver paste (DuPont 5220) and fired at 150 °C for 20 min. Polarization–electric field hysteresis loops were measured at room temperature by a Radiant precision ferroelectric analyzer. The samples were poled under a DC electric field of 20-80 kV/cm for 20 min in silicone oil at room temperature. After aging for 24 h, the piezoelectric constant d33 was measured with a quasi-static piezoelectric d33 meter. The Curie temperature was determined indirectly by determining the depolarization temperature. The electrical properties of samples at room temperature were measured using an Agilent 4263B LCR meter at 1 kHz and 1 V.

Measurements of the high-temperature piezoelectric constant were carried out by a direct method using a laboratory setup from Kistler Instrumente AG at their lab in Winterthur. To this aim samples were clamped between two Al_2O_3 discs with static preload of 1 MPa (100 N). To measure the piezoelectric response a dynamic load of 0.1 MPa (10 N) with a frequency of 1, 2, 5, 10, 20 , 50, 100 Hz was applied. Such measurements were performed at 22, 50, 100, 150, 200, 250, 300, 350 °C. When changing the temperature either during heating or cooling, the preload was removed. Up to 5 temperature cycles up to increasing maximum temperatrures have been performed to check the stability of the temperature dependency of the properties.

5.3 RESULTS

5.3.1 MICROSTRUCTURE AND CRYSTAL STRUCTURE

Figure 5.1 show two illustrative SEM images of a fresh fracture surface for the 0.6BFO-0.2PT-0.3ST ceramic. The surface features of the broken granules shows equiaxed grains and randomly oriented domains and it can be seen that they have rather large dimensions of more than 100 nm. The grain size was determined from SEM images measuring a large number of grains. The

microstructure of ceramics does not depend much on the composition as shown in Supporting Information **Figure 5.1S**. All binary and ternary ceramics produced in this work exhibit an average grain size of about 4-7 μm. An earlier study on BFO-PT ceramics reported a grain size of about 1 μm [1], while single-phase BFO sintered to a fully dense state could have a grain size of 10 μm [2]. The increase in the grain size in the ternary system with respect to the binary system might be due to a decrease in tetragonality upon the addition of ST. The relative density of the samples made was at least 97%. No correlation between sintered density and composition was observed.

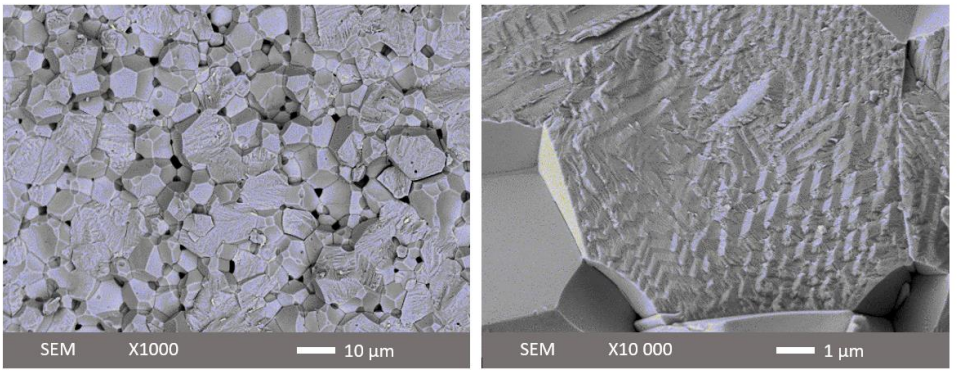

Figure 5.1 – (SEM) images of a fractured $0.6BiFeO_3$-$0.2PbTiO_3$-$0.3SrTiO_3$ ceramic after sintering

Table 5.1 shows the unit cell parameters for all obtained compositions. The material crystallises in a rhombohedral perovskite structure type with space group R3c at low $SrTiO_3$ concentrations and undergoes a change to a pseudocubic structure at high concentrations of $SrTiO_3$. All ceramics are found to exhibit a single-phase perovskite structure with no detectable secondary phases, indicating that the BFO-PT-ST have formed a stable ternary perovskite solid solution. All systems could be classified into 3 possible types: cubic (C), pseudocubic (PC) and rhombohedral (Rh). We will consider a system to be of the rhombohedral type when the rhombohedral angle γ_{rh} is less than 89.95; of the pseudocubic type when γ_{rh} is close to 90 degrees but piezoelectric properties are still present; of the cubic type when γ_{rh} is 90 degrees and there are no piezoelectric properties. It can be seen from the obtained data that the addition of ST increases the symmetry of the unit cell.

It can be assumed that there should be a morphotropic phase boundary (MPB) or polymorphic phase boundary (PPB) region in the BFO-PT-ST ternary system. It is located at the edge of the compositional domain where we have detected the pseudocubic crystal structure (0.45BFO-0.20PT-0.35ST; 0.50BFO-0.15PT-0.35ST; 0.40BFO-0.25PT-0.35ST).

Table 5.1 – Unit cell parameter in hexagonal and tetragonal representation (C – cubic, PC – pseudocubic, Rh – rhombohedral, a_h, a_{rh}, c_h, γ_{rh} – unit cell parameters in h-hexagonal and rh-rhombohedral representation)

	Composition	*Type*	a_h (Å)	c_h (Å)	a_{rh} (Å)	γ_{rh} (deg)
I	0.40BFO-0.20PT-0.40ST	C	5.634	13.802	3.9846	90.001
	0.45BFO-0.20PT-0.35ST	PC	5.635	13.803	3.9846	89.998
	0.50BFO-0.20PT-0.30ST	PC	5.637	13.809	3.9861	89.995
	0.55BFO-0.20PT-0.25ST	PC	5.635	13.811	3.9862	89.991
	0.60BFO-0.20PT-0.20ST	PC	5.637	13.813	3.9864	89.984
	0.70BFO-0.20PT-0.10ST	Rh	5.631	13.861	3.9881	89.810
	0.80BFO-0.20PT-0.00ST *	Rh	5.624	13.904	3.9891	89.645
II	0.70BFO-0.00PT-0.30ST*	PC	5.597	13.727	3.9594	89.952
	0.55BFO-0.15PT-0.30ST	PC	5.635	13.811	3.9862	89.991
	0.50BFO-0.20PT-0.30ST	PC	5.637	13.809	3.9861	89.995
	0.45BFO-0.25PT-0.30ST	PC	5.636	13.804	3.9848	89.997
	0.40BFO-0.30PT-0.30ST	PC	5.641	13.808	3.9859	89.995
III	0.40BFO-0.25PT-0.35ST	C	5.639	13.811	3.9856	90.00
	0.50BFO-0.15PT-0.35ST	PC	5.635	13.811	3.9862	89.991
	0.55BFO-0.10PT-0.35ST	C	5.641	13.813	3.9863	90.00
	0.60BFO-0.15PT-0.25ST	PC	5.637	13.813	3.9864	89.984
	0.50BFO-0.25PT-0.25ST	PC	5.636	13.813	3.9867	89.989
	0.70BFO-0.10PT-0.20ST	Rh	5.635	13.829	3.9872	89.932
	0.70BFO-0.10PT-0.10ST	Rh	5.631	13.861	3.9881	89.810

5.3.2 PIEZO- AND FERROELECTRIC PROPERTIES AT ROOM TEMPERATURE

Figure 5.2 shows the dependence of d_{33} at room temperature on the composition. It can easily be seen that an increase in piezoelectric properties occurs upon transition from a pseudocubic to a cubic crystal structure at a ST concentration of about 0.3. With a further increase in the ST concentration, although the transition from the pseudocubic to cubic phase does not occur yet, the piezoelectric properties decrease.

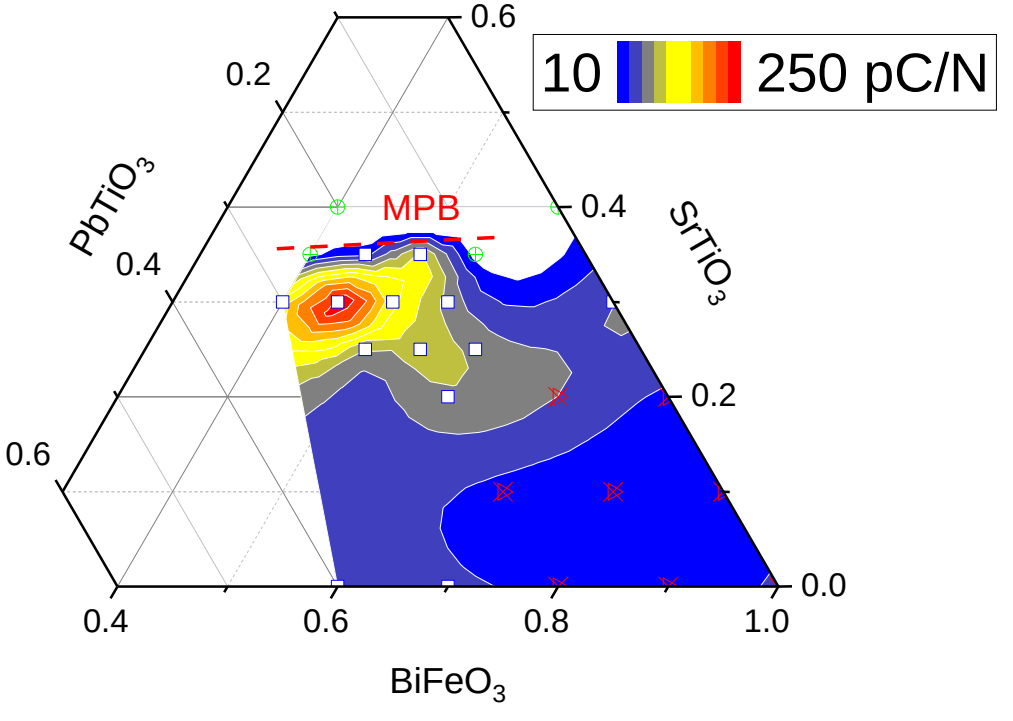

Figure 5.2 – Values for the piezoelectric constant at room temperature for the ternary diagram of BFO-PT-ST (square – pseudocubic PC; triangle – rhombohedral Rh; circle – cubic C)

Figure 5.3 shows the variation of the Curie temperature with compositions in the BFO-PT-ST system. From **Figure 5.3**, it is evident that the Curie temperature decreases with decreasing BFO level. The range of Curie temperatures measured for these ternary systems is rather wide compared to

those of modified PZT systems. The composition near the phase boundary showed a low Curie temperature down to 30°C, while as the concentration of ST decreases, it rises quite rapidly up to 600 °C at 0.1 mol ST. The difference in the contour plot between **Figure 5.2** and **5.3** (Especially for high concentrations of BFO) can be rationalized by taking into account that for some compositions it was not possible to measure the piezoelectric constant, due to difficulties in prior polarization, as some BFO-based piezoceramics had a high coercive field, which made proper poling impossible. It should be pointed out that piezoelectric properties in samples depend not only on the crystallographic structure and composition, but also on the polarizability of the material. A proper analysis of compositional effects requires that proper poling has been achieved in all samples. In the present work all poling was done at room temperature with a maximum field strength of 50 kV/mm. The poling aspect will be further discussed in the Discussion section.

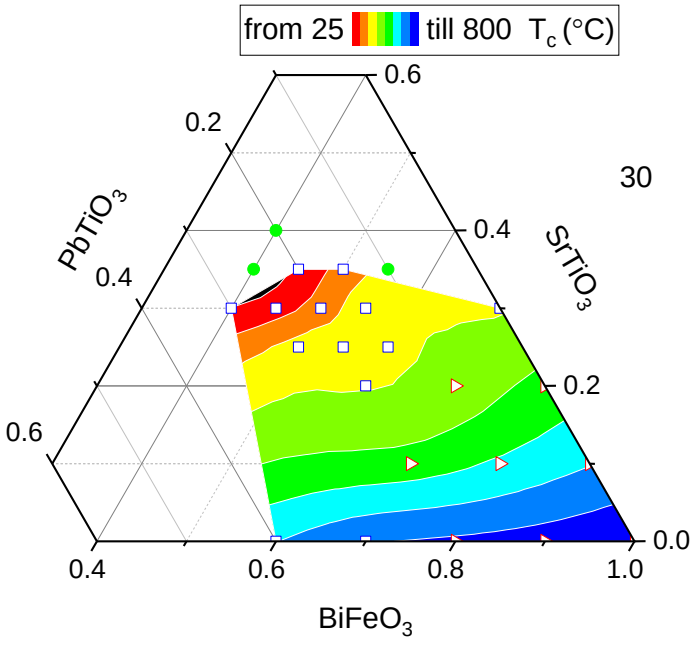

Figure 5.3 – Isothermal map of Curie temperatures with various compositions in BFO-PT-ST ternary system (square – pseudocubic PC; triangle – rhombohedral Rh; circle – cubic C)

Figure 5.4 shows the correlation between the piezoelectric constant at room temperature and the Curie temperature for the ternary compositions explored As can be seen from **Figure 5.4**, there is a clear and seemingly unique correlation between the Curie temperature and the piezoelectric properties over the composition ranges explored. To put these values into perspective the figure also shows the piezoelectric charge constants of commercial high-temperature piezoceramics: lead-based and lead-free. Although lead-based piezoceramics have high piezoelectric properties, they are limited to about 200-300 °C, while lead-free ceramics allow this barrier to be exceeded by sacrificing high piezoelectric properties. For some concentrations the ternary systems obtained in this study can compete with commercial materials.

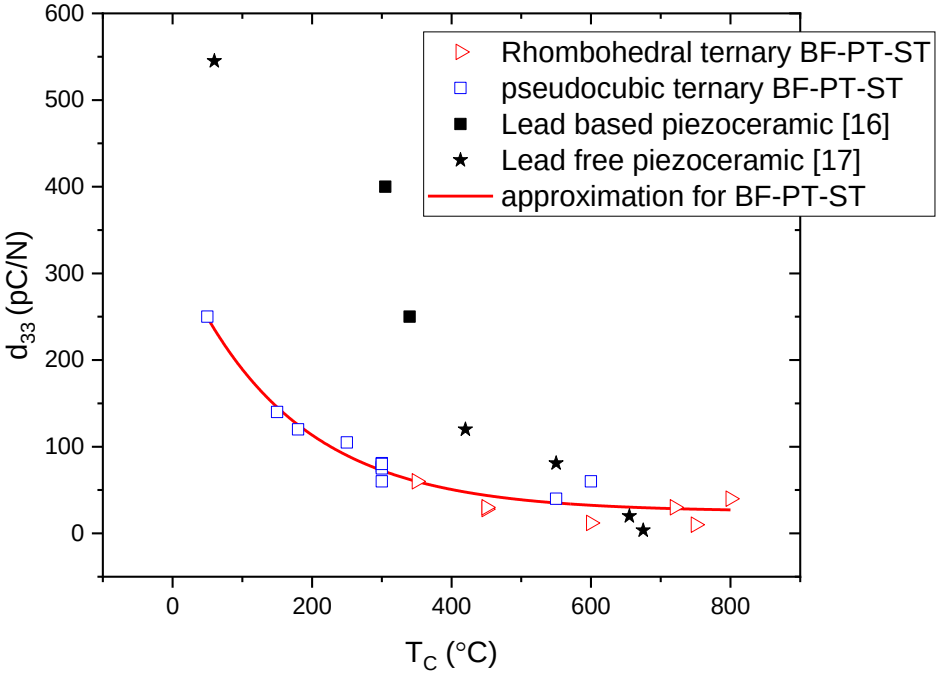

Figure 5.4 – Relationship piezoelectric properties at room temperature and Curie temperature.

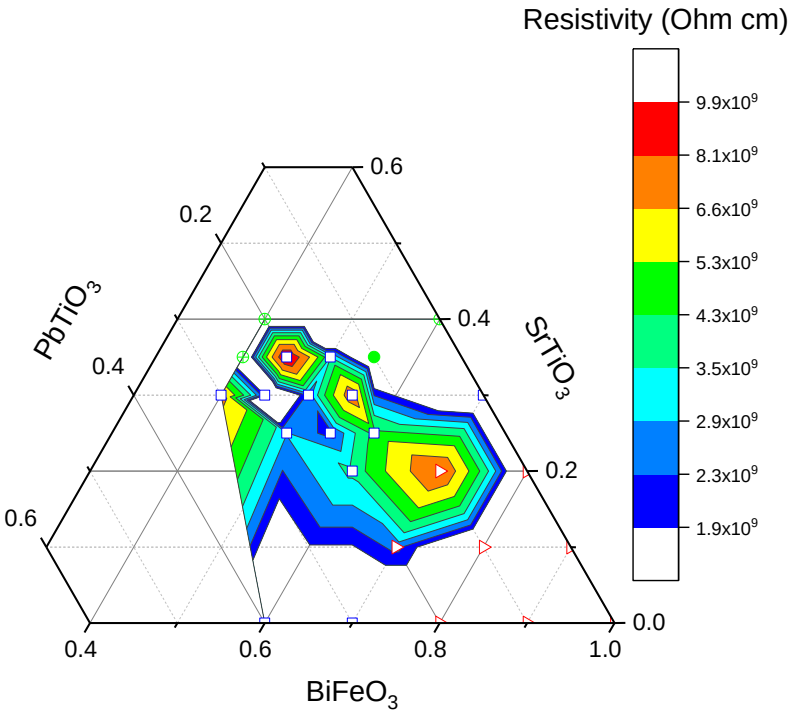

Figure 5.5 – Electrical resistivity at room temperature for ternary diagram of BFO-PT-ST. The symbols correspond to the crystal structure as listed in **Figure 5.3**.

Figure 5.5 presents the electrical resistivity values at room temperature for the compositions studied in the BFO-PT-ST system. At room temperature, all samples have a high resistivity in excess of 2. 10^9 Ohm.cm. The variations between the various samples show no obvious correspondence to crystal structure and may be due to slight variations in sintering temperature, precursor stoichiometry, presence of impurities, or moisture that occurred during laboratory sample preparation.

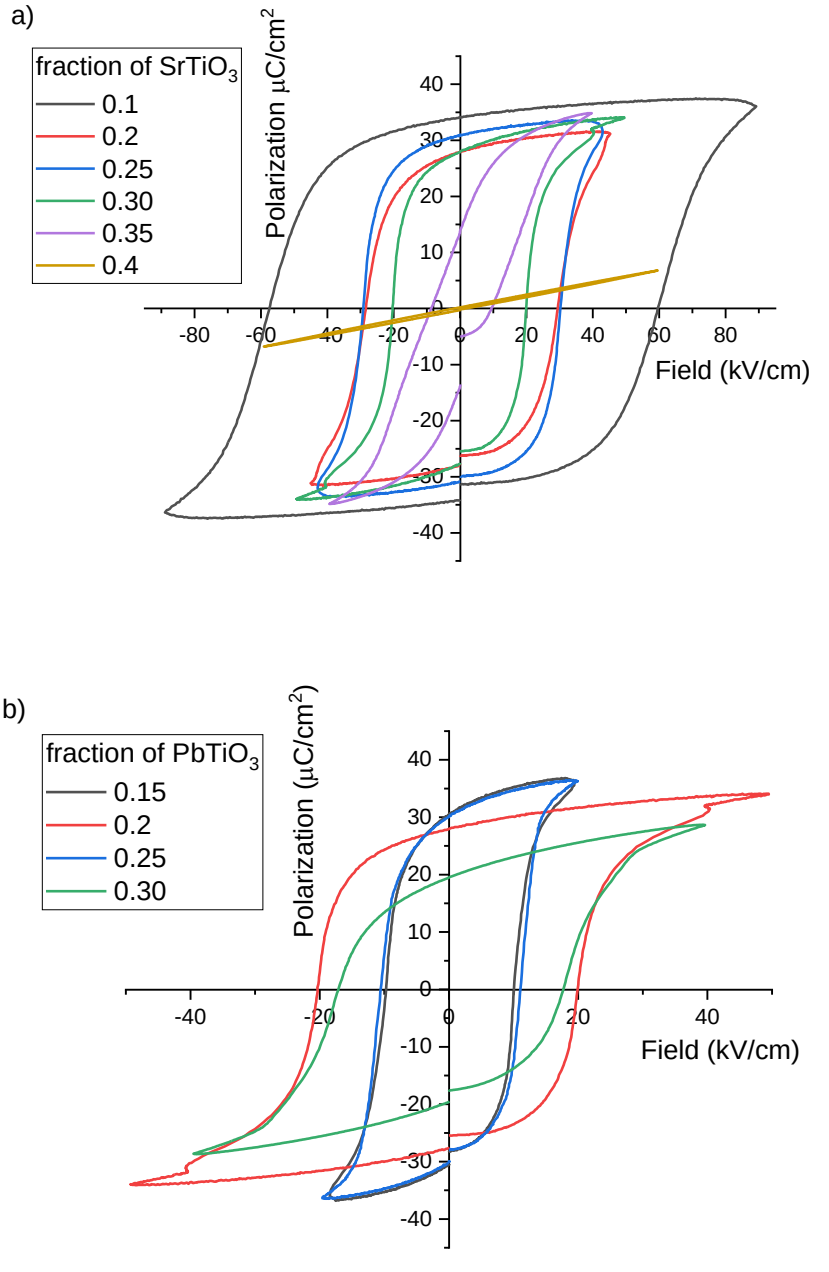

Figure 5.6 – Polarization-electric field (P-E) hysteresis loop of the BFO-PT-ST sintered ceramics with a) a fixed PT concentration (0.2PT) and b) a fixed ST concentration (0.3ST)

It was noted earlier that the piezoelectric properties depend not only on the composition and coupled to this to the Curie temperature, but also on the poling ability of the samples. Hence it is important to determine the coercive field for the newly synthesized ceramics. **Figure 5.6** shows P-E hysteresis loops measured at 5 Hz at room temperature for ceramics with different concentrations of ST or PT. The difference in the resulting changes in the ferroelectric properties is obvious. With an increase in the ST concentration at a fixed PT concentration, the remnant polarization does not change, while the coercive field strongly decreases with an increase in the ST concentration, till it disappears at ST = 0.4. In contrast, the PT concentration not only affects the coercive field, but also the remnant polarization and the shape of the hysteresis loop. The polarization value is more gradually saturated with increasing electric field. A possible reason for this broad transition is the distribution of the locally required electric field to complete the switching mechanism, due to the coexistence of rhombohedral and tetragonal phase at pseudocubic region. The coercive field in this case varies non-linearly with the change in the PT, but it behavior is consistent with that of the Curie temperature.

5.3.3 PERFORMANCE AT ELEVATED TEMPERATURES

The effect of temperature on the piezoelectric charge constant (d_{33}) values of three fully polarized ceramic (0.8-x)BFO-0.2PT-xST (x=0.1, 0.2 and 0.3) ceramics, measured in-situ, is shown in **Figure 5.7**. These compositions were chosen to study the temperature behaviour of ceramics with significantly different Curie temperatures ($T_c \approx$ 600 °C for x=0.1; $T_c \approx$450 °C for x=0.2; $T_c \approx$350 °C for x=0.3). For each material the temperature dependence is measured in the pristine state and in three aged states (see section 5.2 and the captions). All measurements per composition were done successively on one sample each.

As the temperature increases, for the three studied compositions the piezoelectric response d_{33} also increases, with the temperature dependence being strongest for the highest ST concentration. It should also be noted that the temperature dependence of d_{33} decreases during subsequent measurement cycles. This may indicate some changes in the defect structure in the samples during annealing leading to stabilization of the piezoelectric properties. Interestingly the d_{33} value continuously increases with temperature except for one case (**Figure 5.7c**, 2nd annealing run) where the d_{33}

drops between 300 and 350 °C. This special behaviour will be explained in the Discussion.

Thermal stability was also determined by measuring d_{33} at a fixed temperature of 300 °C as a function of the holding time. The results are shown in **Figure 5.8**. As can be seen, for all three compositions, d_{33} remains stable up to around 4 10^4 seconds and then starts to decrease. The most stable ceramic is the one with the lower ST concentration, probably because it has the highest Curie temperature of 600 °C.

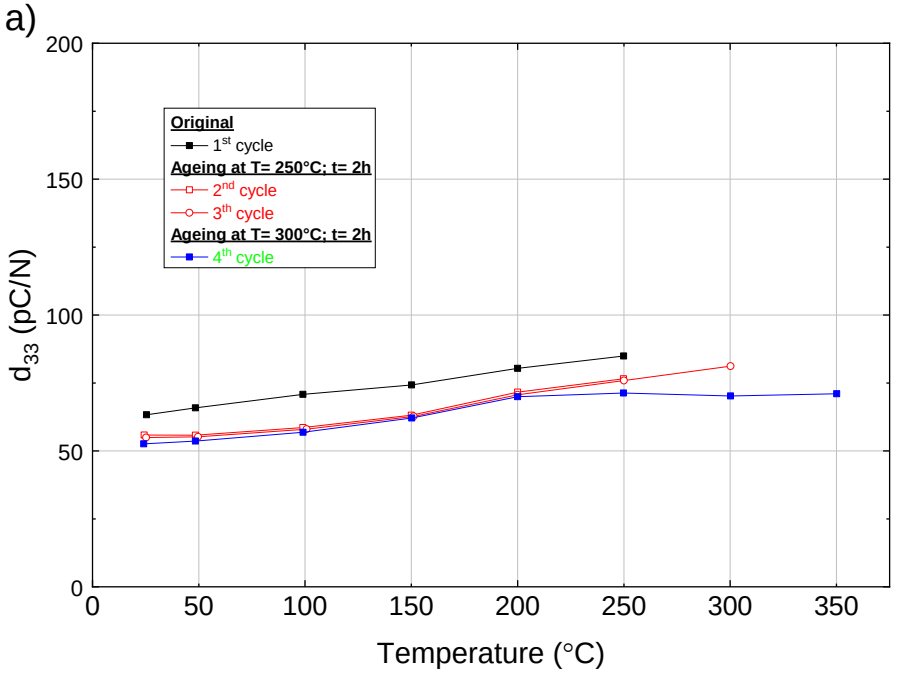

Figure 5.7 – Temperature dependence of the piezoelectric properties of the (0.8-x)BFO-0.2PT-xST ceramics for : a) x=0.1

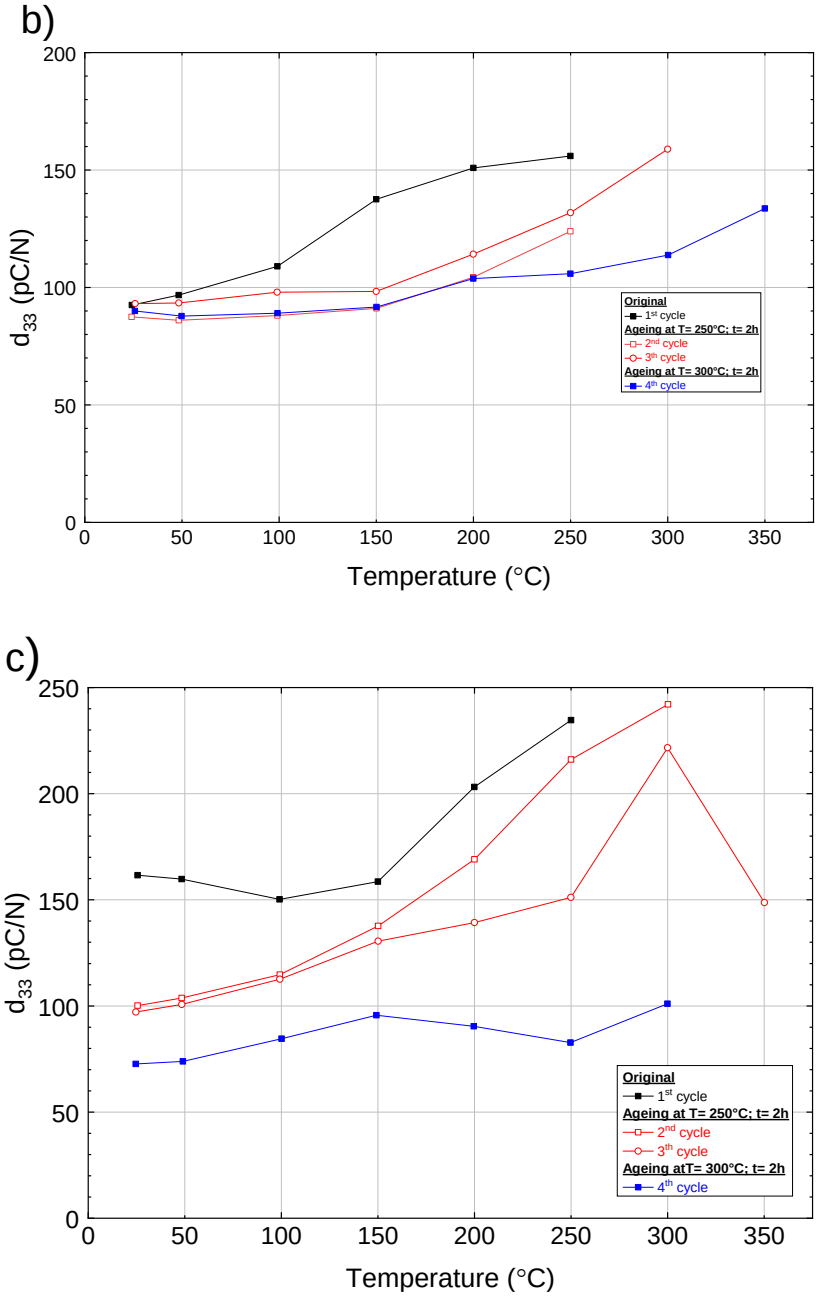

Figure 5.7 (continued) – Temperature dependence of the piezoelectric properties of the (0.8-x)BFO-0.2PT-xST ceramics for : b) x=0.2 ; c) x=0.3

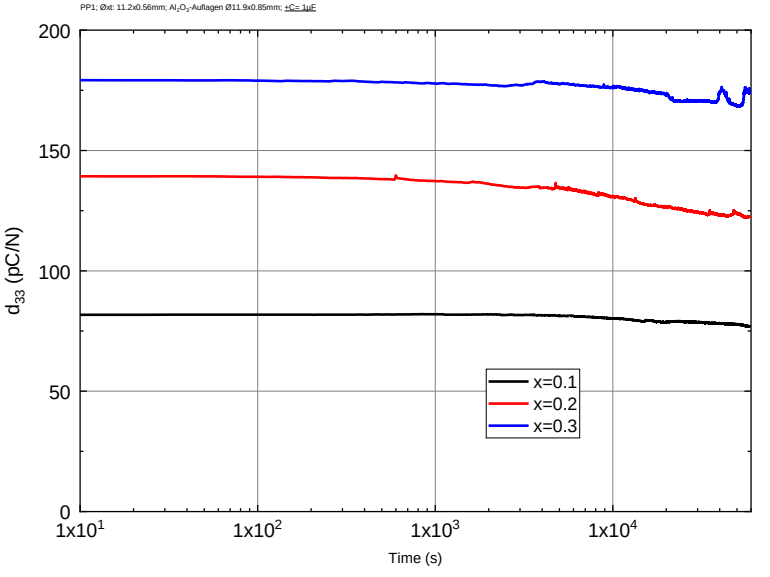

Figure 5.8 – Dependence of piezoelectric constant d_{33} on holding time at 300°C for (0.8-x)BFO-0.2PT-xST ceramics

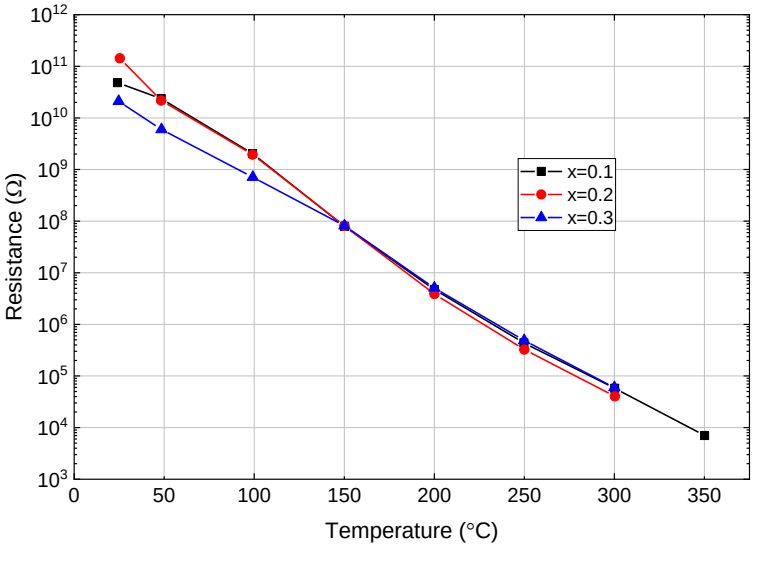

Figure 5.9 – Temperature dependence of electrical resistance for (0.8-x)BFO-0.2PT-xST ceramics

Finally, **Figure 5.9** shows the temperature dependence of the electrical resistance of the three materials studied in more depth. At room temperature, all samples exhibit comparable high-resistance characteristics, which decreases rapidly as temperature increases. The temperature dependence did not seem to depend on composition and compares with that of pure BFO [3,4]. This observed low resistance at high temperatures restricts the suitability of this type of material for applications as the amplifying electronic circuitry cannot work effectively with such conductive materials. The high electrical losses originated from defect genetation at elevated temperatures ultimately constrain the overall performance of the material. Therefore, the low resistance at high temperatures remains a critical issue that needs to be addressed in future studies.

To determine the effect of temperature on the defect dipoles and the internal bias field, the S-E loops of the poled 0.6BFO-0.2PT-0.3ST ceramics were measured at successively higher temperatures and the results are shown in **Figure 5.10** for temperatures up to 125 °C (holding time 15 min). This effect is reversible and after cooling to RT we got the asymmetric behaviour again (cooling is slow). With increasing temperature, the shape of the S-E loops gradually changes from the initial asymmetric shape to a symmetric shape; The symmetric shape being the regular shape for poled ceramics. The above results indicate that the defect dipole effect weakens with increasing the temperature. The reason is mainly due to the oxygen vacancies having a large energy to migrate at high temperature, resulting in the rearrangement of defect dipoles in the direction of the applied electric field. In this case, the defect dipoles of the poled ceramics decouple, and the internal bias field disappears, resulting in asymmetrical S-E loops. In future studies, it would be useful to study this effect at higher temperatures and the reversibility at faster cooling rates. In the experiments of **Figure 5.10** the temperature circuit was limited by the capability of the measuring setup.

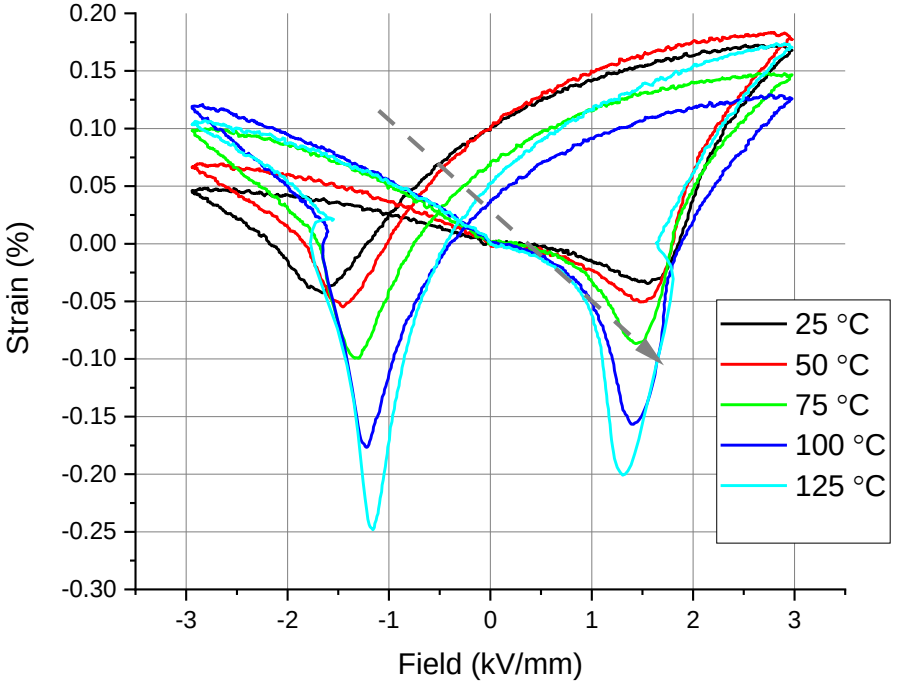

Figure 5.10 – Bipolar strain curves of the 0.5BFO-0.2PT-0.3ST ceramic measured at different temperatures

5.4 DISCUSSION

BFO-PT-ST was fabricated across the compositional space with the intention of replicating the MPB observed in PZT. The perovskite structure was formed across the entire compositional space with the absence of secondary phases. As can be seen from **Table 5.1**, the $BiFeO_3$-rich end of the phase diagram belonging to the rhombohedral phase was indexed to the R3c space group. The phase changed from pseudocubic to cubic as the concentration of BFO in the solution decreased. Similar to PZT [12], the piezoelectric properties significantly increase upon transitioning from the pseudocubic phase to the cubic phase, as opposed to the transition from the pseudocubic phase to the rhombohedral phase. As expected, this also reduces the giant tetragonality

1.18 [5] and the electric coercive field of the system near the MPB, which hinders its use in applications. Possible explanation is an increase in polling efficiency due to a decrease in the coercive field with decreasing amount of BFO in system.

The ferroelectric Curie temperature was in wide range between 30-650 °C across the entire phase diagram as can be seen in **Figure 5.3**, the depolarization temperature was also largely commensurate with the Curie temperature. High temperature stability is recorded for d_{33} until 20–50 °C below T_C. **Figure 5.4** shows that all compositions fit a simple and unique relationship between the piezoelectric properties (at room temperature) and the Curie temperature very well. It should be noted that, according to the Landau theory [6], if the system experiences a second-order phase transition, all secondary parameters (dielectric permittivity, piezoelectric coefficient) increase a lot. This also explains the absence of a jump during the transition from the rhombohedral phase to the pseudocubic one, since this is a first-order phase transition.

Based upon this preliminary research into the BFO-PT system [11][12][15] it was hypothesized that the partial substitution of ST may reduce long-range non-centrosymmetric structural order and enhanced piezoelectric performance. This could provide an explanation for the potential relationship between the increase in properties with similar ST and PT contents. Moreover, the influence of the relative concentrations of ST and PT on the crystal structure and the resultant piezoelectric properties merits further investigation.

The selected compositions for the d_{33} test at elevated temperatures demonstrated an increase in the magnitude of the d_{33} coefficient as the temperature increases, consistent with the Landau theory [6]. The d_{33} coefficient exhibited strong temperature dependence, as depicted in **Figure 5.7** for compositions in the vicinity of the MPB. The increase of the piezoelectric charge coefficients d_{33} with increasing temperature is observed in many ferroelectrics including barium titanate and PZT [10,11]. Such an increase has also been reported in the binary $BiScO_3$-$PbTiO_3$ solid solutions [12].

The ternary system with the highest ST content displayed a prominent peak (i.e., the d_{33} coefficient increased by two times compared to room temperature)

in piezoelectric properties at 300 °C. This observation was attributed to a phase transition, as the Curie temperature for this sample was determined to be in the region of 350 °C.

Based on the obtained data, it is concluded that the sample 0.7BFO-0.2PT-0.1ST can be utilized up to a temperature of 350 °C, 0.6BFO-0.2PT-0.2ST up to 150-200 °C, and 0.5BFO-0.2PT-0.3ST only at room temperature. At these maximum use temperatures, the d_{33} coefficient does not vary by more than 10%. But in contrast to PZT the depolarization temperature is relatively high and approaches the phase transition temperature. The unusual enhancement of the d_{33} which we observe at 250-300 °C in the 0.5BFO-0.2PT-0.3ST ceramics can be practically useful. These findings provide important insights for the selection of appropriate compositions for piezoelectric applications under varying temperature conditions. However the risk of depolarization in the vicinity of a phase transition can be a strong obstacle for practical applications at such high temperatures.

In practical applications, the repeatability of the material's d_{33} during thermal cycling is maybe even more significant than the magnitude of its change. After several annealing cycles, as shown on **Figure 5.7**, not only d_{33} at room temperature decreased, but also the temperature dependence became weaker. As for example for the sample 0.6BFO-0.2PT-0.2ST: in the first annealing cycle, noticeable changes in d_{33} occur upon reaching a temperature of 150 °C, while during the second or third cycle this occurs already in the region of 200–250 °C. And for a sample 0.5BFO-0.2PT-0.3ST: during annealing up to 300 °C, the d_{33} curves did not change, apart from after the 3rd cycle, when the temperature exceeded 350 °C (which is presumably higher than the Curie temperature). Hence in the fourth cycle the piezoelectric response was significantly reduced. However, once this treatment was received the sample became more stable and showed no peaks in d_{33} at 300 °C. Similar results are seen when analyzing the bipolar strain curve; as the sample is heated, the stress asymmetry vanishes. This effect can presumably be explained by the domain pinning by oxygen defects similar to what occurs in hard-PZT ceramics [13–15]. When, at elevated temperatures, oxygen defects become more mobile and start concentrating on domain walls, thereby reducing the dipole moment (as a consequence of d_{33}) but also preventing reorientation of domains (domain pinning) at lower temperatures, which leads to stabilization of d_{33}. As can been

seen from **Figure 5.8** is interesting that the decrease in piezoelectric properties at elevated temperatures does not occur immediately, but after some time. It is possible that defects need time to diffuse to the domain walls and accumulate before a noticeable effect appears.

Although for all materials synthesized the electrical conductivity was high and adequate for use in sensors, the observed high electrical conductivity of the studied material at elevated temperatures, as shown on **Figure 5.9**, remains problematic. Varying the ST level had no noticeable effect on the temperature dependence of conductivity. Consequently, this makes the material unsuitable for high-temperature applications where stability and low electric conductivity are key factors. The high electrical conductivity may have originated from intrinsic defects or impurities present in the material. Further studies may be conducted to elucidate the origin of the high electrical conductivity, and potentially mitigate this undesired effect in the material.

5.5 CONCLUSIONS

$BiFeO_3$-rich $BiFeO_3$-$PbTiO_3$-$SrTiO_3$ bulk piezoceramics with a perovskite structure can be made using a conventional solid-state process with density >97%. In perovskite $BiFeO_3$ ceramic – $PbTiO_3$ and $SrTiO_3$ were well-soluble at least until 35mol%; no secondary phases were discovered. For samples close to the cubic-pseudo cubic phase boundary in phase diagram, the highest piezoelectric properties at room temperature are obtained. The Curie temperature is significantly reduced as a result of dual doping, and the relationship between it and $BiFeO_3$ level is almost linear. Both $SrTiO_3$ and $PbTiO_3$ additions result in comparable Curie temperature depressions. For all compositions investigated, a unique relationship between T_c and d_{33} was found. Compared to pure $BiFeO_3$ and binary systems, dual doping with $PbTiO_3$ and $SrTiO_3$ added at comparable levels results in significantly higher piezoelectric properties. It is discovered that the temperature dependence varies based on the previous thermal history. When an earlier heat treatment is done at a temperature higher than the used temperature, the temperature dependence decreases and stabilizes. For $0.6BiFeO_3$-$0.2PbTiO_3$-$0.2SrTiO_3$, the combination of a high T_C and an appropriate heat treatment result in superior stable d_{33} value of 90 pC/N ar room temperature (120 pC/N at 300 °C). But the material is still unsuitable for applications at high temperatures because the electrical

conductivity rises so quickly with temperature. The $SrTiO_3$ and $PbTiO_3$ level seems to have no effect on the temperature dependency of conductivity. Future research should focus on these areas to gain a deeper understanding of the $BiFeO_3$-$PbTiO_3$-$SrTiO_3$ ternary system and its potential applications.

5.6 SUPPORTING INFORMATION

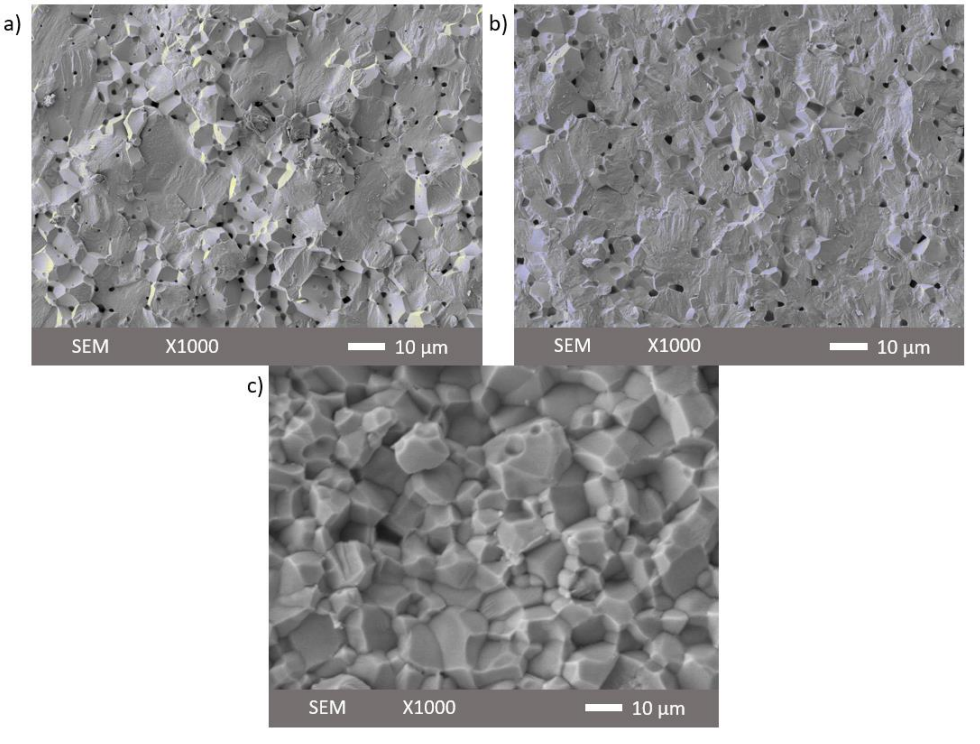

Figure 5.1S – (SEM) images of a fractured a) $0.7BiFeO_3$-$0.2PbTiO_3$-$0.1SrTiO_3$; b) $0.7BiFeO_3$-$0.1PbTiO_3$-$0.2SrTiO_3$; and c) $0.6BiFeO_3$-$0.2PbTiO_3$-$0.2SrTiO_3$ ceramics after sintering.

REFERENCES:

[1] Z. Ning, Y. Jiang, J. Jian, J. Guo, J. Cheng, H. Cheng, J. Chen, Achieving both large piezoelectric constant and high Curie temperature in BiFeO3-PbTiO3-BaTiO3 solid solution, J. Eur. Ceram. Soc. 40 (2020) 2338–2344. https://doi.org/10.1016/j.jeurceramsoc.2020.01.059.

[2] A.Y. Tuluk, T.R. Mahon, S. van der Zwaag, P. Groen, BiFeO3 synthesis by conventional solid-state reaction, 2019 IEEE Int. Symp. Appl. Ferroelectr. ISAF 2019 - Proc. (2019) 3–6. https://doi.org/10.1109/ISAF43169.2019.9034976.

[3] A. Tuluk, T. Mahon, S. van der Zwaag, P. Groen, Estimating the true piezoelectric properties of BiFeO3 from measurements on BiFeO3-PVDF terpolymer composites, J. Alloys Compd. 868 (2021) 159186. https://doi.org/10.1016/j.jallcom.2021.159186.

[4] A. Hussain, X. Xu, G. Yuan, Y. Wang, Y. Yang, J. Yin, J. Liu, Z. Liu, The development of BiFeO 3 -based ceramics, Chinese Sci. Bull. 59 (2014) 5161–5169. https://doi.org/10.1007/s11434-014-0648-0.

[5] A. Siddaramanna, V. Kothai, C. Srivastava, R. Ranjan, Stabilization of metastable tetragonal phase in a rhombohedral magnetoelectric multiferroic BiFeO3-PbTiO3, J. Phys. D. Appl. Phys. 47 (2014). https://doi.org/10.1088/0022-3727/47/4/045004.

[6] I. Kim, K. Jang, I. Kim, L. Li, Higher-order Landau phenomenological models for perovskite crystals based on the theory of singularities: a new phenomenology of BaTiO 3, Phase Transitions. 91 (2018) 239–253. https://doi.org/10.1080/01411594.2017.1350960.

[7] C.M. Fernández-Posada, H. Amorín, C. Correas, O. Peña, M. Algueró, A. Castro, Mechanosynthesis and multiferroic properties of the BiFeO3-BiMnO3-PbTiO3 ternary system along its morphotropic phase boundary, J. Mater. Chem. C. 3 (2015) 2255–2266. https://doi.org/10.1039/c4tc02053g.

[8] J. Bennett, T.R. Shrout, S.J. Zhang, P. Mandal, A.J. Bell, T.J. Stevenson, T.P. Comyn, Temperature dependence of the intrinsic and extrinsic contributions in BiFeO3-(K0.5Bi0.5)TiO3-PbTiO3piezoelectric ceramics, J. Appl. Phys. 116 (2014). https://doi.org/10.1063/1.4894443.

[9] A.J. Bell, T.P. Comyn, T.J. Stevenson, Expanding the application space for piezoelectric materials, APL Mater. 9 (2021). https://doi.org/10.1063/5.0035416.

[10] D. Damjanovic, A morphotropic phase boundary system based on polarization rotation and polarization extension, Appl. Phys. Lett. 97

(2010) 24–27. https://doi.org/10.1063/1.3479479.

[11] M.J. Haun, E. Furman, S.J. Jang, L.E. Cross, Thermodynamic theory of the lead zirconate-titanate solid solution system, part v: Theoretical calculations, Ferroelectrics. 99 (1989) 63–86. https://doi.org/10.1080/00150198908221440.

[12] R.E. Eitel, C.A. Randall, T.R. Shrout, P.W. Rehrig, W. Hackenberger, S.E. Park, New high temperature morphotropic phase boundary piezoelectrics based on Bi(Me)O3-PbTiO3 ceramics, Japanese J. Appl. Physics, Part 1 Regul. Pap. Short Notes Rev. Pap. 40 (2001) 5999–6002. https://doi.org/10.1143/jjap.40.5999.

[13] M.I. Morozov, D. Damjanovic, Hardening-softening transition in Fe-doped Pb (Zr,Ti) O3 ceramics and evolution of the third harmonic of the polarization response, J. Appl. Phys. 104 (2008). https://doi.org/10.1063/1.2963704.

[14] N. Horchidan, C.E. Ciomaga, R.C. Frunza, C. Capiani, C. Galassi, L. Mitoseriu, A comparative study of hard/soft PZT-based ceramic composites, Ceram. Int. 42 (2016) 9125–9132. https://doi.org/10.1016/j.ceramint.2016.02.179.

[15] M.I. Morozov, M.A. Einarsrud, J.R. Tolchard, P.T. Geiger, K.G. Webber, D. Damjanovic, T. Grande, In-situ structural investigations of ferroelasticity in soft and hard rhombohedral and tetragonal PZT, J. Appl. Phys. 118 (2015) 0–7. https://doi.org/10.1063/1.4934615.

6

CONTROLLING THE PIEZOELECTRIC PROPERTIES IN BULK $BiFeO_3$-$PbTiO_3$-$Li_{0.5}Bi_{0.5}TiO_3$ CERAMIC BY QUENCHING AND ANNEALING

ABSTRACT

Chemical modification is the main way to control the ferroelectric and piezoelectric properties of piezoceramic, but it is also known that their properties can be varied using a heat treatment. Quenching can be a valuable technique not only to minimize the formation of secondary phases as shown in previous studies on bismuth ferrite, but also to increase the piezoelectric and ferroelectric properties by stabilizing the high temperature phases. In the present work, we study the effect of quenching and annealing on the ferroelectric and piezoelectric properties at room and elevated temperatures of a new ternary $BiFeO_3$-$PbTiO_3$-$Li_{0.5}Bi_{0.5}TiO_3$ bulk piezo ceramic. While sacrificing part of the maximally obtainable piezoelectric constant value, using an optimal heat treatment retention of good properties up to 600 °C was achieved. The quenching and annealing process are completely reversible and can be used in combination with additional chemical modifications to tailor the properties of this new high-temperature piezoelectric ceramic to the intended use conditions. Unfortunately, no completely satisfying physical explanation of the many interesting observations was found, but all experimental results point into the direction of unusual defect behavior in this novel ternary system.

6.1 INTRODUCTION

Electro-mechanical interactions between charged point defects and domain walls (DW) play a key role in controlling the functional properties of bulk and thin-film ferroelectrics. Since the discovery of the presence and role of conducting domain walls in thin films of bismuth ferrite, it has been suggested that local conductivity increases with the presence of charged point defects [1]. Various types of defects have been proposed to maximize the effect, including oxygen vacancies, bismuth vacancies, holes and electrons, highlighting the key role of defect chemistry and hence the material preparation processes (such as annealing temperature and cooling rate, as well as annealing atmosphere) [2][3]. In previous studies on $BiFeO_3$ (BFO) thermally treated in air, it was shown that in this material the dominant defects at the domain walls are electron holes and bismuth vacancies. A reasonable assumption is that accumulated defects will lead to DW pinning effects affecting DW dynamics, such as displacements over short distances under the action of an applied electric field. It is possible that this mechanism will differ from that in prototype ferroelectrics, such as acceptor-doped hard $Pb(Zr,Ti)O_3$ (PZT) and $BaTiO_3$, in which strong attachment of DW is controlled by the acceptor-oxygen-vacancy defect complexes [4][5][6]. In addition to the type of defects, the pinning of DW is highly dependent on the spatial distribution of the defects [7,8]. Lacking evidence at the atomic level, macroscopic data on polarization switching in hard ferroelectrics based on PZT [9] and $BiFeO_3$ [10] suggest that the degree of defect ordering can be controlled by the cooling rate from the high temperature annealing stage. It was proposed that quenching (i.e. fast cooling) the sample from a temperature above the Curie temperature (T_C) maintains the high temperature disordered state of the defects, while slow cooling promotes ordering of defects. This hypothesis is confirmed by a number of works on quenching of $BiFeO_3$-based piezoceramic [11][12], which show an increase in piezoelectric properties and a decrease in the coercive field in bulk samples after quenching from above the Curie temperature.

Quenching in itself is a classic tool for constructing phase diagrams [13], in addition to being widely used in heat treatment in the production of ferrous sheet metal and machined components and is used to tailor the general and local hardness respectively [14,15]. For non-transforming metals and non-metallic ceramic and polymeric materials, quenching is mainly used to retain

the high temperature phase and to prevent undesirable phases from forming during cooling. Quenching is not widely used as a treatment option to control ferroelectric or piezoelectric properties of piezo ceramics, where property optimization is done more commonly via chemical modifications. The preference for chemical modification route is primarily due to the problems related to thermally initiated stresses leading to microcracks and failure of quenched ceramics [16,17]. Despite the obvious disadvantages, the quenching method, apart from being cheap and versatile, could be a promising tool for tailoring electromechanical properties and phase transitions in various ferroelectric and related materials. A recent work demonstrated that quenching from high sintering temperatures is beneficial in significantly increasing the thermal depolarization temperature in $Na_{0.5}Bi_{0.5}TiO_3$ [17]. In earlier studies on BFO ceramics, the quenching method was used for two different reasons. The first is to effectively avoid an unstable region in the phase diagram. Quenching has been found to be a valuable technique to minimize the formation of secondary phases rich in Bi and Fe, which are commonly observed in BFO bulk ceramics synthesized via conventional processing [18–20]. The second reason relates to the behaviour of charged point defects, in particular in relation to domain wall pinning, in which quenching was used to tune the distribution of defects [21]. The results showed the reason for the hardening behaviour of BFO, which made it possible to truly reveal the influence of point defects on the switching properties of BFO and to provide insight even on the atomistic details of domain walls [22]. Quenching also has provided a new paradigm for improving the piezoelectric properties of BFO-based systems. As an example, the piezoelectric charge constant of $BiFeO_3$–$BaTiO_3$-based (BFO-BT) ceramics is significantly enhanced by the quenching process compared to the non-quenched state (commonly referred to furnace cooling, slow cooling, as-sintered) [17,23]. Therefore, a quenching process is found to be one of the successful methods to improve piezoelectricity in BFO-based systems, and this has led to further research on the effect of quenching processes, such as quenching temperature and cooling rate.

There is a wide variety of BFO-base systems, but it is well known that systems which form a solid solution at or near the morphotropic phase boundary (MPB) region [24], generally have the best properties including the highest piezoelectric constants. One such system is the MPB composition in $BiFeO_3$–

$PbTiO_3$ which offers a high Curie temperature (T_c = 635 °C), but which is hard to pole without cracking due to the large spontaneous strain. Furthermore, their p-type conductivity is too high for high temperature operation. On the other hand, other tetragonal end-members result in the breakdown of long-range order, a reduction in T_C, and the onset of relaxor behavior. As a general rule, increasing the number of cations in a solid solution tends to further undermine polar coherence and deepen the relaxor nature [25]; however, incorporation of $PbTiO_3$ in nano-polar systems tends to overcome the loss of coherence and favors the formation of long-range polar order. This can be clearly seen in the example of $BiFeO_3$–$PbTiO_3$–$(K_{0.5}Bi_{0.5})TiO_3$ in which the largest weak-field d_{33} is located virtually mid-way between the $BiFeO_3$–$PbTiO_3$ MPB composition and the pseudo-cubic region of $BiFeO_3$–$(K_{0.5}Bi_{0.5})TiO_3$ [26].

In order to address the problem of the $BiFeO_3$-$PbTiO_3$ system's high electrical conductivity and prevent spontaneous sample destruction during the phase transition due to the substantial volume difference between the tetragonal and cubic phases, the addition of a third component, $Li_{0.5}Bi_{0.5}TiO_3$, was made. With this approach we do not introduce new elements at the B position, but only introduce aliovalent doping at the A position of the perovskite structure, which must locally compensate for electrical charges. , Due to the large difference in the ionic radii of bismuth (lead) ions and lithium ion, doping with a lithium based titanate lead to reduced local stresses in the structure that will reduce the macroscopic stresses in the material in general.

The main goal of this work was to study the effect of quenching and annealing on the piezoelectric properties of the most promising BFO ternary alloy of this latter type: $0.60BiFeO_3$-$0.25PbTiO_3$-$0.15Li_{0.5}Bi_{0.5}TiO_3$. The idea of rapid cooling is to maintain the randomized defect structure at the high temperature (above T_c) and to prevent (or control) the defect ordering on domain walls formed at temperature below T_c. The mechanisms responsible for the observed quenching effects in BFO-based ceramics are related to the role of oxygen vacancies similar to the better-known mechanism of domain stabilization in acceptor-doped ferroelectric ceramics (e.g., $BaTiO_3$ and PZT) involving a dipolar ion-oxygen acceptor vacancy [27–29]. This concept has used to study hardening-softening transitions in PZT ceramics [8]. However, no detailed study of this transition in BFO-based ternary ceramics has been reported in the literature yet. The ability to reverse the quenching effect by a subsequent heat

treatment has also not been studied in previous works, but could be an important aspect when studying the possibility of using this ceramic at elevated temperatures. The study of various heat treatments (such as quenching and annealing) for piezoelectric materials can open up new possibilities in tuning of their final properties. Such studies indirectly also deepen the understanding of the interaction of point defects and domain walls in ferroelectric materials.

6.2 EXPERIMENTAL PROCEDURE

$BiFeO_3$-$Bi_{0.5}Li_{0.5}TiO_3$-$PbTiO_3$ (BFO-BLT-PT) samples were prepared by a conventional solid-state reaction using analytical-grade commercially supplied raw materials: Bi_2O_3, Fe_2O_3, TiO_2, PbO and Li_2CO_3. Dried powders were weighed and ground separately before mixing. The $Bi_{0.5}Li_{0.5}TiO_3$ and $PbTiO_3$ levels were fixed at 0.15 and 0.25 respectively. Hence the final composition can be written as $0.60BiFeO_3$-$0.25PbTiO_3$-$0.15Li_{0.5}Bi_{0.5}TiO_3$. Grinding and mixing processes were performed in isopropanol using yttria-stabilized ZrO_2 balls. The particle size distributions of the milled powder are in the range of 0.5-1 microns according to SEM images. Mixed powders after drying were calcined at 800°C for 1 h using a heating rate of 600°C/h. Then the calcined powders were reground, granulated by mixing with 2 wt% QPAC 40 binder, and uniaxially pressed into disks (13 mm in diameter and 1 mm in thickness) under 200-250 MPa. The pellets were sintered at 1025 °C for 1 h using a heating and cooling rate of 600°C/h. The sintering procedure is shown in detail in **Figure 6.1S** of the SI section.

Scanning Electron Microscope (SEM) images were taken using a Jeol JSM-7500F field emission scanning electron microscope. Prior to SEM measurements a thin (15 nm) layer of gold was deposited on the sample. To determine the phase purity X-ray diffraction studies with Cu Kα radiation were done using a Bruker D8 Discover diffractometer. Scans were recorded at set temperatures: RT, 200° to 700 °C in steps of 25 °C and again at RT after cooling down by switching off the heating. The density was determined by the Archimedes' method in an aqueous medium.

Polarization–electric field hysteresis loops were measured at room temperature using a Radiant precision ferroelectric analyzer. The electrical properties of samples were measured at room temperature using an Agilent

4263B LCR meter at 1 kHz and 1 V. For these measurements, silver electrodes were applied on the ceramics by firing silver paste at 150 °C. For the actual research, electrode coated samples were thermally treated by gradual heating to a predetermined temperature of 600-750 °C, temperature stabilizing for 30 minutes and then abrupt cooling in air or other media (silicone oil, ceramic plate, liquid nitrogen) to vary the cooling rate. Cooling rate variations were achieved in the range from 0.1 ^{o}C /s (furnace cooling) to 50-80 ^{o}C/s (metal contact). The process of quenching of the samples are shown in detail in **Figure 6.2S** in the SI section. After dielectric measurements, the samples were polarized under a DC electric field of 70 kV/cm for 20 min in silicone oil at room temperature. After aging for 24 hours at ambient laboratory conditions, the piezoelectric constant d_{33} was measured with a PM300 Berlincourt-type piezometer from Piezotest with a static force of 10 N and a dynamic force of 0.25 N peak to peak with sinusoidal excitation at 110 Hz. Samples were then annealed by placing them in a preheated furnace at temperature of 150 to 600 °C for a period of 7 minutes up to 2 weeks. After annealing and air cooling, the dielectric and piezoelectric parameters at room temperature were measured again.

6.3 RESULTS

6.3.1 MICROSTRUCTURE AND CRYSTAL STRUCTURE

Figure 6.1 shows the microstructure of a polished sample after chemical etching. The grain size is approximately 2-3 microns. Ferroelectric and ferroelastic domain walls are partially visible, but the resolution is too small to properly show the domain size of 50-100 nm. The microstructure of the quenched and annealed samples does not differ from that of the as-sintered sample and are shown in the Supporting Information **Figure 6.3S** for the sake of completeness.

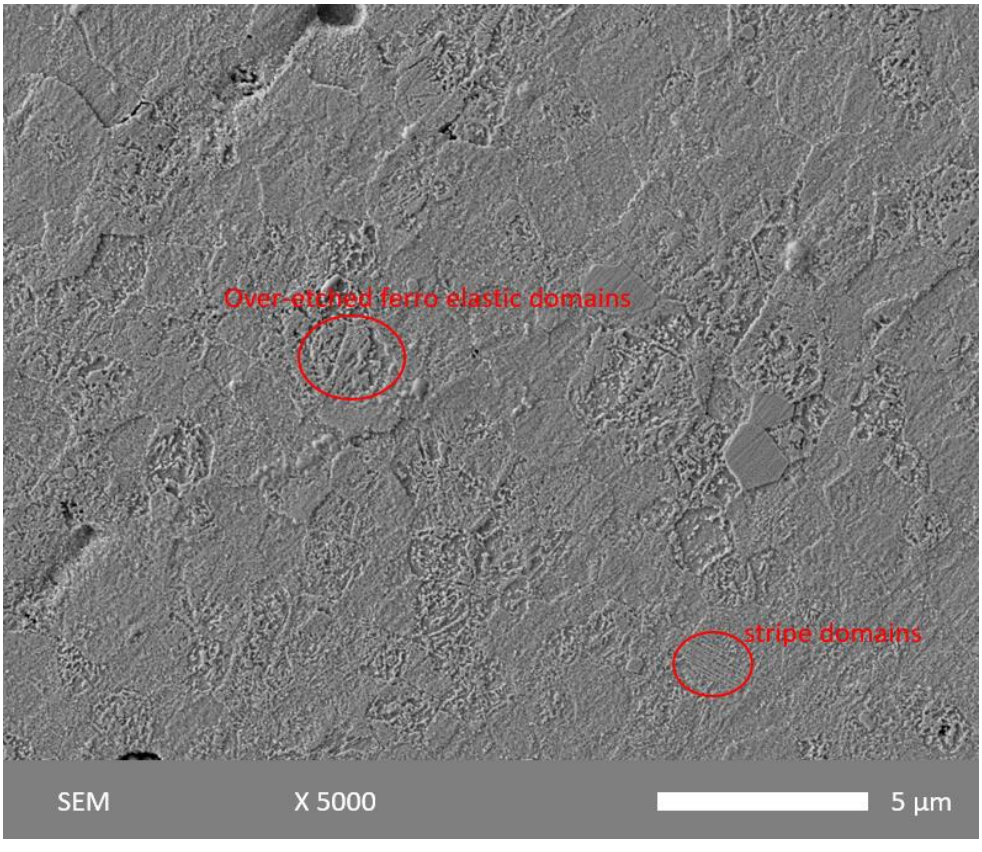

Figure 6.1 – SEM picture of a polished as-sintered sample after chemical etching. The encircled regions show the domain structure.

The XRD pattern is shown in **Figure 6.2** for three samples: 1) as-sintered which was oven cooled (i.e. cooling rate 0.05 °C/s) from 700 °C, 2) oil quenched (i.e. cooling rate 60 °C/s) from 700 °C and 3) annealed for 12 hours at 450 °C after oil quenching. The figure shows that two phases, rhombohedral and tetragonal, are coexisting (some non-overlapping peaks were marked on figure). The diffraction peak at 37 degrees (marked with blue circle) is an artefact and is associated with the aluminum sample holder material. No peaks belonging to secondary phases were found indicating good solubility of all components and the formation of a solid solution. Upon annealing of the quenched sample, the peaks change in intensity, but no change in the peak position (i.e. the crystal structure) is observed.

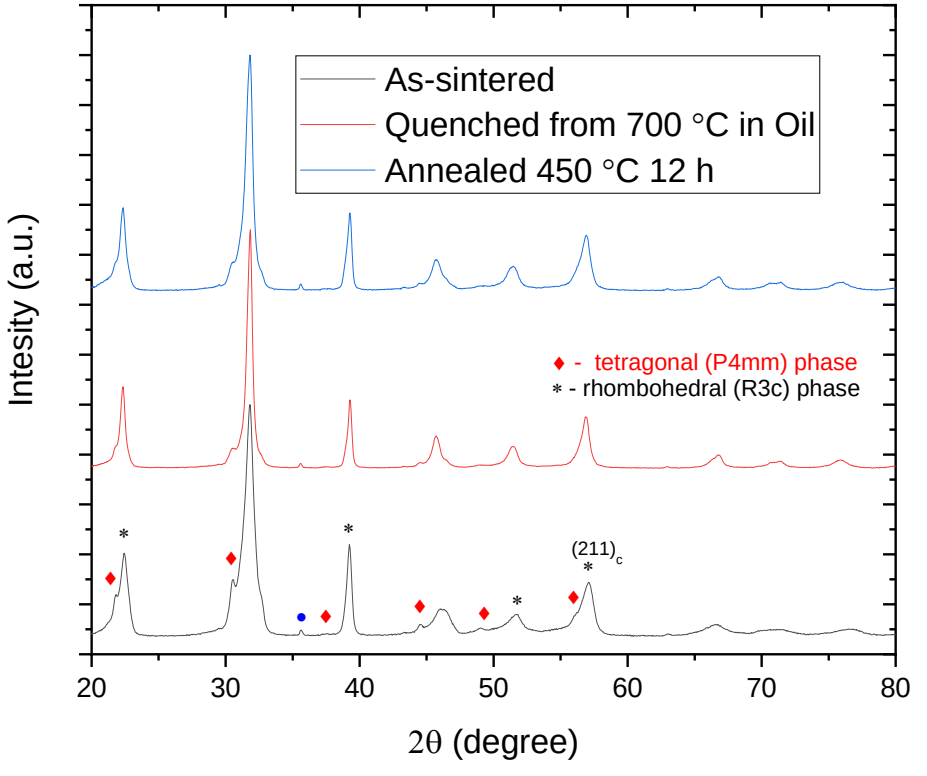

Figure 6.2 – X-ray diffraction patterns of the as-sintered, oil quenched from 700 ^{0}C and 12 h, 450 ^{0}C annealed after oil quenching samples

6.3.2 INFLUENCE OF TEMPERATURE ON THE CRYSTAL STRUCTURE

Figure 6.3 shows the evolution of the rhombohedral into the cubic phase as evidenced by the (associated) $(211)_C$ peak for the same three sample conditions used in **Figure 6.2**. This peak was chosen for the following reasons: a relatively high intensity while being located at a high angle, and no strong overlap with peaks of tetragonal phase. Both the curves of the peak position and the average peak width indicate that the phase transition occurs over a temperature range of 600-625 °C. The peak position curves for the quenched and annealed samples show an unexpected plateau between 500 and 575 °C but are otherwise linear. The peak position curve of the as-sintered material only shows a linear temperature dependence up to the transformation

temperature. **Figure 6.3a** also shows that the peak position changes markedly upon quenching, but that annealing has no effect on the peak position. This is in contrast with **Figure 6.3b** which shows that the reduction of the peak position due to quenching is partially reverted by the annealing treatment. FWHM plotted after deconvolution of the recorded peak. The unit cell parameter shown in **Figure 6.3c** and **6.3d** is almost identical for all three samples, and also show a phase transition in the temperature range of 600-625 °C. The interpretation of the observed changes is discussed in the Discussion.

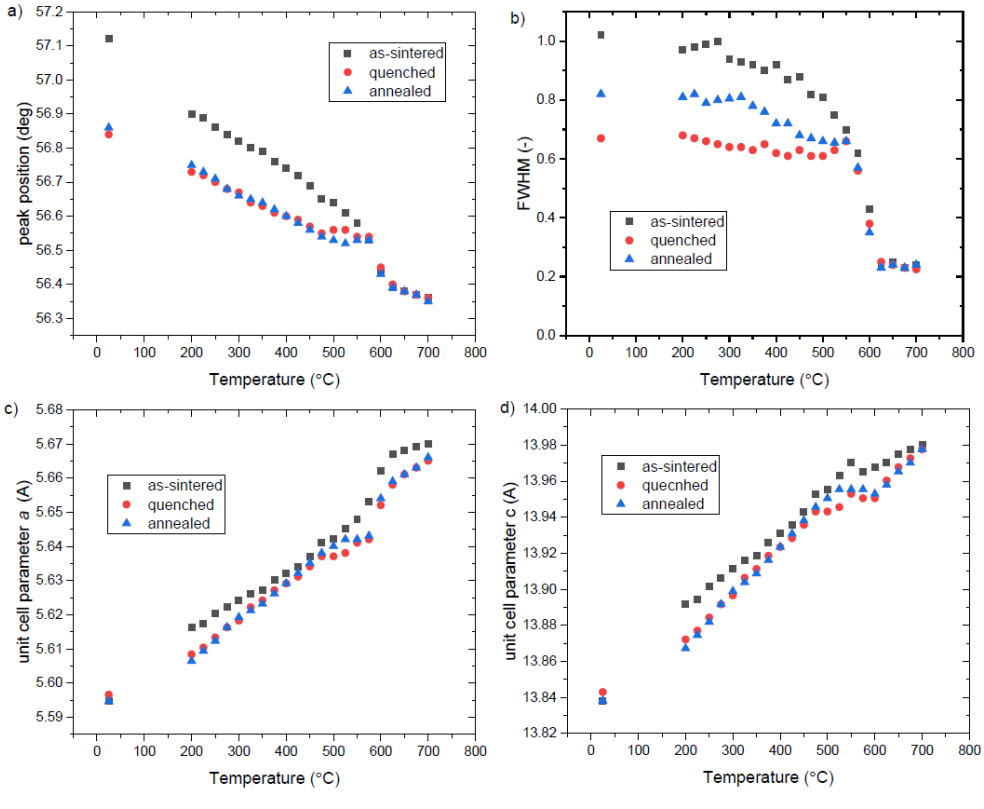

Figure 6.3 – a) Peak position; b) full with at half maximum of (211) cubic reflection; c) and b) unit cell parameter *a* and *c* of R3c phase depending on temperature for samples as-sintered, oil quenched from 700 °C and annealed 12 hours at 450 °C

6.3.3 THE EFFECT OF THE PRE-QUENCHING TEMPERATURE ON THE FERROELECTRIC PROPERTIES

To study the minimal annealing temperature required to mobilize the defects, the P-E hysteresis loops were obtained for the as-sintered condition and for oil-quenched (silicon oil at room temperature) samples quenched from different temperatures. These P-E hysteresis loops are shown in **Figure 6.4**. The well-saturated loops for samples quenched from temperatures from 650 to 750 °C demonstrate remnant polarization in range of 20-25 μC/cm², but there is no visible trend in the change of the maximum and remnant polarization values depending on quenching temperature for this temperature range. But there is a clear trend in the reduction of the coercive field from 42 kV/cm to 40 kV/cm with an increase in the quenching temperature from 650 to 750 °C. At quenching temperatures below 650 °C, we no longer observe saturated ferroelectric hysteresis loops. The transition temperature of around 625-650 ˚C is a bit higher than the transition temperature, 600-625 ˚C obtained from high temperature XRD data (**Figure 6.3**). Nevertheless, we believe that the phase transformation is responsible for opening the P-E loop.

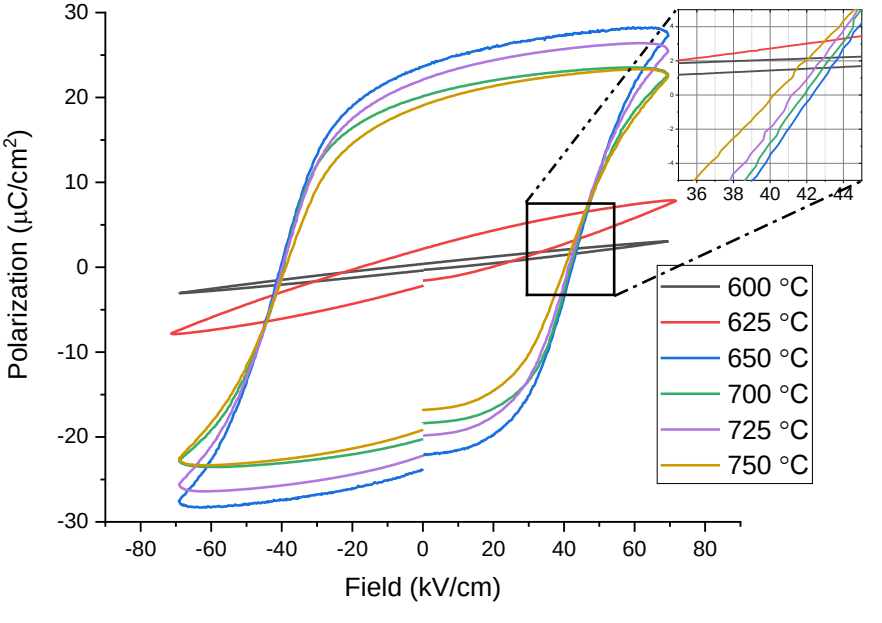

Figure 6.4 – Ferroelectric hysteresis of samples quenched from different temperatures in silicone oil.

The P-E hysteresis loop obtained for the sample oil quenched from 700 °C and poled at 70 kV/cm for 20 min at room temperature is shown in **Figure 6.5**, which exhibits a bias field (Piezoelectric charge constant after poling reached 95 pC/N). This clearly indicates the presence of a sufficient number of defects that participate in polarization [30]. This result may indicate a hardening-softening transition similar to acceptor doped PZT [8].

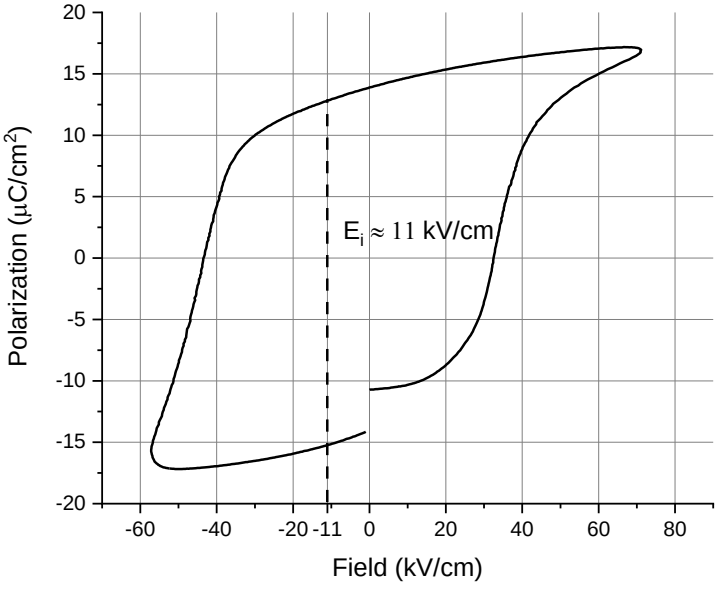

Figure 6.5 – Typical ferroelectric hysteresis loop after poling at 70 kV/cm for an oil quenched sample quenched from 700 ^{0}C.

For indirect determination of the transition temperature to the paraelectric state, the thermal depolarization of d_{33} was measured, and the results are shown in **Figure 6.6**. It can be seen that both for the as poled and for the annealed samples, a rapid depolarization occurs at a temperature above 600 °C and an approximate transition lies in the region of 625-650 °C. It can also be seen that for as-poled sample, a smooth decrease in the piezoelectric constant d_{33} occurs at temperatures above 125-150 °C. This effect is studied in more detail in section 6.3.5

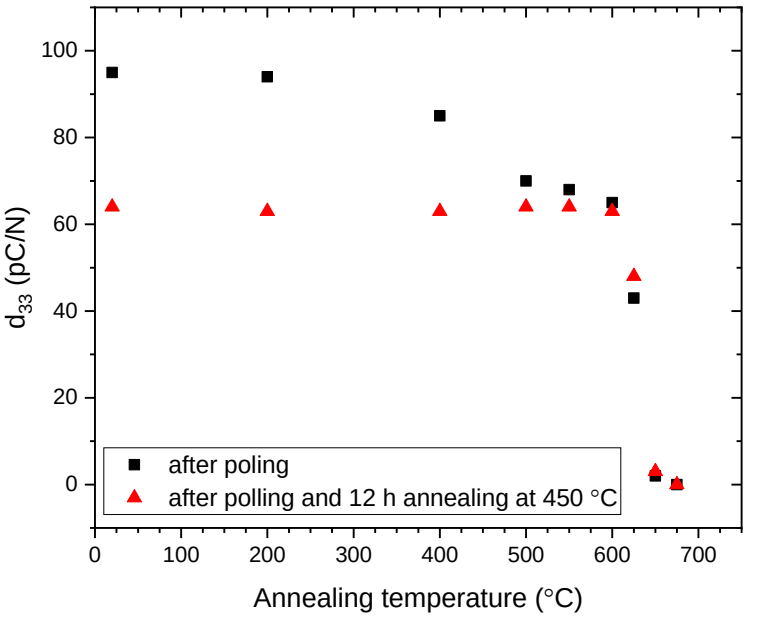

Figure 6.6 – Effect of thermal depolarization on d_{33} values of poled samples after poling and after annealing at 450 °C measured *ex situ* (at room temperature after heating up till target temperature for 15 min)

6.3.4 EFFECT OF COOLING RATE DURING QUENCHING FROM 700 °C ON FERROELECTRIC PROPERTIES

In **Figure 6.7a** the P-E loops up to 80 kV/cm are shown for various cooling rates from a fixed annealing temperature of 700 °C. The figure shows that for cooling rates higher than 10 °C/s the P-E loops open up at a coercive field of about 50 kV/cm. At lower cooling rates the P-E loops do not open up properly. As shown in **Figure 6.7b** the remnant field strength shows an increase with increasing the cooling rate and the polarization for a cooling rate slower than 0.2 °C/s the ferroelectric loop will not differ from that for the as-sintered sample. Data do not allow draw conclusion on the dependence of remnant polarization on cooling rate. All measurements shown in **Figure 6.7** were successively performed on a single sample with the return of its original properties (as-sintered) upon annealing at 450 °C for 12 hours.

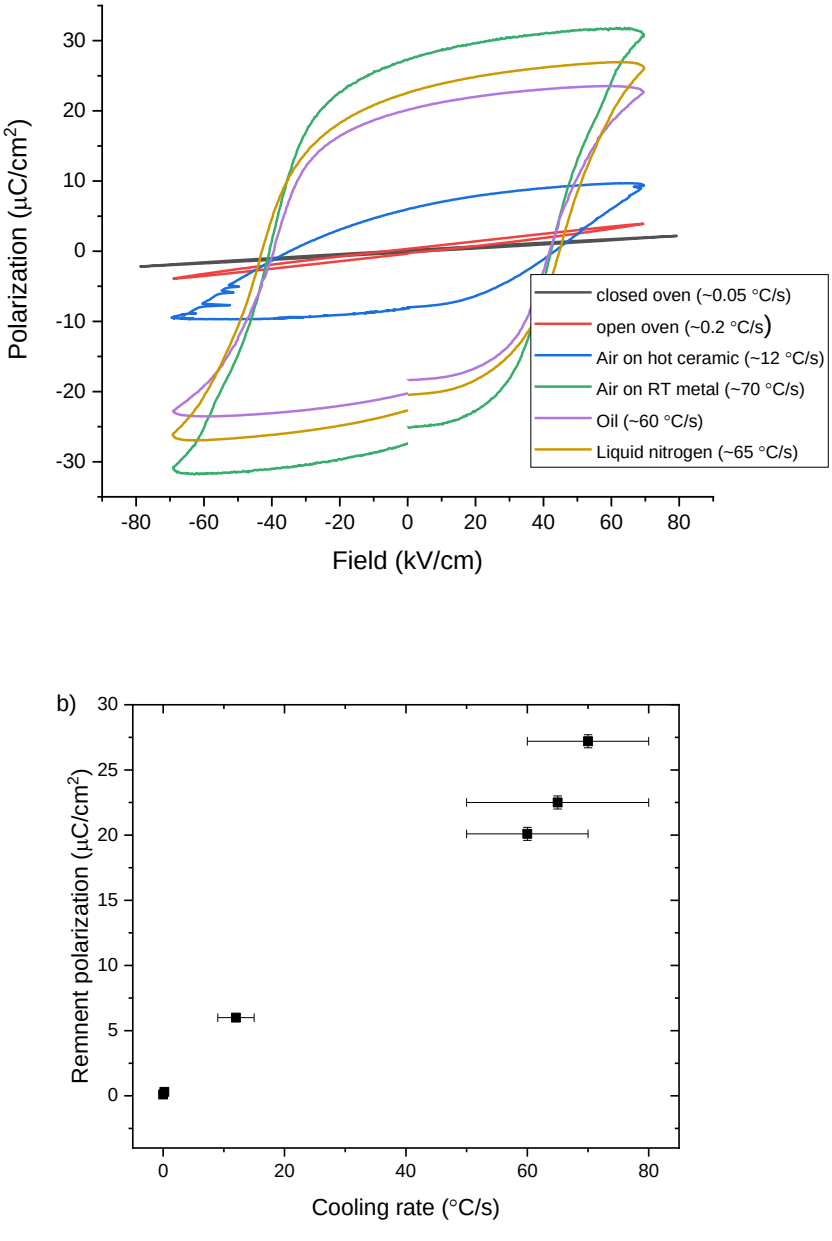

Figure 6.7 – a) Ferroelectric hysteresis loops of a single sample quenched from 700 °C at different cooling rates, b) remnant polarization as a function of the cooling rate.

6.3.5 EFFECT OF POST-QUENCHING ANNEALING ON PIEZOELECTRIC AND ELECTRIC PROPERTIES

If the sample is quenched from 700 °C at a rate of around 50 °C/s and subsequently poled at a field of 70 kV / cm, the material is piezoelectrically activated and values of d_{33} of 95 pC/N (at room temperature) are achieved. **Figure 6.8** shows the dynamics of changes in the (room temperature) piezoelectric and dielectric properties of optimally quenched samples upon subsequent isothermal annealing in air at different temperatures (a) 150 °C, b) 300 °C, c) 450 °C and d) 600 °C). We observe that a noticeable decrease in the piezoelectric property values occurs upon annealing at 300 °C or higher temperatures. Interestingly, the actual temperature does not affect the final value of the piezoelectric constant, which reaches a value of 63 pC/N, but only affects the kinetics of the change. All high temperature annealed samples eventually reach the same piezoelectric property value, which we consider to be the thermodynamically meta-stable state (intermedium) for our material.

Finally, we performed a number of successive annealing treatments at different temperatures to get a better insight into the apparent intermedium state leading to a d_{33} of 63 pC/N. To this aim a sample was first annealed at 150 °C for times up to 20.160 minutes (i.e. 2 weeks), subsequently at 300 °C again for times up to 20,160 minutes (i.e. 2 weeks) and finally 2 weeks at 450 °C; and the piezo and dielectric properties were measured intermittently. The results are shown in **Figures 6.9a-c** for the d_{33}, the dielectric constant and the tan δ respectively. The figure clearly shows that in the case of successive annealing the final values for d_{33} and the dielectric constant finally obtained, 63 pC/N and 225 respectively, are the same as those for the samples directly annealed at 450 °C , but that the total annealing time required was considerably longer. It should be especially noted that no matter what the temperature history of the sample, if the depolarization temperatures are not reached, the piezoelectric properties of the material will be in the region of 63 pC/N.

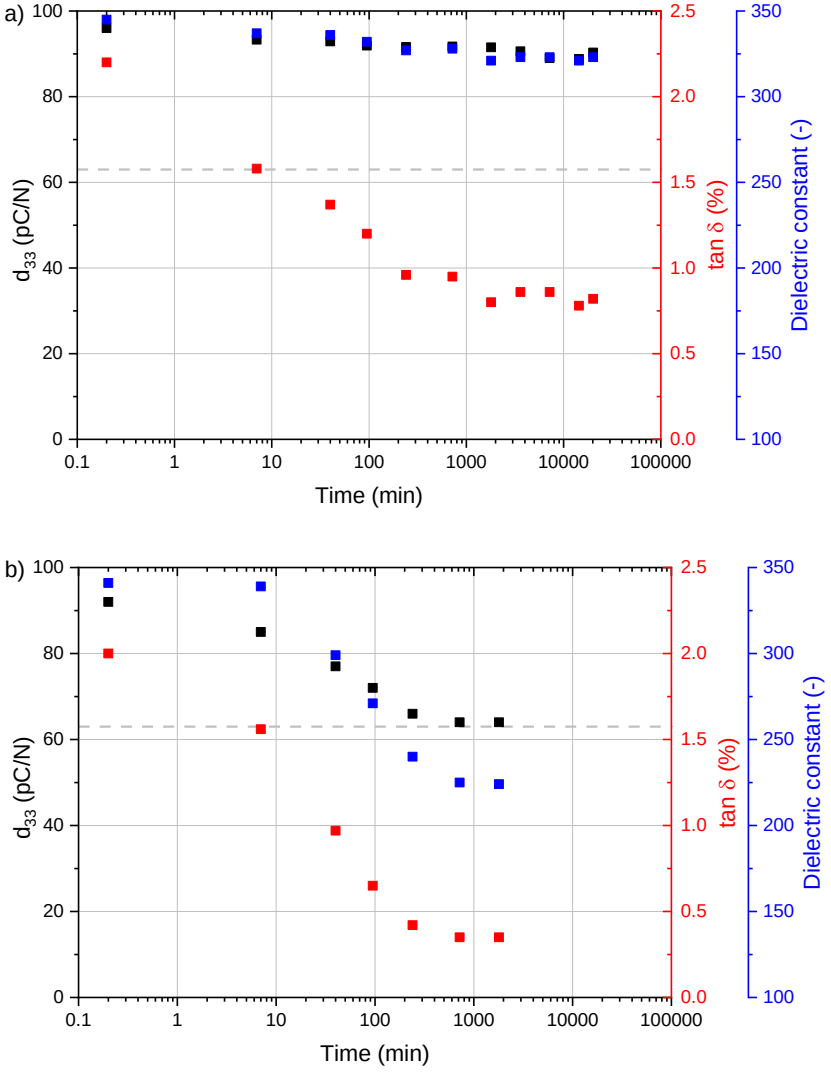

Figure 6.8 – Effect of post annealing at a) 150 °C and b) 300 °C on piezoelectric and dielectric properties of sample. Symbol colour corresponds to the colour of the parameter mentioned on they Y-axes. Dashed line shows the stable value of piezoelectric constant at 63 pC/N.

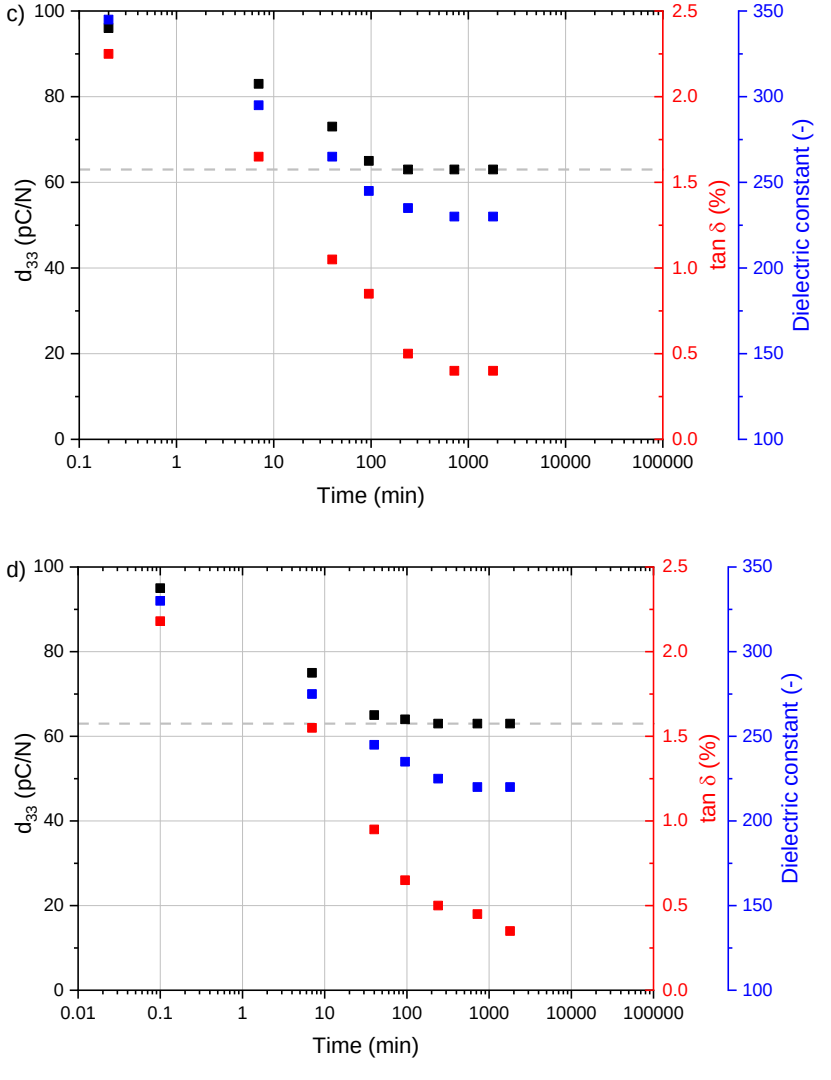

Figure 6.8 (continued) – Effect of post annealing at c) 450 °C and d) 600 °C on piezoelectric and dielectric properties of sample. Symbol colour corresponds to the colour of the parameter mentioned on they Y-axes. Dashed line shows the stable value of piezoelectric constant at 63 pC/N.

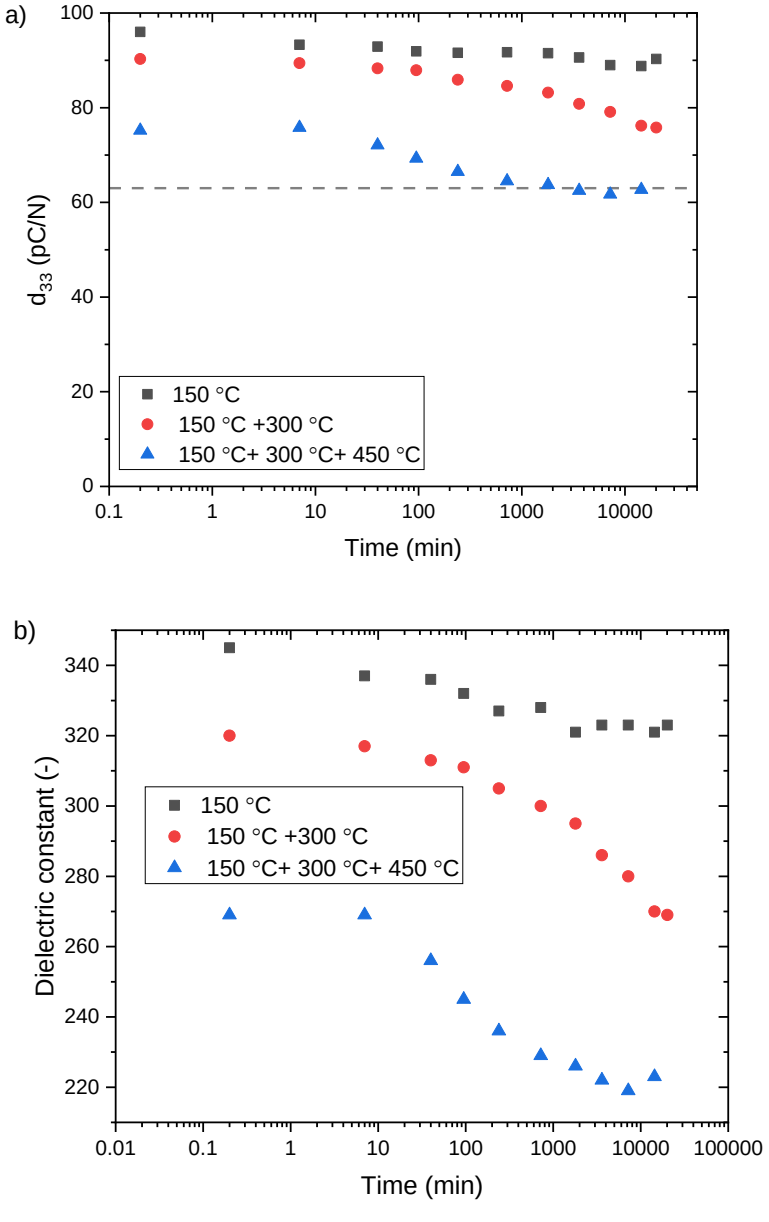

Figure 6.9 – a) Piezoelectric charge constant (Dashed line shows the stable value of piezoelectric constant at 63 pC/N) and b) dielectric constant of quenched sample depending on total time at annealing temperature 150 °C, 150+300, and 150°C +300°C +450°C (detailed thermal history shown on Figure 6.4S)

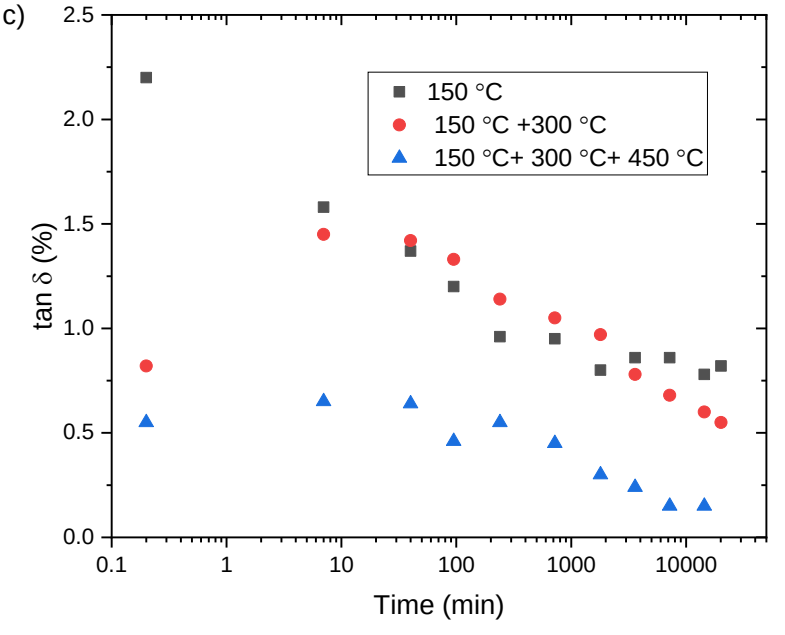

Figure 6.9 (continued) – c) dielectric losses of quenched sample depending on total time at annealing temperature 150 °C, 150+300, and 150°C +300°C +450°C (detailed thermal history shown on **Figure 6.4S**)

6.3.6 REPEATABILITY OF THE QUENCHING-ANNEALING CYCLE

Figure 6.10 shows the results of measurements of ferroelectric hysteresis loops after multiple quenching cycles from 700 °C in oil and subsequent 12 hours annealing at 450 °C at which conditions the piezoelectric properties should reach a plateau. It can be seen that the remnant polarization of the material decreases with each subsequent quenching cycle. The result obtained is similar to the result of the fatigue phenomenon for piezoelectric materials [31], but in contrast to it, the original polarization value is not restored when the sample is re-annealed at a temperature above the Curie temperature [27].

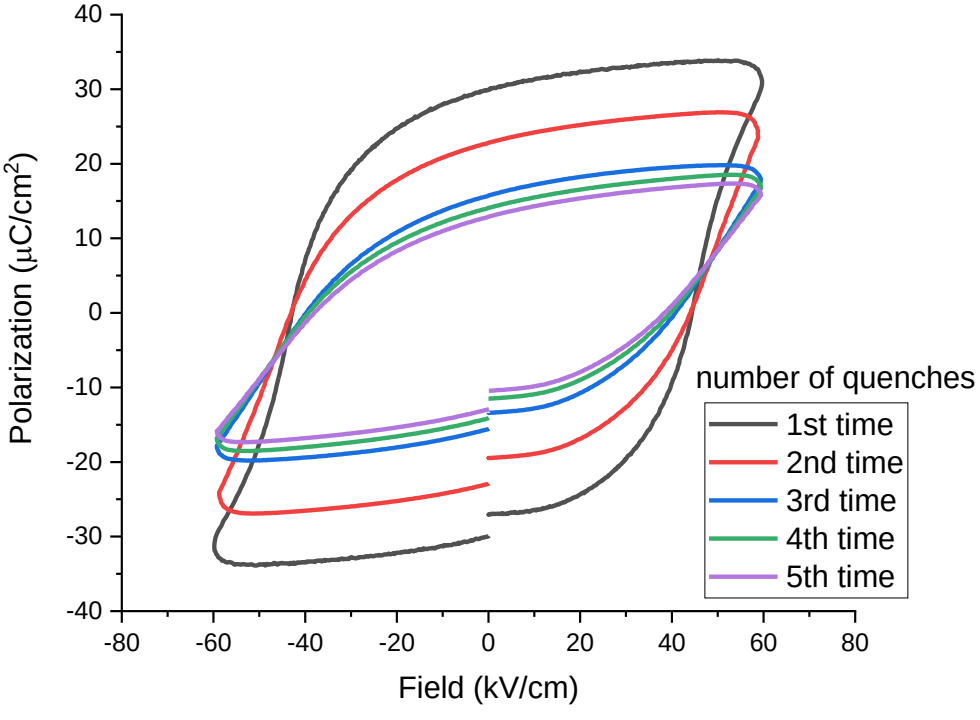

Figure 6.10 – P-E loops after multiple cycles of quenching from 700 °C in oil with subsequent 12 hours annealing in air at 450 °C

However, as can been seen from **Figure 6.11** the piezoelectric properties, unlike the remnant polarization, of the material practically do not change after multiple annealing and quenching cycles.

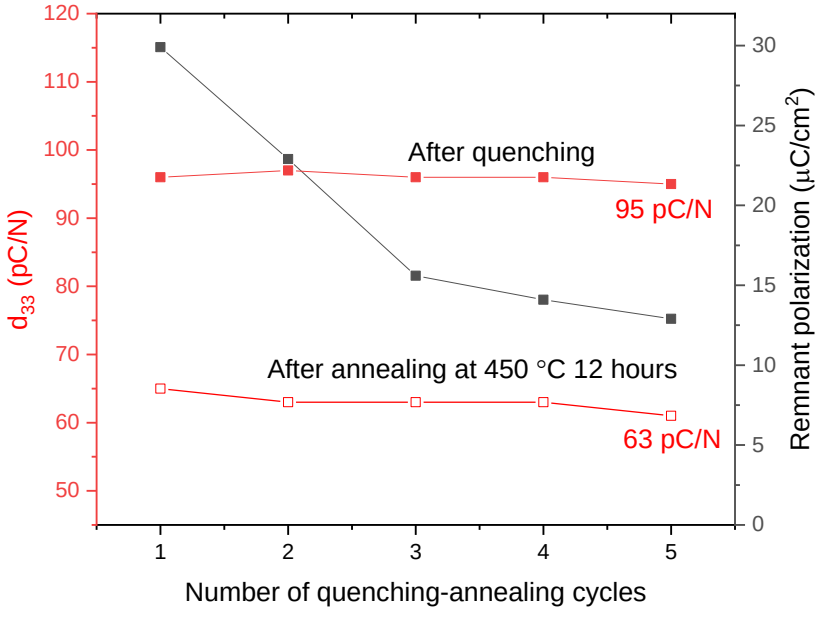

Figure 6.11 – Piezoelectric and ferroelectric properties after multiple quenching-annealing cycles. Symbol colours correspond to the label colours on the X and Y-axes

6.4 DISCUSSION

6.4.1 "QUENCHING" EFFECT MECHANISM

The primary explanation of quenching may be the transformation of ferroelectric domains during cooling into a certain quasi-stable state, not associated with surrounding defects [8]. Based on the fact that the cooling rate should exceed a certain value (higher than 10 °C/s) to open ferroelectric loops as shown on **Figure 6.7b**, it can be assumed that defects that are free at high temperatures, have a limited lifetime before they take a more thermodynamically stable position near the domain walls. The transition from a closed ferroelectric hysteresis loop to an open loop occurs only upon quenching from a temperature of 650°C and higher, so it can be assumed that the phase transition from the ferroelectric state to the para-electric state plays an important role in the formation of this effect [11,23]. It is shown indirectly by the thermal depolarization curve of d_{33} that all the piezoelectric properties

of the material disappear when heated above 650 °C as a result of the phase transition in material (**Figure 6.6**). It should be remembered that the actual in-situ high temperature XRD data show that the phase transition does occur at a slightly lower temperature (600-625 °C). We have no real physical explanation for the observed temperature difference and blame it on instrumental issues. But it is also worth noting that there is no noticeable change in the crystallographic structure of the samples directly after quenching from 700 °C and after subsequent annealing at 450 °C while the difference in piezoelectric behaviour is extreme. Only for the sintered sample a slight phase shift of the (211) peak is observed at room temperature. As shown in **Figure 6.3b**, all samples achieve a similar full width at half maximum at high temperature, which indicates a diffusive phase transition at temperatures above 600 °C, which correlates well with the presence of a minimally required quenching temperature, while the width depends on the temperature history of the sample. The synthesized sample has the largest peak width at room temperature, and the quenched sample has the smallest. While the width of the peak may be responsible for the internal stresses accumulated in the ceramic, it is not typical to have a lower stress in the quenched samples [32].

6.4.2 Annealing after quenching

During subsequent annealing, two potentially competing processes may occur. One of which is the reorientation of unstable domains, and the second is the diffusion of defects to the domain walls, which, as a result, bind them. This may explain the decrease in the piezoelectric response upon subsequent annealing to a certain stable value. But it cannot explain the fact that the piezoelectric constant value at the intermediate state does not depend on the annealing temperature. Another assumption is that the change in the piezoelectric properties may be caused by a change in the dielectric constant of the material during annealing due to the binding of mobile charges. Since the piezoelectric constant is directly proportional not only to the polarizability but also to the dielectric constant, then, at a constant polarizability and with a decrease in the permeability, the piezoelectric constant of the material can be reduced [33]. Contrary to this expected correlation it was noticed (**Figure 6.8a**) that a decrease in dielectric losses occurs also upon low-temperature annealing while the piezoelectric constant remains more or less constant. High dielectric losses after quenching are presumably associated with the generation of free

charge carriers, which, upon subsequent annealing, form dipole complexes or recombine [17]. Therefore, it can be assumed that annealing mainly affects free charge carriers, and not bound dipoles.

Figure 6.6 shows the thermal depolarization curves obtained in our work. The main difference between results obtained in our work and the usual published depolarization curves for piezoelectric ceramics [34] is that after annealing above a certain temperature (100-150 °C), the samples transform into an intermediate state, which is characterized by a lower yet significant value for the piezoelectric constant (**Figure 6.12**). This is different from depolarization curves for conventional piezo ceramics, for which the value decreases to zero during long enough annealing.

So during annealing, the quenched state of the more mobile domain walls and point defects is destroyed, and the material pass into an intermediate state, in which the coercive field is much larger. Therefore, poling of the samples is possible only in the quenching state. Value of piezoelectric charge constant of intermediate state does not depend on the annealing temperature as shown in **Figure 6.7**, and an increase of this temperature only accelerates the process of transition to this state as long as the depolarization temperature is not exceeded.

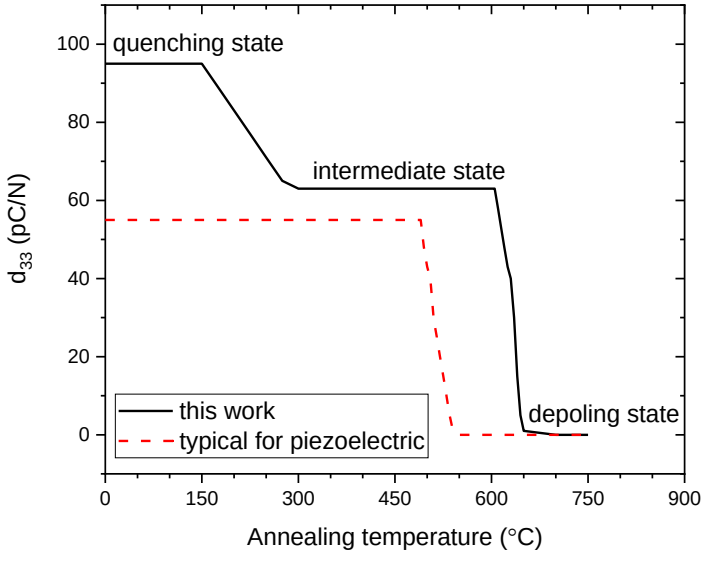

Figure 6.12 – d_{33} values of poled samples depends on annealing temperature [34]

6.4.3 REVERSIBILITY OF THE QUENCHING-ANNEALING

As shown in section 6.3.6, the effect of quenching and annealing can be reversed. Re-quenching of re-annealed samples fully restores the quenched state, while subsequent annealing brings the sample to an intermediate state again. These cyclic changes in both electrical and piezoelectric parameters indirectly indicate a change in the mobility of domain walls and point defects. The absence of a change in the piezoelectric parameters in cycles shows the complete reversibility of this transition. Based on the reversibility of the quenching, we can assume that it is associated with defects and a similar hardening mechanism as that which occurs in acceptor-doped PZT [35], is involved. The mechanism of precipitation hardening [36] as a result of the formation of secondary phases can be considered as being unlikely due to the fact that no secondary phases after quenching could be detected in XRD. The effect of fatigue of ceramics during repeated reproduction of the effect cannot be directly explained by defects and phase transition and can be caused by microcrakes arising from aggressive impact on ceramics.

6.5 CONCLUSIONS

Piezoelectric properties of $BiFeO_3$-$Bi_{0.5}Li_{0.5}TiO_3$-$PbTiO_3$ ceramic can be changed by thermal processing. Good properties at room temperature can be obtained by sufficiently fast cooling from temperature above phase transition temperature (T > 650 °C). The cooling rate is essential in this process and must be above a certain threshold (In our study, above 10 °C/s).

The non-equilibrium state can be mediated by proper annealing, shifting material to an unusual but clearly identifiable intermediate state. The transition to intermediate state occurs spontaneously at annealing temperature above 150 °C. An increase in annealing temperature leads to an acceleration of this transition but not to a change in final properties. For this ternary system it is possible to distinguish 3 states obtained for this material: quenched (full polarization), intermediate and depoled, while for common piezoceramics there is only a poled and depoled state. Thermal depolarization takes place when annealing at T > 650° C

Although the nature of this effect is not fully understood, all observed changes can be attributed to defect reorganisation. The nature of the defects has not been investigated here. Our assumption is that this effect is related to the

uniform distribution of point defects over the sample during quenching and the subsequent movement of these defects to domain walls that connect them during tempering. This is supported by the fact that this effect is completely reversible, if we properly reheat and adequately quench the ceramic again, we will release the domains and we can bind them again when annealed. For further research, it would be useful to find another mechanism for controlling the distribution of defects and study the processes on the domain walls *in-situ*.

6.6 SUPPORTING INFORMATION

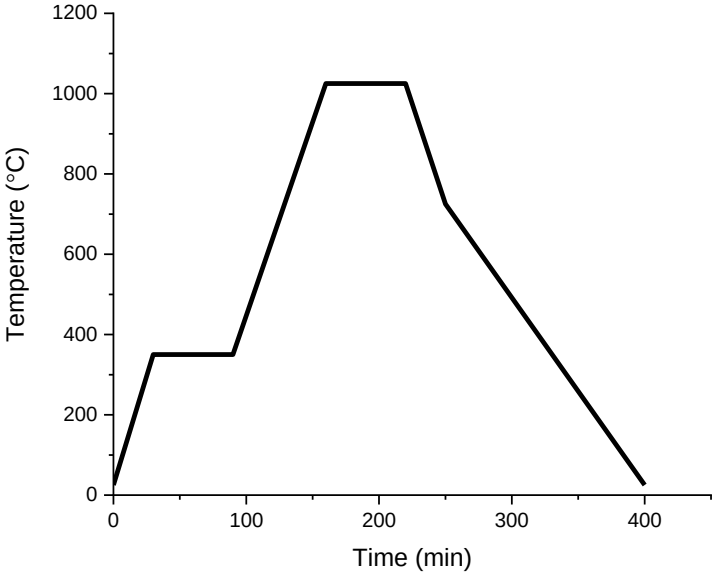

Figure 6.1S – Temperature profile of sintering procedure (The first plateau is binder burning, the second plateau is sintering process)

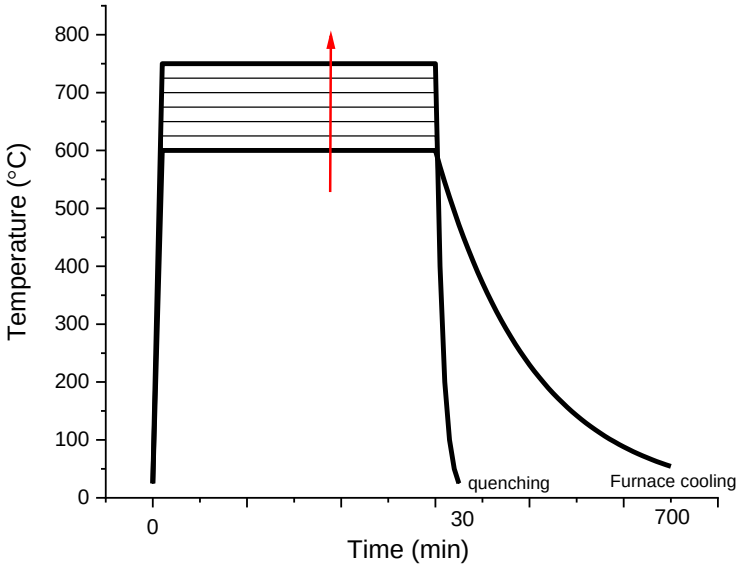

Figure 6.2S – Temperature profile of quenching procedure (Cooling time and quenching temperature varied)

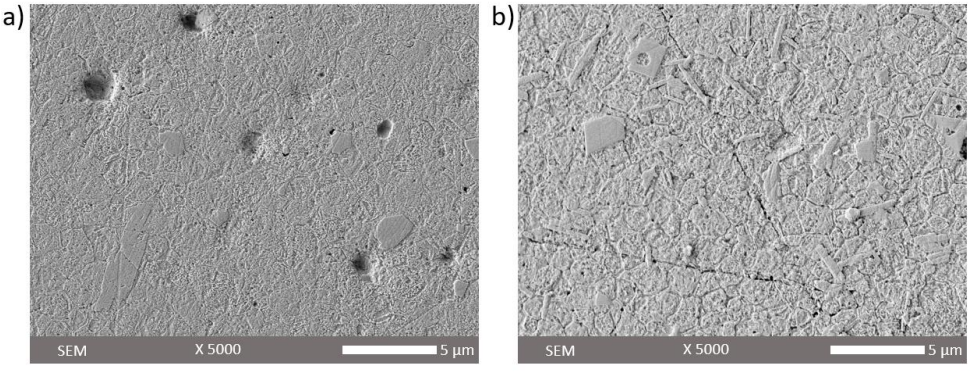

Figure 6.3S – SEM picture of a polished a) quenched and b) annealed sample after chemical etching (both samples over etched)

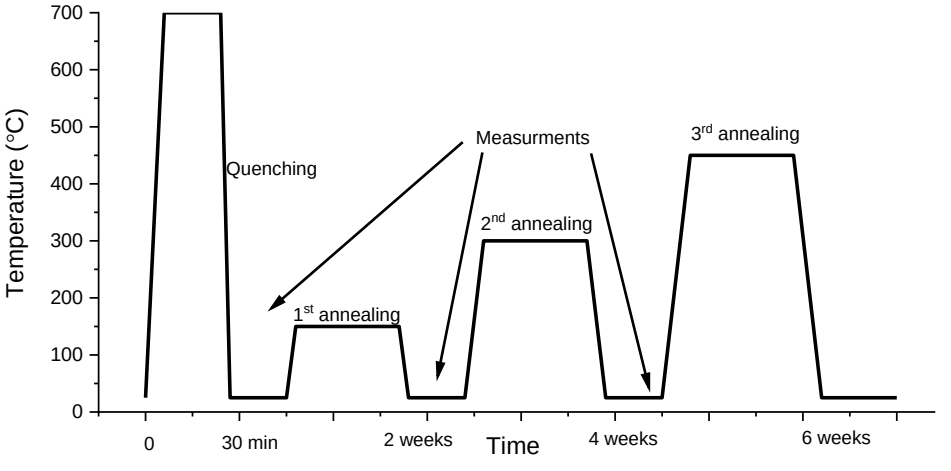

Figure 6.4S – Thermal history of annealing procedure.

REFERENCES:

[1] J. Seidel, L.W. Martin, Q. He, Q. Zhan, Y.H. Chu, A. Rother, M.E. Hawkridge, P. Maksymovych, P. Yu, M. Gajek, N. Balke, S. V. Kalinin, S. Gemming, F. Wang, G. Catalan, J.F. Scott, N.A. Spaldin, J. Orenstein, R. Ramesh, Conduction at domain walls in oxide multiferroics, Nat. Mater. 8 (2009) 229–234. https://doi.org/10.1038/nmat2373.

[2] T. Rojac, A. Bencan, G. Drazic, N. Sakamoto, H. Ursic, B. Jancar, G. Tavcar, M. Makarovic, J. Walker, B. Malic, D. Damjanovic, Domain-wall conduction in ferroelectric BiFeO 3 controlled by accumulation of charged defects, Nat. Mater. 16 (2017) 322–327. https://doi.org/10.1038/nmat4799.

[3] A.N. Morozovska, R.K. Vasudevan, P. Maksymovych, S. V. Kalinin, E.A. Eliseev, Anisotropic conductivity of uncharged domain walls in BiFeO 3, Phys. Rev. B - Condens. Matter Mater. Phys. 86 (2012) 1–9. https://doi.org/10.1103/PhysRevB.86.085315.

[4] U. Robels, G. Arlt, Domain wall clamping in ferroelectrics by orientation of defects, J. Appl. Phys. 73 (1993) 3454–3460. https://doi.org/10.1063/1.352948.

[5] X. Ren, Large electric-field-induced strain in ferroelectric crystals by point-defect-mediated reversible domain switching, Nat. Mater. 3 (2004) 91–94. https://doi.org/10.1038/nmat1051.

[6] R.A. Eichel, Structural and dynamic properties of oxygen vacancies in perovskite oxides - Analysis of defect chemistry by modern multi-frequency and pulsed EPR techniques, Phys. Chem. Chem. Phys. 13 (2011) 368–384. https://doi.org/10.1039/b918782k.

[7] M.I. Morozov, M.A. Einarsrud, J.R. Tolchard, P.T. Geiger, K.G. Webber, D. Damjanovic, T. Grande, In-situ structural investigations of ferroelasticity in soft and hard rhombohedral and tetragonal PZT, J. Appl. Phys. 118 (2015) 0–7. https://doi.org/10.1063/1.4934615.

[8] M.I. Morozov, D. Damjanovic, Hardening-softening transition in Fe-doped Pb (Zr,Ti) O3 ceramics and evolution of the third harmonic of the polarization response, J. Appl. Phys. 104 (2008). https://doi.org/10.1063/1.2963704.

[9] N. Horchidan, C.E. Ciomaga, R.C. Frunza, C. Capiani, C. Galassi, L. Mitoseriu, A comparative study of hard/soft PZT-based ceramic composites, Ceram. Int. 42 (2016) 9125–9132. https://doi.org/10.1016/j.ceramint.2016.02.179.

[10] T. Rojac, A. Bencan, B. Malic, G. Tutuncu, J.L. Jones, J.E. Daniels, D. Damjanovic, BiFeO3 ceramics: Processing, electrical, and electromechanical properties, J. Am. Ceram. Soc. 97 (2014) 1993–2011. https://doi.org/10.1111/jace.12982.

[11] J. Lv, X. Lou, J. Wu, Defect dipole-induced poling characteristics and ferroelectricity of quenched bismuth ferrite-based ceramics, J. Mater. Chem. C. 4 (2016) 6140–6151. https://doi.org/10.1039/c6tc01629d.

[12] I. Calisir, A.A. Amirov, A.K. Kleppe, D.A. Hall, Optimisation of functional properties in lead-free BiFeO3-BaTiO3 ceramics through La3+ substitution strategy, J. Mater. Chem. A. 6 (2018) 5378–5397. https://doi.org/10.1039/c7ta09497c.

[13] S. Lee, C.A. Randall, Z.K. Liu, Modified phase diagram for the barium oxide-titanium dioxide system for the ferroelectric barium titanate, J. Am. Ceram. Soc. 90 (2007) 2589–2594. https://doi.org/10.1111/j.1551-2916.2007.01794.x.

[14] J.M. Vitek, A. Dasgupta, S.A. David, Microstructural Modification of Austenitic Stainless Steels By Rapid Solidification., Metall. Trans. A, Phys. Metall. Mater. Sci. 14 A (1983) 1833–1841. https://doi.org/10.1007/BF02645553.

[15] W. Deng, D. Zhang, H. Wu, Z. Huang, K. Zhou, L. Jiang, Prediction of yield strength in a polycrystalline nickel base superalloy during interrupt cooling, Scr. Mater. 183 (2020) 139–143. https://doi.org/10.1016/j.scriptamat.2020.03.034.

[16] T.K. GUPTA, Strength Degradation and Crack Propagation in Thermally Shocked Al2O3, J. Am. Ceram. Soc. 55 (1972) 249–253. https://doi.org/10.1111/j.1151-2916.1972.tb11273.x.

[17] K. V. Lalitha, B. Wang, P. Ren, D.A. Hall, T. Rojac, Quenching effects and mechanisms in bismuth-based perovskite ferroelectrics, Open Ceram. 10 (2022) 100259. https://doi.org/10.1016/j.oceram.2022.100259.

[18] M. Čebela, D. Zagorac, K. Batalović, J. Radaković, B. Stojadinović, V. Spasojević, R. Hercigonja, BiFeO3 perovskites: A multidisciplinary approach to multiferroics, Ceram. Int. 43 (2017) 1256–1264. https://doi.org/10.1016/j.ceramint.2016.10.074.

[19] G.L. Yuan, S.W. Or, Y.P. Wang, Z.G. Liu, J.M. Liu, Preparation and multi-properties of insulated single-phase BiFeO 3 ceramics, Solid State Commun. 138 (2006) 76–81. https://doi.org/10.1016/j.ssc.2006.02.005.

[20] Y.P. Wang, L. Zhou, M.F. Zhang, X.Y. Chen, J.-M. Liu, Z.G. Liu, Room-temperature saturated ferroelectric polarization in BiFeO3 ceramics synthesized by rapid liquid phase sintering, Appl. Phys. Lett. 84 (2004) 1731–1733. https://doi.org/10.1063/1.1667612.

[21] T. Rojac, M. Kosec, B. Budic, N. Setter, D. Damjanovic, Strong ferroelectric domain-wall pinning in BiFeO3 ceramics, J. Appl. Phys. 108 (2010). https://doi.org/10.1063/1.3490249.

[22] A. Bencan, G. Drazic, H. Ursic, M. Makarovic, M. Komelj, T. Rojac, Domain-wall pinning and defect ordering in BiFeO3 probed on the atomic and nanoscale, Nat. Commun. 11 (2020) 1–9. https://doi.org/10.1038/s41467-020-15595-0.

[23] B. Wang, Y. Li, D. A. Hall, Surface structure and quenching effects in BiFeO3-BaTiO3 ceramics, J. Am. Ceram. Soc 105 (2021) 1265–1275. https://doi.org/10.1111/jace.18188.

[24] M. Ahart, M. Somayazulu, R.E. Cohen, P. Ganesh, P. Dera, H.K. Mao, R.J. Hemley, Y. Ren, P. Liermann, Z. Wu, Origin of morphotropic phase boundaries in ferroelectrics, Nature. 451 (2008) 545–548. https://doi.org/10.1038/nature06459.

[25] T. Sebastian, I. Sterianou, D.C. Sinclair, A.J. Bell, D.A. Hall, I.M. Reaney, High temperature piezoelectric ceramics in the Bi(Mg1/2Ti 1/2)O3-BiFeO3-BiScO3-PbTiO 3 system, J. Electroceramics. 25 (2010) 130–134. https://doi.org/10.1007/s10832-010-9600-0.

[26] A.J. Bell, T.P. Comyn, T.J. Stevenson, Expanding the application space for piezoelectric materials, APL Mater. 9 (2021). https://doi.org/10.1063/5.0035416.

[27] Y.A. Genenko, J. Glaum, M.J. Hoffmann, K. Albe, Mechanisms of aging and fatigue in ferroelectrics, Mater. Sci. Eng. B Solid-State Mater. Adv. Technol. 192 (2015) 52–82. https://doi.org/10.1016/j.mseb.2014.10.003.

[28] E.M. Bourim, H. Tanaka, M. Gabbay, G. Fantozzi, B.L. Cheng, Domain wall motion effect on the anelastic behavior in lead zirconate titanate piezoelectric ceramics, J. Appl. Phys. 91 (2002) 6662–6669. https://doi.org/10.1063/1.1469201.

[29] M.M. Kumar, A. Srinivas, S. V. Suryanarayana, Structure property relations in BiFeO3/BaTiO3solid solutions, J. Appl. Phys. 87 (2000) 855–862. https://doi.org/10.1063/1.371953.

[30] S. Takahash, Effects Of Impurity Doping In Lead Zirconate-Titanate Ceramics, Ferroelectrics. 41 (1982) 143–156. https://doi.org/10.1080/00150198208210617.

[31] L. Zhang, X. Ren, Aging behavior in single-domain Mn-doped BaTiO3 crystals: Implication for a unified microscopic explanation of ferroelectric aging, Phys. Rev. B - Condens. Matter Mater. Phys. 73 (2006) 17–19. https://doi.org/10.1103/PhysRevB.73.094121.

[32] Y. Takagi, H. Nagata, T. Takenaka, Effects of quenching on bending strength and piezoelectric properties of (Bi0.5Na0.5)TiO3 ceramics, J. Asian Ceram. Soc. 8 (2020) 277–283. https://doi.org/10.1080/21870764.2020.1732020.

[33] S. Zhang, F. Yu, Piezoelectric materials for high temperature sensors, J. Am. Ceram. Soc. 94 (2011) 3153–3170. https://doi.org/10.1111/j.1551-2916.2011.04792.x.

[34] T.L. Zhao, A.A. Bokov, J. Wu, H. Wang, C.M. Wang, Y. Yu, C.L. Wang, K. Zeng, Z.G. Ye, S. Dong, Giant Piezoelectricity of Ternary Perovskite Ceramics at High Temperatures, Adv. Funct. Mater. 29 (2019). https://doi.org/10.1002/adfm.201807920.

[35] M.I. Morozov, D. Damjanovic, Charge migration in Pb(Zr,Ti)O3 ceramics and its relation to ageing, hardening, and softening, J. Appl. Phys. 107 (2010). https://doi.org/10.1063/1.3284954.

[36] C. Zhao, S. Gao, T. Yang, M. Scherer, J. Schultheiß, D. Meier, X. Tan, H.J. Kleebe, L.Q. Chen, J. Koruza, J. Rödel, Precipitation Hardening in Ferroelectric Ceramics, Adv. Mater. 33 (2021). https://doi.org/10.1002/adma.202102421.

SUMMARY

The main objective of the research as described in this thesis was to enhance the piezo- and electrical properties of bismuth ferrite-based ($BiFeO_3$ or BFO) piezoceramics at room and elevated temperatures, using both chemical and physical approaches.

Chapter 1 gives a BFO-focused introduction into the field of piezoceramics. It describes the physical origin of the piezoelectric effect and the complex interplay between the intrinsic properties of a material and the poling conditions in case of bulk piezoceramics. The chapter ends with the formulation of the sub-aims of the work.

In **Chapter 2** I successfully achieved the suppression of secondary phases in BFO through a careful analysis of all aspects of the synthesis. Adding 1% Bi_2O_3 to the precursors mixture and optimizing process temperatures resulted in the formation of a phase-pure ceramic with significantly lower electrical conductivity compared to the untreated material. To gain a deeper understanding of the factors influencing the (intrinsic) electrical conductivity of the optimized $BiFeO_3$ material, dedicated annealing experiments in different oxygen-nitrogen gas atmospheres were performed. The results revealed that the high conductivity of the material is related to the concentration of defects associated with oxygen. It was also found that by carefully controlling the partial pressure of oxygen during annealing, the concentration of defects and the resulting conductivity of the material can be further fine-tuned. In particular, at lower partial pressures of oxygen ($pO_2 \leq 10\%$), the conductivity of the material is primarily determined by intrinsic charge carriers, highlighting the significance of oxygen concentration in modulating the electrical behavior of BFO ceramics. The ability to control the conductivity of BFO ceramics through specific annealing conditions and controlled oxygen concentration opens up exciting possibilities to tailor their properties to meet specific requirements in different applications.

Chapter 3 focuses on the use of unstructured composites of BFO particles in a non-conductive PVDF terpolymer matrix for improving the local poling conditions by significantly reducing the overall leakage current and to evaluate

the piezoelectric properties of well-poled BFO ceramic particles. In this chapter, we systematically varied the volume fraction of BFO in the composites and carefully measured the piezoelectric charge constants to explore the relationship between volume fraction and performance. We discovered that the composites with a 60% volume fraction of BFO particles exhibited the highest piezoelectric properties, with a d_{33} value of 31 pC/N and a g_{33} value of 47 mV·m/N after poling under extremely high electric field of 200 kV/cm. To gain a understanding a relationship of the volume fraction dependence of the dielectric constant and piezoelectric charge constant, we employed various analytical models, including the well-known Yamada models and modified Poon models. These models provided valuable insights into the complex interplay between the fraction of ceramic in the composite and its piezoelectric behavior. By extrapolation of the obtained result this study suggested that the maximum possible piezoelectric constant for fully poled bulk BFO in theory could reach a value around 56 pC/N.

In **Chapter 4** the impact of cobalt and titanium doping on the electrical conductivity and piezoelectric properties in BFO synthesized with the protocol presented in Chapter 2 was investigated. Our findings revealed that cobalt doping leads to a decrease in the coercive field of the piezoelectric ceramic and an increase in the electrical conductivity, which could be attributed to the acceptor nature of cobalt doping, resulting in an increased concentration of oxygen vacancies in the material. In contrast, titanium doping resulted in a decrease in electrical conductivity, possibly due to a decrease in the concentration of oxygen vacancies but leads to the disappearance of piezoelectric properties of BFO. Interestingly this study also revealed that dual doping with cobalt and titanium at appropriate levels, specifically 0.25 at% each, resulted in a synergistic effect. The dual-doped material exhibited a decrease in the coercive field for polarization, similar to that for cobalt doping, and a decrease in the conductivity, similar to that due to titanium doping. The resulting piezoelectric ceramic material showed an excellent room temperature performance with a piezoelectric constant (d_{33}) of 40 pC/N, a dielectric constant in the range of 100, and low dielectric losses of less than 1%.

In **Chapter 5** it was demonstrated that newly conceived BFO-rich $BiFeO_3$-$PbTiO_3$-$SrTiO_3$ bulk piezoceramics can be synthesized successfully using a conventional solid-state process resulting in a density of >97%. Both $BiFeO_3$-$SrTiO_3$ and $BiFeO_3$-$PbTiO_3$ systems contain the MPB region which leads to a

triple point MPB in the resulting ternary system. Samples near the cubic-pseudo cubic phase boundary (possible triple point MPB region) exhibit the highest piezoelectric properties at room temperature with piezoelectric constants reaching a value of 250 pC/N. However, the Curie temperature is significantly reduced due to unit cell dual doping with $PbTiO_3$ and $SrTiO_3$, and an exponential relationship is observed between the Curie temperature and the piezoelectric property d_{33}. The study also found that the temperature dependence of piezoelectric properties varies with the thermal history of the samples. Heat treatment at a temperature higher than the use temperature results in decreased piezoactivity but also stabilized the temperature dependence. For the composition of 0.6BiFeO3-0.2PbTiO3-0.2SrTiO3, a combination of a high Curie temperature and an appropriate heat treatment resulted in a superior stable piezoelectric coefficient (d_{33}) value of 90 pC/N at room temperature and a value of 120 pC/N at 300 °C. However, the material still showed a rapid rise in electrical conductivity with temperature, which is unaffected by the levels of $SrTiO_3$ and $PbTiO_3$ doping. Future research should focus on gaining a deeper understanding of the electrical conductivity at elevated temperatures for the $BiFeO_3$-$PbTiO_3$-$SrTiO_3$ ternary system to open this system for potential applications.

In **Chapter 6**, we investigated the impact of a post-synthesis heat treatment on the piezoelectric properties of the most promising $BiFeO_3$-$Bi_{0.5}Li_{0.5}TiO_3$-$PbTiO_3$ ceramic developed in Chapter 5. We observed that the rate of cooling from temperatures above the phase transition temperature (T > 650 °C) played a critical role in obtaining favorable properties at room temperature. Specifically, we observed that a cooling rate of above 10 °C/s resulted in a decrease in the coercive field to 45 kV/cm, which allowed effective poling, resulting in a relatively high piezoelectric constant of around 95 pC/N. We discovered an unusual intermediate state after annealing at temperatures above 150 °C but lower than 600 °C with a quasi-stable piezoelectric constant of around 63 pC/N. Regardless of the thermal history of the sample, provided the depolarization temperature (around 650°C) is not exceeded, the piezoelectric properties of the material (at room temperature) will be around 63 pC/N. This intermediate state exhibited the presence of a non-equilibrium state that could be mediated and reversed through proper quenching and annealing. We hypothesize that the uniform distribution of point defects during quenching and their subsequent movement to domain walls during annealing could be responsible for this phenomenon. However, the exact

nature of these defects and the processes occurring at the domain walls require further investigation.

In conclusion, using a combination of chemical and thermal modifications, it was possible to obtain a piezoelectric ceramic based on BFO with high (even exceeding the theoretical prediction for pure BFO shown in chapter 3) piezoelectric properties at room temperature of 63 pC/N, a high depolarization temperature above 600 °C, and stable and only weakly temperature dependent properties.

SAMENVATTING

Het belangrijkste doel van het onderzoek zoals beschreven in dit proefschrift was om de piëzo- en elektrische eigenschappen bij kamer- en verhoogde temperatuur van piëzo-keramiek op basis van bismutferriet(BiFeO3 or BFO) te verbeteren, daarbij gebruikmakend van zowel chemische als fysische processen.

Hoofdstuk 1 geeft een inleiding tot het gebied van piëzo-keramiek met specifieke aandacht voor BFO-gebaseerde systemen. Het beschrijft de fysische oorsprong van het piëzo-elektrisch effect en het complexe samenspel tussen de intrinsieke eigenschappen van een materiaal en het polariseergedrag in het geval van bulk piëzo-keramieken. Het hoofdstuk sluit af met het formuleren van de sub-doelen van het onderzoek.

In **hoofdstuk 2** wordt beschreven hoe de vorming van secundaire fasen in BFO voorkomen kan worden door aandacht te besteden aan alle aspecten van de synthese. De toevoeging van 1% Bi_2O_3 aan het precursor mengsel en de optimalisatie van de procestemperaturen leidden tot de vorming van een fase-puur keramiek met een belangrijk lagere waarde voor de elektrische geleidbaarheid dan die van normaal geproduceerd materiaal. Om een beter inzicht te krijgen in de factoren die een rol spelen in de intrinsieke elektrische geleidbaarheid van het geoptimaliseerde BFO materiaal, werden specifieke gloeiproeven gedaan in diverse zuurstof-stikstof gasmengsels. De resultaten lieten zien dat een hoge elektrische geleidbaarheid gerelateerd is aan de aanwezigheid van zuurstof-defecten. Ook werd gevonden dat door verlaging van de zuurstof partiaaldruk in het gasmengsel de concentratie van defecten en daarmee de geleidbaarheid verder gestuurd kon worden. Bij een zuurstof concentratie lager dan 10% wordt de geleidbaarheid vooral bepaald door de intrinsieke ladingsdragers. De mogelijkheid om de geleidbaarheid van BFO keramiek te sturen middels een juiste combinatie van zuurstofpotentiaal en temperatuur biedt de mogelijkheid om BFO met verschillende eigenschappen voor specifieke toepassingen te realiseren.

Hoofdstuk 3 richt zich op het gebruik van ongestructureerde composieten van BFO deeltjes in een niet-geleidende PVDF terpolymere matrix om door

verlaging van de lekstromen te komen tot verbeterde lokale poling condities van afzonderlijke deeltjes, en om zo de eigenschappen van perfect gepolariseerde BFO keramische deeltjes te kunnen bepalen. In dit hoofdstuk varieerden we de volume fractie BFO en bepaalden de piëzo-elektrische ladingsconstante om zo de relatie tussen beide nauwkeurig te bepalen. We ontdekten dat composieten met een volume fractie van 60% BFO deeltjes, na polen onder een extreem hoog veld van 200 kV/cm, de hoogste piëzo-elektrische eigenschappen hadden met een d_{33} waarde van 31 pC/N en een g_{33} waarde van 47 mV.m/N. We gebruikten verschillende analytische modellen zoals het Yamada en het Poon model, om de volume fractieafhankelijkheid van de di-elektrische contante en de piëzo-elektrische constante en hun onderliggende interacties beter te begrijpen. Door extrapolatie bepaalden we dat de waarde van de piëzo-elektrische constante van perfect gepolariseerde chemisch zuivere BFO deeltjes 56 pC/N zou moeten zijn.

In **hoofdstuk 4** wordt het effect van doping met Kobalt en Titanium op de elektrische geleidbaarheid en de piëzo-elektrische eigenschappen van het BFO gesynthetiseerd via het protocol beschreven in Hoofdstuk 2, gepresenteerd. Onze metingen lieten zien dat doping met Kobalt leidt tot een afname in het coërcief veld en een toename in de elektrische geleidbaarheid. Dit is een gevolg van het donor-karakter van Kobalt wat een verhoogde concentratie van zuurstof defecten induceert. Doping met Titanium daarentegen gaf een verlaging van de elektrische geleidbaarheid, mogelijk als gevolg van het verdwijnen van zuurstof defecten, maar zorgde er ook voor dat het BFO zijn piëzo-elektrische eigenschappen verloor. Het onderzoek liet ook zien dat gelijktijdig legeren van BFO met gelijke hoeveelheden Kobalt en Titanium (0.25 at % elk) een synergistisch effect had. Het 'dual doped' materiaal had zowel een lager coërcief veld als een lagere elektrische geleidbaarheid. Het materiaal heeft bij kamertemperatuur uitstekende eigenschappen zoals een d_{33} van 40 pC/N, een di-elektrische contante rond de 100 en lage di-elektrische verliezen van minder dan 1 %.

In **hoofdstuk 5** wordt een nieuw-bedacht BFO-rijk ternair $BiFeO_3$-$PbTiO_3$-$SrTiO_3$ systeem gepresenteerd. Het materiaal werd gesynthetiseerd via een conventioneel vaste stof proces en bereikte een dichtheid groter dan 97%. Zowel de binaire $BiFeO_3$-$SrTiO_3$ als de $BiFeO_3$-$PbTiO_3$ systemen bevatten een morphotrope fase grens (MPB) hetgeen zou moeten leiden tot een MPB triple point (en dus superieure piëzo eigenschappen) in het ternaire systeem.

Preparaten met een samenstelling nabij de kubisch/pseudo-kubisch fase grens en het triple point gaven de hoogste waardes voor de piëzo-elektrische constante van 250 pC/N bij kamertemperatuur. Helaas leidde het legeren van BFO met zowel $PbTiO_3$ als $SrTiO_3$ niet alleen tot hogere waardes van de piëzo-elektrische constante d_{33} maar ook tot een sterke verlaging van de Curie temperatuur resulterend in een exponentiele relatie tussen beide. Eveneens werd ontdekt dat de temperatuur afhankelijkheid van de piëzo-elektrische eigenschappen verandert met de voorafgaande warmtebehandeling. Een warmtebehandeling bij een temperatuur die hoger is dan de beoogde gebruikstemperatuur geeft weliswaar een lagere piëzo activiteit maar tevens een lagere temperatuur afhankelijkheid. Bij een samenstelling van $0.6BiFeO_3$-$0.2PbTiO_3$-$0.2SrTiO_3$ werd na een passende warmtebehandeling een hoge Curie temperatuur in combinatie met een vrijwel temperatuur onafhankelijke en stabiele piëzo-elektrische contante verkregen met d_{33} waardes van 90 pC/N bij kamertemperatuur en 120 pC/N bij 300 °C. Helaas vertoonde de elektrische geleidbaarheid nog steeds een hoge temperatuur afhankelijkheid, onafhankelijk van het $SrTiO_3$ en $PbTiO_3$ percentage. Nader onderzoek naar deze veranderbare temperatuur afhankelijkheid van de piëzo eigenschappen van dit ternaire systeem is nodig om de grote potentie van het materiaal voor daadwerkelijke toepassingen te kunnen ontketenen.

In **hoofdstuk 6** onderzochten we het effect van warmtebehandelingen op de piëzo-elektrische eigenschappen van het meest veelbelovende ternaire system ($BiFeO_3$-$Bi_{0.5}Li_{0.5}TiO_3$-$PbTiO_3$) ontwikkeld in **hoofdstuk 5**. We ontdekten dat de afkoelsnelheid van een temperatuur boven de fasegrens (T > 650 °C) tot kamertemperatuur een belangrijke rol speelt voor het verkrijgen van gunstige eigenschappen. We ontdekten dat een afkoelsnelheid groter dan 10 °C/s resulteerde in een afname van het coërcief veld tot 45 kV/cm waardoor effectievere poling en betere eigenschappen zoals een d_{33} van 95 pC/N bij kamertemperatuur mogelijk werden. Tevens ontdekten we het bestaan van een ongebruikelijk en stabiele tussentoestand met een d_{33} van 63 pC/N na gloeien bij een willekeurige temperatuur tussen 150 en 600 °C, en de restrictie dat de temperatuur niet boven de depolarisatie temperatuur van 650 °C komt. Deze niet-evenwichts tussentoestand kan reversibel opgeroepen en uitgeschakeld worden door passende afschrik- en gloei-behandelingen. We stellen de hypothese dat deze tussentoestand het gevolg is van een uniforme verdeling van puntfouten door het afschrikken en hun migratie naar domeinwanden tijdens de gloeibehandeling. Meer onderzoek naar de exacte

aard van deze defecten en hun interactie met, en stabilisatie van de domeinwanden is nodig.

Afsluitend: door gebruik te maken van chemische en fysische processen ben ik er in geslaagd om een BFO-gebaseerd piëzo-elektrisch keramiek te maken, met goede piëzo elektrische eigenschappen op kamertemperatuur (d_{33}= 63 pC/N), hoger dan die van zuiver BFO, een depolarisatie temperatuur boven de 600 °C, een prima stabiliteit en een ongebruikelijk lage temperatuurafhankelijkheid van de piëzo ladingsconstante.

Стислий виклад

Основною метою дослідження, описаного в цій дисертації, було покращення п'єзо- та електричних властивостей п'єзокераміки на основі ферриту вісмута ($BiFeO_3$ або BFO) при кімнатній та підвищеній температурах, використовуючи як хімічні, так і фізичні підходи.

Розділ 1 дає вступ, спрямований на викриття ролі BFO у галузі п'єзокераміки. Він описує фізичне походження п'єзоелектричного ефекту та складну взаємодію між внутрішніми властивостями матеріалу та умовами полярізації у випадку об'ємної п'єзокераміки. Розділ закінчується формулюванням підцілей роботи.

У **розділі 2** мені вдалося досягнути пригнічення вторинних фаз у BFO за допомогою ретельного аналізу всіх аспектів синтезу. Додавання 1% Bi_2O_3 до суміші прекурсорів та оптимізація температур процесу призвели до формування фазово-чистої кераміки з значно нижчою електричною провідністю, порівняно з немодіфікованим матеріалом. Для глибшого розуміння факторів, що впливають на (внутрішню) електричну провідність оптимізованого матеріалу $BiFeO_3$, були проведені спеціальні експерименти з відпалюванням в різних атмосферах кисню-азоту. Результати показали, що висока провідність матеріалу пов'язана з концентрацією дефектів, асоційованих з киснем. Було також знайдено, що шляхом ретельного контролю парціального тиску кисню під час відпалювання можна подальше налаштування концентрації дефектів та відповідної провідності матеріалу. Зокрема, при нижчих парціальних тисках кисню ($pO_2 \leqslant 10\%$), провідність матеріалу в основному визначається внутрішніми носіями заряду, що підкреслює значення концентрації кисню в модулюванні електричної поведінки кераміки BFO. Здатність контролювати провідність кераміки BFO за допомогою специфічних умов відпалювання та контролю концентрації кисню відкриває широкі можливості налаштування властивостей матеріалу для задоволення конкретних вимог у різних застосуваннях.

Розділ 3 зосереджується на використанні неструктурованих композитів з частинок BFO в непровідній матриці терполімеру PVDF для поліпшення

локальних умов полярізації шляхом значного зниження загальних струмів витоку та оцінки п'єзоелектричних властивостей добре поляризованих частинок кераміки BFO. У цьому розділі ми систематично змінювали об'ємну частку BFO в композитах і ретельно вимірювали п'єзоелектричні зарядові константи, щоб дослідити зв'язок між об'ємною часткою та п'єзоелектричними властивостями. Ми виявили, що композити з 60% об'ємною часткою частинок BFO виявили найвищі п'єзоелектричні властивості, з величиною d_{33} 31 pC/N і величиною g_{33} 47 mV·m/N після поляризації під високим електричним полем в 200 kV/cm. Для розуміння залежності від об'ємної частки діелектричної константи та п'єзоелектричної зарядової константи ми використовували різні аналітичні моделі, включаючи відомі моделі Ямади та модифіковані моделі Пуна. Ці моделі дали цінні уявлення про складну взаємодію між часткою кераміки в композиті та її п'єзоелектричною поведінкою. Шляхом екстраполяції отриманих результатів це дослідження натякає на те, що максимальна можлива п'єзоелектрична константа для повністю поляризованого об'ємного BFO в теорії може досягти значення близько 56 pC/N.

У **Розділі 4** було досліджено вплив додавання кобальту та титану на електричну провідність та п'єзоелектричні властивості в BFO, синтезованому за протоколом, представленим у **Розділі 2**. Наші знахідки показали, що додавання кобальту призводить до зниження коерцитивного поля п'єзоелектричної кераміки та збільшення електричної провідності, що може бути пов'язано з акцепторною природою допінга кобальта, що призводить до збільшення концентрації вакансій кисню в матеріалі. На противагу цьому, додавання титану призвело до зниження електричної провідності, можливо, через зменшення концентрації вакансій кисню, але призвело до втрати п'єзоелектричних властивостей BFO. Цікаво, що це дослідження також показало, що подвійне додавання кобальту та титану на відповідних рівнях, специфічно по 0.25 ат.%, призводило до синергетичного ефекту. Матеріал з подвійним додаванням виявив зниження коерцитивного поля для поляризації, подібне до того, як для додавання кобальту, та зниження провідності, подібне до того, що спостерігається при додаванні титану. В результаті п'єзоелектричний керамічний матеріал виявив відмінну продуктивність при кімнатній температурі з п'єзоелектричною

константою (d_{33}) 40 pC/N, діелектричною константою в діапазоні 100 та низькими діелектричними втратами менше 1%.

У **розділі 5** було продемонстровано, що новостворені багаті на ферріт вісмуту кераміки $BiFeO_3$-$PbTiO_3$-$SrTiO_3$ можуть бути успішно синтезовані за допомогою традиційного твердофазного процесу, що призводить до відносної компактності > 97%. Обидві системи $BiFeO_3$-$SrTiO_3$ та $BiFeO_3$-$PbTiO_3$ містять область морфотропної границі фаз (МГФ), що призводить до трійного точкового МРВ у вихідній тернарній системі. Зразки біля межі кубічної-псевдокубічної фази (можлива область трійного точкового МГФ) проявляють найвищі п'єзоелектричні властивості при кімнатній температурі з п'єзоелектричними константами, що досягають значення 250 pC/N. Проте, температура Кюрі значно знижується через подвійне додавання $PbTiO_3$ та $SrTiO_3$, і спостерігається експоненціальний зв'язок між температурою Кюрі та п'єзоелектричною властивістю d_{33}. Дослідження також показало, що температурна залежність п'єзоелектричних властивостей варіюється з термічною історією зразків. Термічна обробка при температурі вищій, ніж температура використання, призводить до зниження п'єзоактивності, але також стабілізує температурну залежність. Для композиції $0.6BiFeO_3$-$0.2PbTiO_3$-$0.2SrTiO_3$ комбінація високої температури Кюрі та відповідна термічна обробка призвела до винятково стабільного значення п'єзоелектричного коефіцієнту (d_{33}) 90 pC/N при кімнатній температурі та значення 120 pC/N при 300 °C. Однак матеріал все ще показував стрімке зростання електричної провідності з температурою, яке не залежить від рівнів додавання $SrTiO_3$ та $PbTiO_3$. Майбутні дослідження повинні бути спрямовані на глибше розуміння електричної провідності при підвищених температурах для тернарної системи $BiFeO_3$-$PbTiO_3$-$SrTiO_3$, щоб відкрити цю систему для потенційних застосувань.

У **розділі 6** ми досліджували вплив післясинтезного теплового оброблення на п'єзоелектричні властивості найбільш обіцяючої кераміки $BiFeO_3$-$Bi_{0.5}Li_{0.5}TiO_3$-$PbTiO_3$. Ми спостерігали, що швидкість охолодження з температур вище температури фазового переходу (T > 650 °C) відіграє критичну роль у досягненні сприятливих властивостей при кімнатній температурі. Зокрема, ми спостерігали, що швидкість охолодження більше 10 °C/с призводила до зниження коерцитивного поля до 45 kV/cm, що дозволило ефективне поляризування, призводячи

до відносно високої п'єзоелектричної константи близько 95 pC/N. Ми виявили незвичайний проміжний стан після відпалювання при температурах вище 150 °C, але нижче 600 °C з квазі-стабільною п'єзоелектричною константою близько 63 pC/N. Незалежно від теплової історії зразка, за умови, що температура деполяризації (близько 650°C) не перевищена, п'єзоелектричні властивості матеріалу (при кімнатній температурі) будуть близько 63 pC/N. Цей проміжний стан виявив присутність нерівноважного стану, який можна було регулювати та змінювати через належне гасіння та відпалювання. Ми робимо гіпотезу, що рівномірне розподілення точкових дефектів під час гасіння та їх подальший рух до доменних стінок під час відпалювання можуть бути відповідальні за це явище. Однак, точна природа цих дефектів та процеси, що відбуваються на доменних стінках, потребують подальшого дослідження.

У висновку, використовуючи комбінацію хімічних та теплових модифікацій, нам вдалося отримати п'єзоелектричну кераміку на основі BFO з високими (навіть перевищуючи теоретичний прогноз для чистого BFO, показаний у **розділі 3**) п'єзоелектричними властивостями при кімнатній температурі 63 pC/N, високою температурою деполяризації понад 600 °C, і стабільними та лише слабко залежними від температури властивостями.

Acknowledgements

First and foremost, as I reflect on the thrilling, challenging, and rewarding almost five-year journey towards earning my PhD in NovAM at the Aerospace faculty of TU Delft, I find myself overwhelmed with gratitude for the people without whom this long voyage would have remained an uncharted dream.

My journey wouldn't have started without the foundational support of my first promotor, the late Pim Groen. His belief in my potential and the opportunity he provided laid the groundwork for everything that followed. I am forever grateful to Pim for setting me on this path and offering unwavering guidance right from the outset. Our enlightening conversations, often over a beer in de Atmosfeer, were times when he generously imparted his wisdom. Pim was not just a mentor but also a reservoir of knowledge, especially in piezoelectrics and ceramics. His deep understanding and infectious passion were important in fueling my motivation to pursue this PhD. While it's deeply saddening that he isn't here to see the conclusion of this journey, his teachings, values, and enduring spirit guide me.

Sybrand van der Zwaag, your steadfast presence and mentorship have been cornerstones of my academic journey. Even though you were my promotor before Pim's passing, the dynamics of our collaboration evolved profoundly afterward. Throughout this transformative phase, you've been a beacon of wisdom and support. I cannot express enough how grateful I am for the ways you have shaped me professionally. Your responsiveness, understanding, and readiness to assist during challenging times have been pivotal. Beyond the academic realm, your guidance has deeply influenced my personal growth and perspectives. I'm indebted to you for the layers of wisdom and insight you've added to my journey. Many thanks for everything; your support has been truly priceless.

Bernard Dam, I'm deeply appreciative of you stepping in as my second promotor. Your critical insights and fresh perspective on my work have been indispensable. Your wisdom and encouragement pushed my work to higher standards, helping me navigate complexities that seemed insurmountable. Your keen eye and sound advice were more than mere professional assistance;

they were lifelines in my academic journey. I thank you sincerely for your dedication and support.

At TU Delft laboratories I am indebted to many people for their assistance. In particular I would like to thank Frans Oostrum, Durga Mainali Sharma, Victor Horbowiec, Alexander Uithol, Mohammed Jafar, Roy Awater. Ed Roessen and Rob van der List, thank you for your help in preparation of sample holders and test setups.

My sincere thanks go to Kistler Instrumente AG and especially to Roland Somer. Their generosity in providing both their expertise and equipment was instrumental for the high-temperature piezoelectric measurements detailed in this thesis (chapter 5). Their collaboration greatly enhanced the depth and quality of our research. I must also a sincere thank you to Hans Brouwer from the Department of Materials Science and Engineering for his assistance with the oxygen control experiments for BFO ceramic (chapter 2). Your expertise and precision have been vital to the success of our experiments. Your collaboration not only enriched the quality of the work but also made the process more engaging and enlightening. Also, I'd like to extend special appreciation to Ruud Hendrix from the Department of Materials Science and Engineering. His expertise in conducting the in-situ high-temperature X-ray measurements was invaluable to this research (chapter 6). His dedication and technical skills greatly enriched the quality of our work.

Also, I would like to say thank you to Siddharth, a master student I had the honour of supervising. Our academic journey not only culminated in invaluable research but also, I hope, forged a friendship. Without him, the doping study of BFO (chapter 4) wouldn't have been possible.

I extend my heartfelt appreciation to our secretary, Shanta Visser. Your cheerful disposition, organizational acumen, and unwavering support have filled workplace with positivity. You played a role that went far beyond ordinary administrative tasks, fostering a vibrant atmosphere within NovAM.

I wish to acknowledge the hidden heroes, those who have contributed in ways less visible but no less meaningful. The people in the NovAM group who have supported, encouraged, challenged, and stood by me through this rewarding phase of my life. Our fun times at the faculty bar, de Atmosfeer, and our daily coffee breaks and lunches made it special. A big thanks to Tinashe, Miisa,

Dimos, Gawel, Jingjing, Mariana, Paul, Satya, Silvia, Vincenzo, Yifan, Riccardo, Siddharth, Krishna, Lakshmi, and others from the past. I especially cherish our boardgame events with Hugo, Vincent, and Tadhg – moments I hope never end. Thanks to everyone in NovAM for making it an incredible experience.

Tadhg, my commendations for being the best office mate one could ever wish for fall short of encapsulating the gratitude I owe you. Your hands-on assistance in the lab and those insightful discussions over 9 am coffee were far from mere routine. They were the spark that often ignited ideas and kept the fire of discovery alive. Your camaraderie has been one of the highlights of this journey, and I thank you wholeheartedly for your unwavering friendship and professional partnership.

I'm not forgetting about Marlon, Vincent and Gawel. Sharing an office with you (and towards the end, only with Marlon) has been a genuine pleasure. The collective brainstorming and light-hearted moments have added immeasurable value to my PhD experience. I am grateful for your support and the laughter we shared, making our workspace truly vibrant and collaborative.

And a special mention to Hugo, who wasn't an office mate but was one of the closest PhD colleagues I had. We began this journey almost at the same time and now we're finishing it side by side. Your support and shared experiences have been a big part of this journey.

И не могу не выразить особую благодарность самому важному человеку в моей жизни — моей маме. Твоя безграничная любовь, поддержка и вера в меня были моим основным источником силы и вдохновения на этом длинном ученом пути. Без твоего участия, твоих жертв и мудрых советов многого бы не произошло. Даже в моменты моих сомнений, ты была той, кто поддерживал и вдохновлял меня двигаться дальше. Ты всегда рядом, готовая прийти на помощь, и за это я безмерно благодарен. Ты — мой основной стержень, моя опора, мое вдохновение.

In conclusion, I hope this dissertation serves as a modest tribute to the collective wisdom, effort, and spirit of all those mentioned above and many others whose names may not have appeared on these pages but whose influence permeates every word and idea.

This long and arduous journey, filled with highs and lows, successes and setbacks, has been made possible by the strength derived from each one of you. Beyond the pages of this dissertation, lie countless hours of dedication, collaboration, and perseverance. I thank you all from the deepest recesses of my heart and dedicate this achievement to you. Together, we have ventured through this academic odyssey, and it's a journey I will cherish forever.

CURRICULUM VITÆ

I was born on the 25th of May 1993 and grew up in Dnipro, Ukraine. In 2016 I obtained my BSc degree Applied Physics at the Oles Honchar Dnipro National University. Driven by a strong passion for knowledge, I enthusiastically enrolled in a Master's program offered collaboratively by Dnipro National University and Cracow Pedagogical University. Throughout this program, my profound interest in material science blossomed. The complexities of materials, their properties, and behaviors fascinated me, sparking an unquenchable thirst to explore this field further. In January 2018, I successfully completed my Master's program, presenting a thesis titled "Impedance Spectra of $Na_{0.5}Bi_{0.5}TiO_3$-$BaTiO_3$ Solid Solutions." Motivated by the discoveries I made during my Master's program, I resolved to continue my scientific journey.

In the same year, 2018, I therefore started on my doctoral trajectory initially under supervision of Prof. dr. Pim Groen and Prof. dr. ir. Sybrand van der Zwaag. Unfortunately, my PhD journey took an unfortunate turn on May 6, 2020, with the tragic passing of my primary supervisor, Pim Groen. However, I was fortunate to have the distinguished presence of Prof. dr. ir. Sybrand van der Zwaag, who graciously assumed the role of my main supervisor. Under his expert guidance and unwavering support, I navigated through the challenges and continued my research with determination. Additionally, I had the invaluable assistance of Prof. dr. Bernard Dam, who served as my second supervisor during the culmination of my PhD trajectory, providing crucial support that contributed to the successful completion of my research.

During my doctoral research, I undertook a comprehensive study centred around the exploration of advanced piezoelectric systems tailored for high temperature applications. The focal point of my investigation revolved around the utilization of bismuth ferrite as a highly promising material for developing piezoelectric sensors capable of withstanding and operating optimally under extreme temperature conditions.

List of Publications

Journal Publications

6. **A. Tuluk** and S. van der Zwaag
Exploring the $BiFeO_3$-$PbTiO_3$-$SrTiO_3$ ternary system to obtain good piezoelectrical properties at low and high temperatures
under review, Materials (2023)

5. **A. Tuluk** and S. van der Zwaag
Controlling the piezoelectric properties in bulk $BiFeO_3$-$PbTiO_3$-$Li_{0.5}Bi_{0.5}TiO_3$ ceramic be quenching and annealing
under review, Journal of Applied Physics (2023)

4. **A. Tuluk**, H. Brouwer, and S. van der Zwaag
Controlling the Oxygen Defects Concentration in a Pure $BiFeO_3$ Bulk Ceramic
Materials 15, 19 (2022)

3. **A. Tuluk**, S. Joshi, T.R. Mahon, and S. van der Zwaag
Tuning Piezoproperties of $BiFeO_3$ ceramic by Cobalt and Titanium Dual Doping
Journal of Applied Physics 131, 21 (2022)

2. **A. Tuluk**, T.R. Mahon, S. van der Zwaag, and P. Groen
Estimating the True Piezoelectric Properties of $BiFeO_3$ from Measurements on $BiFeO_3$-PVDF Terpolymer Composites
Journal of Alloys and Compounds 868: 159186 (2021)

1. **A. Yu. Tuluk**, T. R. Mahon, S. van der Zwaag, and P. Groen
$BiFeO_3$ Synthesis by Conventional Solid-State Reaction.
2019 IEEE International Symposium on Applications of Ferroelectrics, ISAF 2019 - Proceedings: 3–6 (2019)

CONFERENCE CONTRIBUTIONS

5. **A. Tuluk**, S. Joshi, T.R. Mahon, and S. van der Zwaag
Oral presentation: *Study of the effect of heterovalent doping on the piezo-electrical properties of $BiFeO_3$*
Ceramics in Europe, Krakow, Poland 2022

4. **A. Tuluk**, and S. van der Zwaag
Oral presentation: *Reversible control of the properties of $BiFeO_3$-based ferroelectric ceramic with high Curie temperature by quenching and tempering*
International Symposium on Applications of Ferroelectrics, Tours, France 2022

3. **A. Tuluk**, T.R. Mahon, S. van der Zwaag, and P. Groen
Oral presentation: *Measurement of Piezoelectric Properties of $BiFeO_3$-PVDF Terpolymer Composites*
International Symposium on Applications of Ferroelectrics, Sydney, Australia 2021

2. **A. Tuluk**, T.R. Mahon, S. van der Zwaag, and P. Groen
Oral presentation: *Role of oxygen defects in the electrical properties of $BiFeO_3$*
Electroceramics XVII Confererence, Darmstadt, Germany 2020

1. **A. Yu. Tuluk**, T. R. Mahon, S. van der Zwaag and P. Groen
Poster: *$BiFeO_3$ Synthesis by Conventional Solid-State Reaction*
$F^2C\pi^2$ Joint Conference, Lausanne, Switzerland, September 2019